A COMPARATIVE STUDY OF ESTIMATION MODELS FOR SATELLITE RELATIVE MOTION

A Thesis

by

URI PRAKASH DESAI

Submitted to the Office of Graduate Studies of
Texas A&M University
in partial fulfillment of the requirements for the degree of

MASTER OF SCIENCE

Approved by:

Chair of Committee,	Srinivas R. Vadali
Committee Members,	John L. Junkins
	Igor Zelenko
Head of Department,	Rodney D. W. Bowersox

May 2013

Major Subject: Aerospace Engineering

ABSTRACT

The problem of relative spacecraft motion estimation is considered with application to various reference and relative orbits. Mean circular and elliptic orbits are analyzed, with relative orbits ranging in size from 1 km to 10 km. Estimators are built for three propagation models: (i) Gim-Alfriend State Transition Matrix, (ii) the J_2-Linearized Equations of Motion for Circular Orbits, and (iii) the Clohessy-Wiltshire Equations of Motion. Two alternative models were developed in an attempt to account for unmodeled nonlinearities: (i) Biased Clohessy-Whiltshire Equations, and (ii) J_2-Linearized State Transition Matrix. Two estimation techniques are presented in an attempt to explore and determine which propagation model minimizes the error residual: the linear Kalman filter is presented under the assumption of vector based, GPS-type measurements; the extended Kalman filter is analyzed assuming angle-range, optical-type measurements. Sampling time is varied to look at the effect of measurement frequency. It is assumed that the orbit of one of the satellites, the chief, is known reasonably well.

This work showed that the error residuals from the state estimates were minimized when the propagation technique utilized was the Gim-Alfriend State Transition Matrix. This supports conclusions that are obtained outside of the estimation problem. Additionally, the error residuals obtained when the propagation technique was the Clohessy-Wiltshire Equations is comparable to the more complicated models. Unmodeled nonlinearities affect the magnitude of the error residuals. As expected, the Gim-Alfriend STM comes closest to the truth; for smaller eccentricities (0.005),

the Clohessy-Wiltshire EOM show minor deviations from the truth. As the eccentricity increases, the linear models begin to diverge greatly from the true response. The additional two models (the biased CW equations, and the linear STM) show decent performance under specific conditions. The former accounts for some of the unaccounted for nonlinearities. The latter exhibits comparable performance to the Gim-Alfrien STM for circular reference orbits. However, in each case, as the nonlinearity of the problem increases, the accuracy of the model decreases.

For my mom and dad, who told me it was possible.

For my sister, who showed me it was possible.

For Jess, who helped me make it possible.

ACKNOWLEDGEMENTS

First and foremost, I would like to thank my advisor, Dr. Srinivas R. Vadali, for his unlimited patience and his never-ending support and guidance. Dr. Vadali never once showed frustration with me, despite the slow goings. He was understanding, and helpful - guiding me through the challenges and helping me to become a better student and a better researcher. The privilege of working with Dr. Vadali has been extremely rewarding, and I am extraordinarily grateful.

I would like to thank my parents, Linda and Prakash Desai, for everything they have done for me over the years. Their unconditional love and support has been invaluable. They were always there to give me the little extra push I needed to continually challenge myself, and to keep raising the bar. And to my sister, Dr. Tasha Zander: I could not have asked for a better role model than her. She set the standard for which I could continually look up.

I would like to thank my fellow graduate students in the Department of Aerospace Engineering for their help, their encouragement, and the distraction they provided when it was needed most. Namely: Dr. Ryan Wiseman for his assistance over the past few years with understanding estimation, the implementation and the nuances associated with filtering; Dr. Christopher Roscoe for his assistance with understanding the relative motion problem, for helping with every question I could possibly dream to ask, and for providing many of the figures utilized over the course of this thesis; and Mr. Francesco de Diletis for being a great sounding board for ideas and problems.

Finally, and most importantly, I would like to thank Jessica. Her support and encouragement over the past few years has been invaluable. There is no way I would have been able to stay sane without having her in my life. For the past 10 years there has always been one person I could count on. She has been there to listen to my frustrations, offer up her support and encouragement, and celebrate with me when things go well.

Uri Prakash Desai December, 2012

TABLE OF CONTENTS

Page

CHAPTER Page

Page

LIST OF FIGURES

FIGURE Page

FIGURE Page

FIGURE Page

LIST OF TABLES

CHAPTER I

INTRODUCTION

Ever since man has left the safety of his shelter, whether to take to sea, or to air, or to space, knowing where one is, has always been of extraordinary significance. From the first days man spent out on the ocean, the need to navigate correctly and accurately has been key. The Greek's invented the astrolabe; the compass and it's north-seeking magnetic needle first came into use in the 12^{th} and 13^{th} centuries; mariners utilized the sextant to determine their location on the surface of the Earth, by measuring the positioning of the sun; each of these navigation instruments were the basis for years of development and planing [1]. Gus Grissom aboard *Gemini 4* utilized the rudimentary, and highly accurate sextant [2]. The development and launch of the Global Positioning System (GPS) allowed man to accurately predict where he is, anywhere on the Earth. Through the use of coordinated satellite information, man could know his exact location [3]. These advances found direct application to spacecraft formation flying.

Formation flying is not a new topic; from the early days of space travel and the rendezvous of the Lunar Module (LM) with the Command Service Module (CSM), to the more advanced science missions of NASA [4], understanding how one spacecraft navigates with respect to another is extremely important. Several techniques exist by which two or more spacecraft can navigate in formation. Escobal [5] presented several of these methods, including the angles-only problem, range-rate and angular data problem, range and range-rate data problem, to name a few. Markley [6]

showed how landmark data provides a highly accurate and consistent method of orbit determination for autonomous navigation, in addition to exploring the conditions for observability. Yim [7], in her dissertation, explored methods by which spacecraft can navigate, independent of ground systems; by looking at three orbital navigation problems, Yim was able to show that in addition to navigation using sun and Earth sensors, relative navigation between two satellites was possible. Angles-only navigation proved to be a feasible method for the solution of the relative navigation problem, given that they are in dissimilar orbits. Schmidt and Lovell [8] looked at the observability problem when applied to the relative orbital element set. They presented a method by which the geometric aspects of the relative trajectory could be determined. However, the unobservability problem persisted for the angles-only problem. The challenges faced by such a problem lies in the loss of observability. Observability is the idea that given the output of a system, the current states are able to be determined; thus, knowing only the output response, the behavior of the entire system is known [9]. Woffinden and Geller looked at the criteria necessary for angles-only navigation, given the linear dynamics [10]; they showed that in the absence of a maneuver, observability was lost. In order to maintain observability over the entire orbit, this thesis focuses on range and angles-range measurements. The observability of this type of system is well known and established, and is without the challenges of the angles-only type measurements.

These problems focus on near-Earth applications. Kim et al [11] presented navigation and estimation techniques utilizing optical measurements coming from VISNAV. Kim was able to show that both relative position and attitude were able to

be estimated from optic-based sensors. With relative orbits of less than 1 km, error residuals on the orders of millimeters were obtained. Fritz [12] looked at estimation using GPS measurements for autonomous rendezvous and docking. Understanding the applications of one type of measurement over another becomes important; for instance, GPS measurements are only valid over specific distances, and degrade as the relative orbit gets smaller. Delpech et al [13] looked at the utilization of radio-frequency measurements that yielded centimeter position accuracy in the short range.

These types of sensors provide the basis for the estimation problem. On board orbiting satellites, it becomes necessary to counter the noise present on the sensors. Fian-feng [14] showed results for the implementation and application of both the extended Kalman filter and unscented Kalman filter to the relative motion problem. Errors on the order of 10 cm and 1 cm/s were observed through use of the extend Kalman filter, while errors on the order of mm and mm/s were observed through use of the unscented Kalman filter at LEO. How and Tilerson [15] showed that relative velocity errors of 2-3 mm/sec can have a very large and adverse effect on estimation and the control problem. This work detailed how small errors in velocity estimates can grow as the spacecraft is propagated, culminating in meter-order errors. It thus becomes necessary to ensure that the estimator predicts the states to within a specific order of magnitude. Only then will the filtered states be feasible solutions to the relative motion problem.

The GA-STM is a very precise method by which the relative elements, in the curvilinear frame can be propagated. It is valid for any elliptical or circular orbit. The J_2-linearized equations and the CW equations are only valid for circular orbits.

However, the nature of the GA-STM is its primary disadvantage: it is a complicated matrix, being a function of the mean elements of the chief, that is computationally intensive to calculate. While the CW equations are not valid for elliptical orbits, they are much simpler than GA-STM. Thus it becomes attractive to use the CW equations; their disadvantage is that they do not account for the nonlinearities and J_2 effects that the GA-STM does. This thesis will present a method by which bias states are added into the filter; these states act to model the unaccounted for perturbations with the goal of improving the response of the CW propagation model to rival the GA-STM. Alfriend and Yan [16] looked a comparison of the relative motion theories, including the CW equations and the GA-STM and several other methods. They developed an index by which the accuracy of the model could be determined; per their results, the CW equations were the least accurate, while the GA-STM proved to be among the most accurate. Two additional theories not explored in this thesis - the unit-sphere approach and the Yan-Alfriend nonlinear theory- were determined to be the most accurate and applicable to the widest range of relative orbits.

The goal of this thesis is to present a comparative study of estimation techniques for the relative motion problem. Given the varying methods of position estimation presented, several scenarios will be examined; in addition to the varying of the propagation model, the types of measurements (GPS-like versus optical), the frequency of measurements, as well as the types of relative orbits will be varied. The goal is to simply answer the question, under what conditions and by how much one estimation model better than another? This thesis approaches these problems from a different direction that previous work. Many applications propagate two spacecraft, simulta-

neously estimating their position and velocity; the relative motion is then determined based off of the estimates of both satellites. Here, an alternative approach is being investigated. It is assumed that the chief's orbit is known reasonably well, and the relative motion is being estimated directly through various models for propagating relative motion.

To answer these questions, this thesis is divided into several parts. Chapter 2 presents the basic orbital mechanics utilized over the course of this thesis; this includes reference frames, coordinate conversions, and the governing equations of motion. Estimation techniques are outlined in Chapter 3. This includes the linear Kalman filter in both its discrete and continuous-discrete forms. Chapter 4 applies these estimation techniques to the orbital mechanics problem. It presents results for the various scenarios selected, and a discussion of their impact Finally, some conclusions are offered in Chapter 5. The appendices to this thesis provide a more detailed look at some of the governing equations as well as the error residual tables from the several scenarios that are analyzed.

CHAPTER II

SPACECRAFT RELATIVE MOTION

Consider two spacecraft orbiting the Earth, both in elliptic orbits, one being identified as the "chief", the other as the "deputy". It is assumed that the spacecraft are under the influence of the Earth only; i.e., the gravitational effects of the Sun and the moon are ignored. Chief and deputy quantities are expressed with a subscript "0"and "1", respectively.

II.A. Reference Orbits and Orbital Geometry

The chief is assumed to be in a reference orbit defined by six, classical orbital elements. These parameters describe the orbit, the orientation, and the timing and are detailed in Table II.1.

Table II.1. Classical orbital elements.

Element	Description
a	Semimajor axis
e	Eccentricity
Ω	Right ascension of the ascending node
i	Inclination
ω	Argument of periapsis
t_0	Time of periapsis passage

The elements Ω, ω, and i define the orientation of the orbital frame, $\vec{\mathcal{F}}_o$, with respect to the inertial frame, $\vec{\mathcal{F}}_i$, shown in Figure II.1. The transformation from the inertial reference frame to the orbital frame is described by the rotation matrix of

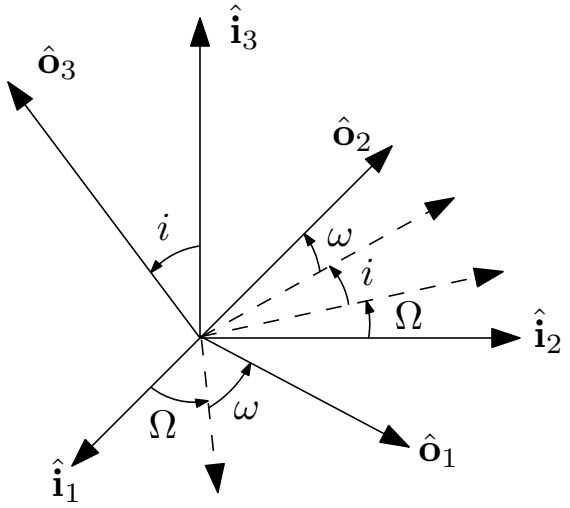

Figure II.1. Inertial frame to orbital frame rotations.

Eq. (2.1):

$$\vec{\mathcal{F}}_o = \mathbf{C}_{oi}\vec{\mathcal{F}}_i \tag{2.1}$$

$$\mathbf{C}_{oi} = \mathbf{C}_3(\omega)\mathbf{C}_1(i)\mathbf{C}_3(\Omega) \tag{2.2}$$

$$\mathbf{C}_{oi} = \begin{bmatrix} c_\omega & s_\omega & 0 \\ -s_\omega & c_\omega & 0 \\ 0 & 0 & 1 \end{bmatrix} \begin{bmatrix} 1 & 0 & 0 \\ 0 & c_i & s_i \\ 0 & -s_i & c_i \end{bmatrix} \begin{bmatrix} c_\Omega & s_\Omega & 0 \\ -s_\Omega & c_\Omega & 0 \\ 0 & 0 & 1 \end{bmatrix}$$

$$\mathbf{C}_{oi} = \begin{bmatrix} c_\omega c_\Omega - s_\omega c_i s_\Omega & c_\omega s_\Omega + s_\omega c_i c_\Omega & s_\omega s_i \\ -s_\omega c_\Omega - c_\omega c_i s_\Omega & -s_\omega s_\Omega + c_\omega c_i c_\Omega & c_\omega s_i \\ s_i s_\Omega & -s_i c_\Omega & c_i \end{bmatrix}$$

where the abbreviations $c_\alpha = cos(\alpha)$ and $s_\alpha = sin(\alpha)$.

The reference orbit that is formed on the plane of $\vec{o}_1$ and $\vec{o}_2$ is defined by the geometric and timing parameters, a, e, and t_0, the time at perigee. Figure II.2 details the construction of the orbit ellipse from the semimajor axis, a, and the eccetricity, e.

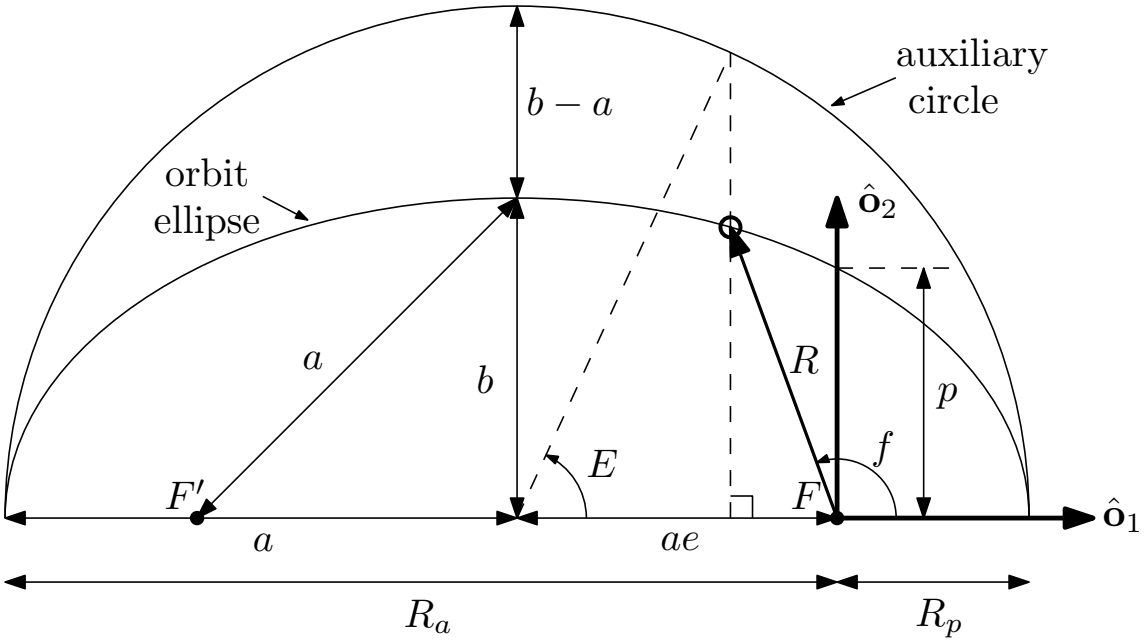

Figure II.2. Orbital geometry.

The geometrical parameters a and e are utilized to obtain the ellipse geometry, including the semiminor axis, b, the semi-latus rectum, p, the radius of periapsis, and the radius of apoapsis, R_p and R_a, respectively.

$$b = a\sqrt{1 - e^2} \tag{2.3}$$

$$p = a(1 - e^2) \tag{2.4}$$

$$R_p = a(1 - e) \tag{2.5}$$

$$R_a = a(1+e) \tag{2.6}$$

The timing parameter, t_0, is transformed into an angular measurement through the conversions of Eq. (2.7).

$$M = n_0(t - t_0) \tag{2.7a}$$

$$M = E - e\sin E \tag{2.7b}$$

$$\tan\frac{f}{2} = \sqrt{\frac{1+e}{1-e}}\tan\frac{E}{2} \tag{2.7c}$$

where M is the mean anomaly, calculated from the chief's mean motion, n_0, and the current time, t, and the time at perigee, t_0. The eccentric anomaly, E, can not be determine analytically from Eq. (2.7b), and must be solved numerically (using a Newton root solver, for instance). f is the true anomaly, easily solved for once the eccentric anomaly is known. The eccentric and true anomaly are depicted in Figure II.2.

II.A.1. Converting between Orbital Element Sets

Throughout the course of this thesis, two types of orbital element sets will be used. The first is the classical orbital element set, presented in Table II.1. The second is the non-singular orbital element set, useful for situations in which a specific element is undefined. For instance, in the case of a circular orbit, ω is undefined. The non-singular set, as defined in [17] and shown in Table II.2, helps account for these problems. Eq. (2.8) shows the simple conversions from the classical element set to the non-singular element set.

Table II.2. Non-singular orbital elements.

Element	Description
a	Semimajor axis
q_1	$-$
q_2	$-$
i	Inclination
Ω	Right ascension of ascending node
λ	Mean argument of latitude

where

$$q_1 = e\cos\omega \tag{2.8a}$$

$$q_2 = e\sin\omega \tag{2.8b}$$

$$\lambda = \omega + M \tag{2.8c}$$

The reverse transformation, from the non-singular element set to the classical set its easily performed, according to Eq. (2.9). The only terms requiring calculation are the eccentricity, the argument of periapsis, and the true anomaly.

$$e = \sqrt{q_1^2 + q_2^2} \tag{2.9a}$$

$$\omega = \arctan\frac{q_2}{q_1} \tag{2.9b}$$

The transformation of the mean anomaly into the true anomaly follows the procedure outlined in Eq. (2.7).

The orbital element sets can be expressed in the Cartesian reference frame; this is a necessary conversion for the propagation using the perturbed two-body equations of motion. Given the non-singular elements of Table II.2, the Cartesian position and

velocity can be extracted from Eq. (2.10), where the rotation matrices present are defined in Eq. (2.2).

$$r_s = \frac{p}{1 + q_1 \cos\theta + q_2 \sin\theta} \begin{bmatrix} \cos\theta \\ \sin\theta \\ 0 \end{bmatrix} \tag{2.10a}$$

$$v_s = \sqrt{\frac{\mu}{p}} \begin{bmatrix} -q_2 - \sin\theta \\ q_1 + \cos\theta \\ 0 \end{bmatrix} \tag{2.10b}$$

$$R = \left[\mathbf{C}_1(i)\mathbf{C}_3(\Omega)\right]^T r_s \tag{2.10c}$$

$$V = \left[\mathbf{C}_1(i)\mathbf{C}_3(\Omega)\right]^T v_s \tag{2.10d}$$

where p is the *semilatus rectum*, defined by:

$$p = a\left(1 - q_1^2 - q_2^2\right) \tag{2.11}$$

II.A.2. Relative Orbits

The deputy spacecraft's orbit can be defined via absolute elements (in a similar fashion to how the chief was defined), or by relative elements. More specifically, rather than defining a separate orbit for the deputy, the relative orbit can be defined, and from such definition, the inertial orbit can be extracted.

Using the development presented in [18] and [19], it is possible to define the relative orbit in terms of a sizing parameter, ρ, and a phase angles, ϕ and ψ; Figure II.3 defines the orbit in terms of the relative range, ρ, and the phase angle α, which is

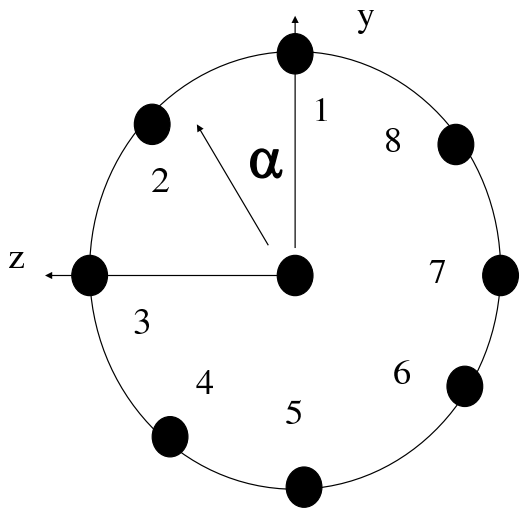

Figure II.3. Relative orbit phase angle.

interchangeable with the angles ϕ and ψ. The relative, non-singular elements are defined by Eq. (2.12).

$$\delta a = \frac{1}{2} J_2 \left(\frac{R_e^2}{a_0}\right) \frac{3\eta + 4}{\eta^4} \left[-\left(1 - 3\cos^2 i_0\right) \delta e \frac{e_0}{1 - e_0^2} - \sin\left(2i_0\right) \delta i \right] \tag{2.12a}$$

$$\delta\theta = \gamma_1 \delta\lambda + \gamma_2 \delta q_1 + \gamma_3 \delta q_2 \tag{2.12b}$$

$$\delta i = \frac{\rho_z}{a_0} \cos\psi \tag{2.12c}$$

$$\delta q_1 = \frac{q_{1,0} q_{2,0} \rho_x \cos\phi}{a_0} - \frac{\left(1 - q_{1,0}^2\right) \rho_x \sin\phi}{a_0} - q_{2,0} \left(\frac{\rho_y}{a_0} - \delta\Omega \cos i_0\right) \tag{2.12d}$$

$$\delta q_2 = \frac{q_{1,0} q_{2,0} \rho_x \sin\phi}{a_0} - \frac{\left(1 - q_{2,0}^2\right) \rho_x \cos\phi}{a_0} + q_{1,0} \left(\frac{\rho_y}{a_0} - \delta\Omega \cos i_0\right) \tag{2.12e}$$

$$\delta\Omega = -\frac{\rho_z}{a_0} \frac{\sin\psi}{\sin i_0} \tag{2.12f}$$

where

$$\delta\lambda = \frac{\rho_y}{a_0} - \delta\Omega\cos i_0 - \frac{\left(1+\eta+\eta^2\right)\rho_x\left(q_{1,0}\cos\phi - q_{2,0}\sin\phi\right)}{\left(1+\eta\right)a_0} \tag{2.13}$$

$$\eta = \sqrt{1-e_0^2} \tag{2.14}$$

$$\delta e = \sqrt{\delta q_1^2 + \delta q_2^2} \tag{2.15}$$

$$\gamma_1 = \frac{\alpha^2}{\eta^3} \tag{2.16}$$

$$\gamma_2 = \frac{q_{2,0}\alpha^2}{\eta^2\left(1+\eta\right)} + \frac{\alpha\sin\theta_0}{\eta^2} + \frac{q_{2,0}+\sin\theta_0}{\eta^2} \tag{2.17}$$

$$\gamma_3 = -\frac{q_{2,0}\alpha^2}{\eta^2\left(1+\eta\right)} - \frac{\alpha\cos\theta_0}{\eta^2} - \frac{q_{1,0}+\cos\theta_0}{\eta^2} \tag{2.18}$$

and where

$$\alpha = 1 + q_{1,0}\cos\theta_0 + q_{2,0}\sin\theta_0 \tag{2.19}$$

Note that unlike in the case of unperturbed relative orbits, $\delta a \neq 0$ in the presence of the J_2 perturbation. Condition (2.12a) is a result of enforcing a no-along track drift condition, as discussed extensively in [20].

II.B. Reference Frames

For the purposes of this thesis, three reference frames will be utilized: the Earth Centered Inertial (ECI) frame is Earth-fixed, and does not rotate with the planet; the Local Vertical Local Horizontal (LVLH) frame is fixed to the chief spacecraft - as the chief rotates and precesses about the Earth, the frame does as well; and finally, the curvilinear reference frame, a variant of the LVLH frame.

II.B.1. Earth Centered Inertial (ECI) Frame

As per [21], the Earth Centered Inertial (ECI) frame places the Earth's center at the origin of the frame. The XY plane coincides with Earth's equatorial plane, where in the X-axis points in the direction of the vernal equinox. The Z-axis points in the direction of the north pole, and the Y-axis completes the right handed coordinate system. Figure II.4 presents the ECI frame, denoted by $\vec{\mathcal{F}}_i$.

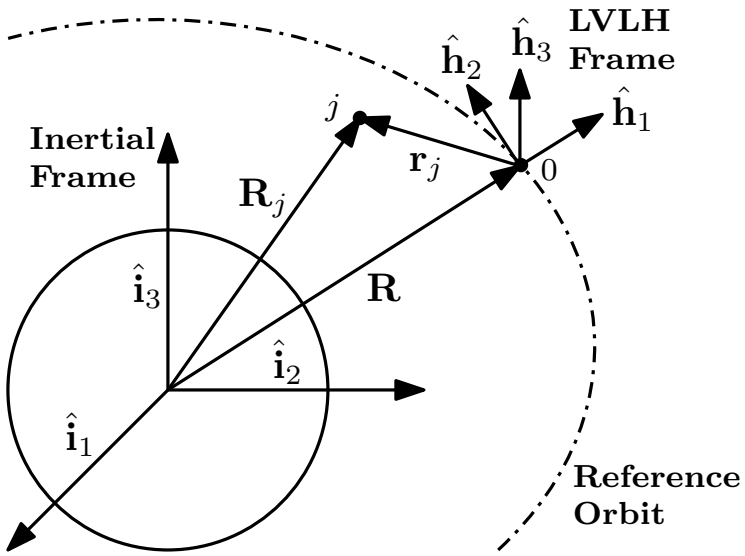

Figure II.4. Earth Centerted Inertial (ECI) and Local Vertical Local Horizontal. (LVLH) frame.

II.B.2. Local Vertical Local Horizontal (LVLH) Frame

The LVLH frame is chief-fixed and rotates with the chief as it orbits the Earth. Figure II.4 depicts this reference frame, denoted by $\vec{\mathcal{F}}_h$, relative to the ECI frame. The X-axis is directed from the spacecraft radially outward. The Z-axis is normal

to the orbital plane, and the Y-axis completes the right handed coordinate frame, customarily pointing in the along-track direction.

II.B.3. Curvilinear Frame

For a special set of governing equations, the customary reference frame is forgone in place of a curvilinear description. This frame is formed by creating an imaginary circle that lies tangent to the reference orbit at the current orbital position. As with the LVLH frame, a triplet (x_c, y_c, z_c) describes the relative position of the deputy with respect to the chief. However, unlike the LVLH frame, the three coordinates describe different quantities. The x coordinate is the radial distance from the imaginary circle to the deputy spacecraft, in the direction of the inertial radial position. The y coordinate is the arc length from the chief, along the imaginary circle, to the point of intersection of the deputy's inertial radial direction. The z coordinate is similar to the y coordinate, but lies out of plane along a second imaginary circle.

II.B.4. Converting between Reference Frames

In order to provide an accurate comparison of results, the position and velocity may need to be converted from one reference frame to another; this includes taking a vector in the ECI frame and expressing it in the LVLH or vice versa, and taking a vector in the LVLH and expressing it in the curvilinear frame, or vice versa.

II.B.4.a. Transformation of Varaiables from ECI to LVLH Frames(and LVLH to ECI)

The relative position and velocity of the deputy with respect to the chief, expressed in the ECI frame are defined by Eq. (2.20):

$$\delta\mathbf{r} = \mathbf{r}_1 - \mathbf{r}_0 \tag{2.20a}$$

$$\delta\mathbf{v} = \mathbf{v}_1 - \mathbf{v}_0 \tag{2.20b}$$

Taking the relative position from the ECI to the LVLH involves the transformations of Eq. (2.21):

$$\delta x = \frac{\delta\mathbf{r}^T\mathbf{r}_0}{r_0} \tag{2.21a}$$

$$\delta y = \frac{\delta\mathbf{r}^T(\mathbf{h}_0 \times \mathbf{r}_0)}{\parallel \mathbf{h}_0 \times \mathbf{r}_0 \parallel} \tag{2.21b}$$

$$\delta z = \frac{\delta\mathbf{r}^T\mathbf{h}_0}{h_0} \tag{2.21c}$$

Likewise, the transformation of the relative velocity from the ECI to the LVLH is expressed by Eq. (2.22):

$$\delta\dot{x} = \frac{\delta\mathbf{v}^T\mathbf{r}_0 + \delta\mathbf{r}^T\mathbf{v}_0}{r_0} - \frac{(\delta\mathbf{r}^T\mathbf{r}_0)(\delta\mathbf{r}_0^T\mathbf{v}_0)}{r_0^3} \tag{2.22a}$$

$$\begin{aligned}\delta\dot{y} =& \frac{\delta\mathbf{v}^T(\mathbf{h}_0 \times \mathbf{r}_0) + \delta\mathbf{r}^T(\dot{\mathbf{h}}_0 \times \mathbf{r}_0 + \mathbf{h}_0 \times \mathbf{v}_0)}{\parallel \mathbf{h}_0 \times \mathbf{r}_0 \parallel} \\ & - \frac{\delta\mathbf{r}^T(\mathbf{h}_0 \times \mathbf{r}_0)(\mathbf{h}_0 \times \mathbf{r}_0)^T(\dot{\mathbf{h}}_0 \times \mathbf{r}_0 + \mathbf{h}_0 \times \mathbf{v}_0)}{\parallel \mathbf{h}_0 \times \mathbf{r}_0 \parallel^3}\end{aligned} \tag{2.22b}$$

$$\delta\dot{z} = \frac{\delta\mathbf{v}^T\mathbf{h}_0 + \delta\mathbf{r}^T\dot{\mathbf{h}}_0}{h_0} - \frac{(\delta\mathbf{r}^T\mathbf{r}_0)(\delta\mathbf{r}_0^T\mathbf{v}_0)}{r_0^3} \tag{2.22c}$$

where the cross product from Eq. (2.22) of $\dot{\mathbf{h}}_0 = \mathbf{r}_0 \times \dot{\mathbf{v}}_0$ is obtained directly from the differential equations of motion (see Chapter II.C). Note that $\dot{\mathbf{v}}_0$ is the acceleration of the chief in the ECI frame. Hence, the accuracy of the transformation is dependent on the knowledge of the perturbing accelerations of the chief.

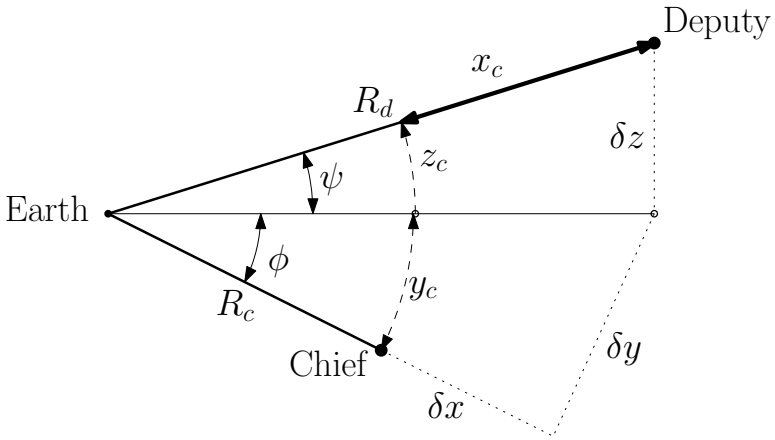

Figure II.5. Converting from LVLH to the curvilinear frame, and vice versa.

II.B.4.b. Transformation of Varaiables from LVLH to Curvilinear Frames (and Curvilinear to LVLH)

While the transformations of II.B.4.a involve the rotation of vectors from one frame to another, the transformation from the LVLH frame to the curvilinear frame is based on the geometry of the frames. The details of this transformation are shown in Figure II.5. For smaller relative orbits, it can be shown that the transformation between the LVLH frame and the curvilinear frame can be approximated as a unity

transformation. This assumption does not hold for larger relative orbits; this being the case, this simplifying assumption is forgone in this work in favor of using the full transformation.

The chief's radius in the orbital frame of the chief, is given by:

$$R_0 = \left(\mathbf{R}_0^T \mathbf{R}_0\right)^{1/2} \tag{2.23}$$

The deputy's radius vector, also in the orbital frame of the chief, is defined by:

$$\mathbf{R}_1 = \begin{bmatrix} R_0 + \delta x \\ \delta y \\ \delta z \end{bmatrix} \tag{2.24}$$

Given the LVLH coordinates of $\delta x, \delta y, \delta z$, the relative position in the curvilinear frame is expressed by Eq. (2.25):

$$x_c = R_1 - R_0 \tag{2.25a}$$

$$y_c = R_0 \phi \tag{2.25b}$$

$$z_c = R_0 \psi \tag{2.25c}$$

While the relative velocity in the curvilinear frame is expressed by Eq. (2.26). These transformations are simply the time derivative of the position equations of Eq. (2.25).

$$\dot{x}_c = \dot{R}_1 - \dot{R}_0 \tag{2.26a}$$

$$\dot{y}_c = \dot{R}_0 \phi + R_0 \dot{\phi} \tag{2.26b}$$

$$\dot{z}_c = \dot{R}_0\psi + R_0\dot{\psi} \tag{2.26c}$$

where the angles ϕ and ψ are defined by Eq. (2.27):

$$\phi = \arctan\left(\frac{\delta y}{R_0 + \delta x}\right) \tag{2.27a}$$

$$\psi = \arcsin\left(\frac{\delta z}{R_1}\right) \tag{2.27b}$$

where R_1 is the radius of the deputy, defined as the scalar of Eq. (2.24). The derivatives of the angles are defined by Eq. (2.28):

$$\dot{\phi} = \frac{\dot{\delta y}\left(R_0 + \delta x\right) - \delta y\left(\dot{R}_0 + \dot{\delta x}\right)}{\delta y^2 + \left(R_0 + \delta x\right)^2} \tag{2.28a}$$

$$\dot{\psi} = \frac{\dot{\delta z}R_1 - \delta z\dot{R}_1}{R_1^2}\sqrt{1 + \frac{\delta z^2}{\delta y^2 + \left(R_0 + \delta x\right)^2}} \tag{2.28b}$$

Finally, the derivative of the chief's radius is defined by Eq. (2.29), and the derivative of the deputy's radius is defined by Eq (2.30):

$$\dot{R}_0 = \frac{\mathbf{V}_C^T\mathbf{R}_0}{R_0} \tag{2.29}$$

$$\dot{R}_1 = \sqrt{\left(\dot{R}_0 + \dot{\delta x}\right)^2 + \dot{\delta y}^2 + \dot{\delta z}^2} \tag{2.30}$$

The reverse transformation from the curvilinear frame to the LVLH frame is defined by the position equations of Eq. (2.31) and the velocity equations of Eq. (2.32):

$$\delta x = R_1\cos\psi\cos\phi - R_0 \tag{2.31a}$$

$$\delta y = R_1\cos\psi\sin\phi \tag{2.31b}$$

$$\delta z = R_1 \sin\psi \tag{2.31c}$$

$$\delta v_x = \dot{R}_1 \cos\psi\cos\phi - R_1 \sin\psi\dot{\psi}\cos\phi - R_1 \cos\psi \sin\phi\dot{\phi} - \dot{R}_0 \tag{2.32a}$$

$$\delta v_y = \dot{R}_1 \cos\psi\sin\phi - R_1 \sin\psi\dot{\psi}\sin\phi + R_1 \cos\psi\cos\phi\dot{\phi} \tag{2.32b}$$

$$\delta v_z = \dot{R}_1 \sin\psi + R_1 \cos\psi\dot{\psi} \tag{2.32c}$$

The angles ϕ and ψ are redefined from the previous section as follows:

$$\phi = \frac{y_c}{R_0} \tag{2.33a}$$

$$\psi = \frac{z_c}{R_0} \tag{2.33b}$$

The time derivative of the chief's scalar position, $\dot{R}_0$, is given by Eq. (2.29), the time derivative of the deptuty's radius, $\dot{R}_1$, is defined by Eq. (2.34), and the time derivatives of the angles ϕ and ψ are defined in Eqs. (2.35):

$$\dot{R}_1 = \dot{R}_0 + \dot{x}_c \tag{2.34}$$

$$\dot{\phi} = \frac{\dot{y}_c - \dot{R}_0\phi}{R_0} \tag{2.35a}$$

$$\dot{\psi} = \frac{\dot{z}_c - \dot{R}_0\psi}{R_0} \tag{2.35b}$$

II.C. Equations of Motion

Expressed in the ECI-Frame, the non-linear differential equations of motion describe the motion of the spacecraft around the Earth, with the option to take into

account several perturbations, including non-spherical Earth gravitational effects, lunar and solar effects, and atmospheric drag.

The governing equations of motion for any object orbiting about the Earth can be solved by any numerical method to express the position and velocity of said object at any point in time, given a set of initial conditions. Eq. (2.36) defines the nonlinear, differential equation:

$$\ddot{\mathbf{r}} = -\frac{\mu}{r^3}\mathbf{r} + \mathbf{a_d} \tag{2.36}$$

where r is the norm of the spacecraft's ECI position, and the disturbing force, $\mathbf{a}_d$ is defined in Eq. (2.37).

$$\mathbf{a}_d = \mathbf{a}_{J_2} + \mathbf{a}_{J_3} + \mathbf{a}_{J_4} + \mathbf{a}_{J_5} + \mathbf{a}_{J_6} + \mathbf{a}_{drag} + \mathbf{a}_{other} \tag{2.37}$$

The individual perturbations are modeled according to Eq. (2.38):

$$\mathbf{a}_{J_2} = -\frac{3}{2}J_2\left(\frac{\mu}{r^2}\right)\left(\frac{R_e}{r}\right)^2\begin{pmatrix}\left(1-5\left(\frac{z}{r}\right)^2\right)\frac{x}{r}\\ \left(1-5\left(\frac{z}{r}\right)^2\right)\frac{y}{r}\\ \left(3-5\left(\frac{z}{r}\right)^2\right)\frac{z}{r}\end{pmatrix} \tag{2.38a}$$

$$\mathbf{a}_{J_3} = -\frac{1}{2}J_3\left(\frac{\mu}{r^2}\right)\left(\frac{R_e}{r}\right)^3\begin{pmatrix}5\left(7\left(\frac{z}{r}\right)^3-3\left(\frac{z}{r}\right)\right)\frac{x}{r}\\ 5\left(7\left(\frac{z}{r}\right)^3-3\left(\frac{z}{r}\right)\right)\frac{y}{r}\\ 3\left(10\left(\frac{z}{r}\right)^2-\frac{35}{3}\left(\frac{z}{r}\right)^4-1\right)\frac{z}{r}\end{pmatrix} \tag{2.38b}$$

$$\mathbf{a}_{J_4} = -\frac{5}{8}J_4\left(\frac{\mu}{r^2}\right)\left(\frac{R_e}{r}\right)^4\begin{pmatrix}\left(3-42\left(\frac{z}{r}\right)^2+63\left(\frac{z}{r}\right)^4\right)\frac{x}{r}\\ \left(3-42\left(\frac{z}{r}\right)^2+63\left(\frac{z}{r}\right)^4\right)\frac{y}{r}\\ -\left(15-70\left(\frac{z}{r}\right)^2+63\left(\frac{z}{r}\right)^4\right)\frac{z}{r}\end{pmatrix} \tag{2.38c}$$

$$\mathbf{a}_{J_5} = -\frac{1}{8} J_5 \left(\frac{\mu}{r^2}\right) \left(\frac{R_e}{r}\right)^5 \begin{pmatrix} 3\left(35\left(\frac{z}{r}\right) - 210\left(\frac{z}{r}\right)^3 + 231\left(\frac{z}{r}\right)^5\right)\frac{x}{r} \\ 3\left(35\left(\frac{z}{r}\right) - 210\left(\frac{z}{r}\right)^3 + 231\left(\frac{z}{r}\right)^5\right)\frac{y}{r} \\ \left(15 - 315\left(\frac{z}{r}\right)^2 + 945\left(\frac{z}{r}\right)^4 - 693\left(\frac{z}{r}\right)^6\right) \end{pmatrix} \tag{2.38d}$$

$$\mathbf{a}_{J_6} = -\frac{1}{16} J_6 \left(\frac{\mu}{r^2}\right) \left(\frac{R_e}{r}\right)^6 \begin{pmatrix} \left(35 - 945\left(\frac{z}{r}\right)^2 + 3465\left(\frac{z}{r}\right)^4 - 3003\left(\frac{z}{r}\right)^6\right)\frac{x}{r} \\ \left(35 - 945\left(\frac{z}{r}\right)^2 + 3465\left(\frac{z}{r}\right)^4 - 3003\left(\frac{z}{r}\right)^6\right)\frac{y}{r} \\ \left(3003\left(\frac{z}{r}\right)^6 - 4857\left(\frac{z}{r}\right)^4 + 2205\left(\frac{z}{r}\right)^2 - 315\right)\frac{z}{r} \end{pmatrix} \tag{2.38e}$$

where the constants R_e, μ, and the zonal harmonics, $J_2 - J_6$, are defined in Table II.3.

Table II.3. Orbital constants.

Constant	Value
J_2	1082.63×10^{-6}
J_3	-2.52×10^{-6}
J_4	-1.61×10^{-6}
J_5	-0.15×10^{-6}
J_6	0.57×10^{-6}
μ	$3.986 \times 10^{-6} \frac{\text{km}^3}{\text{s}^2}$
R_e	6378.1363 km

The disturbance due to atmospheric drag is based upon the model found in [22] and is given in Eq. (2.39):

$$\mathbf{a}_{drag} = -\frac{1}{2} C_D \frac{A}{m} \boldsymbol{\rho} v_a \dot{\mathbf{r}}_a \tag{2.39}$$

where C_D is the dimensionless drag coefficient associated with A, the cross sectional area of the vehicle perpendicular to the direction of motion; m is the vehicle mass, $\boldsymbol{\rho}$ is the atmospheric density at the vehicle's altitude and v_a is the speed of the vehicle

relative to the atmosphere; $\dot{\mathbf{r}}_a$ is defined as:

$$\dot{\mathbf{r}}_a = \begin{bmatrix} \dot{x} + \dot{\theta}y \\ \dot{y} + \dot{\theta}x \\ \dot{z} \end{bmatrix} \tag{2.40}$$

where $\dot{r}$ is the inertial velocity, $[\dot{x}\,\dot{y}\,\dot{z}]^T$, and $\dot{\theta}$ is the rate of rotation of the Earth. The perturbation defined as $\mathbf{a}_{other}$ can include solar radiation pressure, solar gravitation, lunar gravitation, and various other, unmodeled disturbances.

The set of equations that is created by combining Eqs. (2.36) and (2.37) can be formed for two separate spacecraft flying in close formation. Additionally, rather than defining the motions of the two spacecraft separately, one can be defined relative to the other. This becomes the focus of the next section.

II.D. Equations of Relative Motion

II.D.1. Non-Linear Differential Equations

Rather than define the dynamics of two spacecraft flying in close proximity separately, it becomes convenient to define one relative to the other. The relative position of the deputy with respect to the chief is defined in Eq. (2.41), a slight variation of Eq. (2.20).

$$\boldsymbol{\rho} = \mathbf{r}_1 - \mathbf{r}_0 \tag{2.41}$$

Differentiating the expression of Eq. (2.41) twice, yields an expression for the relative acceleration between the chief and the deputy, Eq. (2.42). After building the two-body equations of motion for both the chief and the deputy from Eqs. (2.36)

and (2.38a), substituting into the expression for the relative acceleration, Eq. (2.42), and rearranging, one obtains the perturbed, non-linear differential equation that describes the relative position and velocity of the deputy with respect to the chief, Eq. (2.43):

$$\ddot{\boldsymbol{\rho}} = \ddot{\mathbf{r}}_1 - \ddot{\mathbf{r}}_1 \tag{2.42}$$

$$\ddot{\boldsymbol{\rho}} = -\frac{\mu(\mathbf{r}_0 + \boldsymbol{\rho})}{(r_0 + \rho)^3} + \frac{\mu}{r_0^3}\mathbf{r}_0 + \delta\mathbf{a}_d \tag{2.43}$$

where $\delta\mathbf{a}_d$ are the differential, perturbing accelerations. Note that this result is readily expressed in the ECI frame and can be transformed into the LVLH frame utilizing the transformation of Section II.B.4.a

II.D.2. Gim-Alfriend State Transition Matrix (GA-STM)

The presentation of the developments leading to the Gim-Alfriend State Transition Matrix (GA-STM) is beyond the scope of this thesis. What will be discussed is the basic principle of the GA-STM. The full derivation and expansion of the GA-STM can be found in [23].

The GA-STM takes any set of initial conditions, and propagates them through time. Eq. (2.44) defines this transformation. The objective of this section is to define the matrix, $\Phi_{J_2}(t, t_0)$.

$$\mathbf{x}(t) = \Phi_{J_2}(t, t_0)\mathbf{x}_0 \tag{2.44}$$

The geometric transformation between the Cartesian position and velocity, $\mathbf{x}(t)$,

and the relative, osculating elements, $\delta\mathbf{oe}$, is define in Eq. (2.45), where $A_2 = 3J_2R_e^2$.

$$\mathbf{x}(t) = [A(t) + A_2B(t)]\delta\mathbf{oe} \tag{2.45}$$

The transition matrix for the orbital elements is defined in Eq. (2.46). As with the GA-STM, the transition matrix, $\phi_{\mathbf{oe}}$, takes the initial, osculating orbital elements, and propagates them forward in time. Substituting Eq. (2.45) and Eq. (2.46) into the expression of Eq. (2.44), and rearranging yields the state transition matrix for relative motion, $\Phi_{J_2}(t, t_0)$, Eq. (2.47).

$$\delta\mathbf{oe}(t) = \phi_{\mathbf{oe}}\delta\mathbf{oe}(t_0) \tag{2.46}$$

$$\Phi_{J_2}(t, t_0) = [A(t) + A_2B(t)]\phi_{\mathbf{oe}}(t, t_0)[A(t_0) + A_2B(t_0)]^{-1} \tag{2.47}$$

The GA-STM propagates the relative position and velocity forward in time, assuming that the current relative position and velocity are based upon the instantaneous, osculating elements. Throughout this thesis, any set of orbital initial conditions is given in terms of mean elements. Thus, a conversion from mean to osculating is required. This transformation is given by Eq. (2.48), wherein $\overline{\mathbf{oe}}$ represents the mean elements, and $\mathbf{oe}$ represents the osculating elements.

$$\delta\mathbf{oe}(t) = D(t)\delta\overline{\mathbf{oe}}(t) = D(t)\overline{\phi}_{\mathbf{oe}}(t, t_0)\delta\overline{\mathbf{oe}}(t) \tag{2.48}$$

where the matrix, $\overline{\phi}_{\mathbf{oe}}$, represents the transition matrix for the relative mean elements.

Back substituting yields the GA-STM is given by Eq. (2.49).

$$\Phi_{J_2}(t,t_0) = [A(t) + A_2B(t)]D(t)\overline{\phi}_{\boldsymbol{\alpha e}}(t,t_0)D^{-1}(t_0)[A(t_0) + A_2B(t_0)]^{-1} \tag{2.49}$$

It is convenient to express the GA-STM for two adjacent points in time; rather than propagating the initial conditions forward, it is handy to propagate the previous time step's conditions to the next (t_1 to t_2). This alternate transition matrix is expressed in Eq. (2.50).

$$\Phi_{J_2}(t_2,t_1) = [A(t_2) + A_2B(t_2)]D(t_2)\overline{\phi}_{\boldsymbol{\alpha e}}(t_2,t_1)D^{-1}(t_1)[A(t_1) + A_2B(t_1)]^{-1} \tag{2.50}$$

II.D.3. Linearized Differential Equations for Mean Circular Orbits

The GA-STM provides a method by which the relative position and velocity can be propagated through time, in a curvilinear coordinate system. This can be simplified, given certain assumptions. The GA-STM includes secular, long-period and short-period effects of J_2. For mean, circular orbits, there are no long-periodic terms in the elements, and thus, these effects can be neglected. What follows is a summary of the work presented in [24]. The differential equation model can be augmented with the disturbing acceleration to determine the STM numerically.

The deputy's position is defined in the chief's LVLH frame, denoted by Eq. (2.51). The angular velocity of the LVLH frame is given by Eq. (2.52), where the vector components are defined in Eq. (2.53).

$$\boldsymbol{\rho} = [xyz]^T \tag{2.51}$$

$$\boldsymbol{\omega} = [\omega_x \omega_y \omega_z]^T \tag{2.52}$$

$$\omega_x = \dot{\Omega}_0 \sin i_0 \sin \theta_0 + \dot{i}_0 \cos \theta_0 \tag{2.53a}$$

$$\omega_y = \dot{\Omega}_0 \sin i_0 \cos \theta_0 - \dot{i}_0 \sin \theta_0 = 0 \tag{2.53b}$$

$$\omega_z = \dot{\Omega}_0 \cos i_0 + \dot{\theta}_0 \tag{2.53c}$$

Substituting several expressions (found in [20]) into the differential equation for the relative position (Eq. (2.59) yields the linearized equations of motion for circular orbits: Eq. (2.54).

$$\begin{bmatrix} \dot{\boldsymbol{\rho}} \\ \ddot{\boldsymbol{\rho}} \end{bmatrix} = \begin{bmatrix} 0 & 0 & 0 & 1 & 0 & 0 \\ 0 & 0 & 0 & 0 & 1 & 0 \\ 0 & 0 & 0 & 0 & 0 & 1 \\ a_{41} & a_{42} & a_{43} & 0 & 2\omega_z & 0 \\ a_{51} & a_{52} & a_{53} & -2\omega_z & 0 & 2\omega_x \\ a_{61} & a_{62} & a_{63} & 0 & -2\omega_x & 0 \end{bmatrix} \begin{bmatrix} \boldsymbol{\rho} \\ \dot{\boldsymbol{\rho}} \end{bmatrix} \tag{2.54}$$

where

$$a_{41} = \omega_z^2 + 2\frac{\mu}{r_0^3} + \Upsilon\left(1 - 3\sin^2 \overline{i}_0 \sin^2 \overline{\theta}_0\right) \tag{2.55a}$$

$$a_{42} = \dot{\omega}_z + \Upsilon\left(\sin^2 \overline{i}_0 \sin 2\overline{\theta}_0\right) \tag{2.55b}$$

$$a_{43} = -\omega_x \omega_z + \Upsilon\left(\sin 2\overline{i}_0 \sin \overline{\theta}_0\right) \tag{2.55c}$$

$$a_{51} = -\dot{\omega}_z + \Upsilon\left(\sin^2 \overline{i}_0 \sin 2\overline{\theta}_0\right) \tag{2.55d}$$

$$a_{52} = \omega_x^2 + \omega_z^2 - \frac{\mu}{r_0^3} + \Upsilon\left[-\frac{1}{4} + \sin^2 \overline{i}_0 \left(\frac{7}{4}\sin^2 \overline{\theta}_0 - \frac{1}{2}\right)\right] \tag{2.55e}$$

$$a_{53} = \dot{\omega_x} + \Upsilon \left(-\frac{1}{4} \sin 2\overline{i}_0 \cos \overline{\theta}_0 \right) \tag{2.55f}$$

$$a_{61} = -\omega_x \omega_z + \Upsilon \left(\sin 2\overline{i}_0 \sin \overline{\theta}_0 \right) \tag{2.55g}$$

$$a_{62} = -\dot{\omega_x} + \Upsilon \left(-\frac{1}{4} \sin 2\overline{i}_0 \cos \overline{\theta}_0 \right) \approx 0 \tag{2.55h}$$

$$a_{63} = \omega_x^2 - \frac{\mu}{r_0^3} + \Upsilon \left[-\frac{3}{4} + \sin^2 \overline{i}_0 \left(\frac{5}{4} \sin^2 \overline{\theta}_0 + \frac{1}{2} \right) \right] \tag{2.55i}$$

The relevant variables for the circular orbits case are defined as follows, where $\overline{\theta}_0 = \overline{\theta}_0(0) + \dot{\overline{\theta}}_0 t$, and $J = J_2(\frac{R_e}{\overline{a}_0})^2$:

$$r_0 = \overline{a}_0 \left[1 + J\{ \frac{3}{4}(1 - 3\cos^2 \overline{i}_0) + \frac{1}{4} \sin^2 \overline{i}_0 \cos 2\overline{\theta}_0 \} \right] \tag{2.56a}$$

$$\theta_0 = \overline{\theta}_0(0) + \dot{\overline{\theta}}_0 t + \frac{1}{8} J(1 - 7\cos^2 \overline{i}_0) \sin 2\overline{\theta}_0 \tag{2.56b}$$

$$i_0 = \overline{i}_0 + \frac{3}{8} J \sin 2\overline{i}_0 \cos 2\overline{\theta}_0 \tag{2.56c}$$

$$\Omega_0 = \overline{\Omega}_0(0) + \dot{\overline{\Omega}} t + \frac{3}{4} J \cos \overline{i}_0 \sin 2\overline{\theta}_0 \tag{2.56d}$$

$$\dot{\overline{\theta}}_0 = n_0 \left[1 - \frac{3}{2} J(1 - 4\cos^2 \overline{i}_0) \right] \tag{2.56e}$$

$$\dot{\overline{\Omega}}_0 = -\frac{3}{2} J n_0 \cos \overline{i}_0 \tag{2.56f}$$

The component-wise expression for the angular velocities is given by:

$$\omega_x = 2\dot{\overline{\Omega}}_0 \sin \overline{i}_0 \sin \overline{\theta}_0 \tag{2.57a}$$

$$\omega_y = 0 \tag{2.57b}$$

$$\omega_z = \dot{\overline{\Omega}}_0 \cos \overline{i}_0 + \dot{\overline{\theta}}_0 + \frac{1}{4} J n_0 \cos 2\overline{\theta}_0 \sin^2 \overline{i}_0 \tag{2.57c}$$

These expressions are periodic in $\bar{\theta}_0$ and the frequencies depend on the chief's mean elements. If the mean elements change, the frequencies will change as well. Finally, the constant, Υ, is defined as:

$$\Upsilon = 6 J_2 \left(\frac{\mu R_e^2}{r_0^5} \right) \tag{2.58}$$

II.D.4. Clohessy-Wiltshire-Hill Equations (CWH)

As per the development of [20], the relative acceleration of Eq. (2.43) can be expressed in the local frame, and subsequently simplified for circular chief orbits. What follows is the derivation of the the Clohessy-Wiltshire-Hill Equations of motion.

To begin, the relative acceleration in the LVLH frame is expressed by Eq. (2.59).

$$\ddot{\boldsymbol{\rho}} = \frac{d^2\boldsymbol{\rho}}{dt^2} + 2\boldsymbol{w}_{L/I} \times \frac{d\boldsymbol{\rho}}{dt} + \frac{d\boldsymbol{w}_{L/I}}{dt} \times \boldsymbol{\rho} + \boldsymbol{w}_{L/I} \times (\boldsymbol{w}_{L/I} \times \boldsymbol{\rho}) \tag{2.59}$$

wherein the angular velocity of the local frame with respect to the inertial, is defined by $\boldsymbol{w}_{L/I}$, and is given by Eq. (2.60).

$$\boldsymbol{w}_{L/I} = \left[0, 0, \dot{\theta}_0\right]^T \tag{2.60}$$

Substituting the nonlinear expression for the relative position from Eq. (2.43), along with the expression of the angular velocity, into Eq. (2.59), yields the component-wise expression for the relative motion of the deputy with respect to the chief, Eq. (2.61)

$$\ddot{x} - 2\dot{\theta}_0\dot{y} - \ddot{\theta}_0 y - \dot{\theta}_0^2 x = -\frac{\mu(r_0 + x)}{[(r_0 + x)^2 + y^2 + z^2](\frac{3}{2})} + \frac{\mu}{r_0^2} \tag{2.61a}$$

$$\ddot{y} + 2\dot{\theta}_0\dot{x} + \ddot{\theta}_0 x - \dot{\theta}_0^2 y = -\frac{\mu y}{[(r_0 + x)^2 + y^2 + z^2](\frac{3}{2})} + \frac{\mu}{r_0^2} \tag{2.61b}$$

$$\ddot{z} = -\frac{\mu z}{[(r_0 + x)^2 + y^2 + z^2](\frac{3}{2})} + \frac{\mu}{r_0^2} \tag{2.61c}$$

Eqs. (2.61) hold true for any valid orbit. If the assumption is made that the chief follows a circular orbit, these equations become much simpler. For the circular orbit case, $\dot{\theta}_0$ simply becomes the mean motion of the chief, n_0. Likewise, since the

mean motion is constant, the second derivative, $\ddot{\theta}_0 = 0$. Making the substitution $r_0 = a_0$, yields the expressions of Eq. (2.62).

$$\ddot{x} - 2n_0\dot{y} - n_0^2 x = -\frac{\mu(a_0 + x)}{[(r_0 + x)^2 + y^2 + z^2]^{(\frac{3}{2})}} + \frac{\mu}{a_0^2} \tag{2.62a}$$

$$\ddot{y} + 2n_0\dot{x} - n_0^2 y = -\frac{\mu y}{[(a_0 + x)^2 + y^2 + z^2]^{(\frac{3}{2})}} + \frac{\mu}{a_0^2} \tag{2.62b}$$

$$\ddot{z} = -\frac{\mu z}{[(a_0 + x)^2 + y^2 + z^2]^{(\frac{3}{2})}} + \frac{\mu}{a_0^2} \tag{2.62c}$$

Finally, expanding the right-hand side of Eq. (2.62) in a Taylor's series about the origin, neglecting any higher order terms (taking the series only to first order), simplifying and rearranging, yields the common expression for the CWH equations, in the absence of any disturbing perturbations and controls, Eq. (2.63):

$$\ddot{x} - 2n_0\dot{y} - 3n_0^2 x = 0 \tag{2.63a}$$

$$\ddot{y} + 2n_0\dot{x} = 0 \tag{2.63b}$$

$$\ddot{z} + n_0^2 z = 0 \tag{2.63c}$$

The CWH Equations can be expressed in state-space form, as defined in Eq. (2.64), where the coefficient matrix, A, is defined by Eq. (2.65). Solving this system is straightforward; the state-transition matrix, $e^{A(t-t_0)}$ is not presented in this thesis, but is easily calculated.

$$\dot{\mathbf{x}}(t) = A\mathbf{x}(t) \tag{2.64}$$

$$A = \begin{bmatrix} 0 & 0 & 0 & 1 & 0 & 0 \\ 0 & 0 & 0 & 0 & 1 & 0 \\ 0 & 0 & 0 & 0 & 0 & 1 \\ 3n_0^2 & 0 & 0 & 0 & 2n_0 & 0 \\ 0 & 0 & 0 & -2n_0 & 0 & 0 \\ 0 & 0 & -n_0^2 & 0 & 0 & 0 \end{bmatrix} \tag{2.65}$$

An alternative method to develop the CW equations is to take the J_2-linearized equations of motion of Section II.D.3, and assume that $J_2 = 0$. This reduces the coefficient matrix of Eq. (2.54) to the transition matrix of Eq. (2.65).

II.D.5. Alternative Models

In addition to the models previously presented, this work focuses on two additional models: the first utilizes the coefficient matrix of the J_2-linearized equations of motion to compute the state transition matrix by assuming that the coefficients are piece-wise constants; the second attempts to estimate the unmodeled non-linearities neglected in the CW equations through the addition of a bias term.

II.D.5.a. J_2-Linearized State Transition Matrix

Utilizing the development of SectionII.D.3, and assuming constant time steps as well as a piece-wise constant coefficient matrix, allows for the development of a state transition matrix.

$$\Phi_{LIN} = e^{A\Delta t} \tag{2.66}$$

The linearized equations of motion can then be approximated as:

$$\mathbf{x}(t_2) = \Phi_{LIN}(t_2, t_1)\mathbf{x}(t_1) \tag{2.67}$$

II.D.5.b. Biased Clohessy-Wiltshire (CW) Equations

The CW equations are applicable and reasonable accurate for very small relative orbits if the reference orbit is circular, and nonlinear effects as well as perturbations are negligible. In the scenarios when this is not the case, the CW equations are less accurate due to unmodeled non-linearities. The addition of a linear drift term provides a means for estimating drifts and bias effects. The CW equations of Eq. (2.63) can be altered with the inclusion of a bias, β:

$$\ddot{x} - 2n_0\dot{y} - 3n_0^2 x + \beta_1 = 0 \tag{2.68a}$$

$$\ddot{y} + 2n_0\dot{x} + \beta_2 = 0 \tag{2.68b}$$

$$\ddot{z} + n_0^2 z + \beta_3 = 0 \tag{2.68c}$$

The bias term is governed by Eq. (2.69):

$$\ddot{\boldsymbol{\beta}} = 0 \tag{2.69}$$

This linear term adds an additional 6 states to the A matrix of Eq. (2.65); however, the coefficient matrix remains time-invariant.

CHAPTER III

RELATIVE MOTION ESTIMATION - THE KALMAN FILTER

The focus of this thesis is the estimation of the relative position and velocity of the deputy spacecraft, with respect to the chief. What has been presented previously, are the governing dynamics and equations of motion, as well as an explanation of the reference frames that are used to describe two spacecraft orbiting in formation. This section looks at the estimation problem, and presents a commonly used, linear estimator: the Kalman filter. Further development and explanation can be found in [25].

III.A. Discrete Time Kalman Filter

The linear Kalman filter's objective is to provide an efficient computational method by which the state of a process can be estimated, in such a way that the error is minimized. Given the system of linear, difference equations of Eq. (3.1):

$$\mathbf{x}_{k+1} = \Phi_k \mathbf{x}_k + \Upsilon_k \mathbf{w}_k \tag{3.1a}$$

$$\tilde{\mathbf{y}}_k = H_k \mathbf{x}_k + \mathbf{v}_k \tag{3.1b}$$

where the process noise, $\mathbf{w}(t)$, and measurement noise, $\mathbf{v}(t)$, are again defined to be white, Gaussian noise distributions with zero mean and standard deviations $Q(t)$ and R_k, respectively.

The Kalman filter is initialized through Eq. (3.2), where the "$\wedge$" indicates an

estimated quantity. Eq. (3.2a) defines the initial state estimate, and Eq. (3.2b) defines the initial covariance estimate as the expected value of the error between the estimated state ($\hat{\mathbf{x}}$) and the true state ($\mathbf{x}$), defined to be $\tilde{\mathbf{x}}$. These become the *a priori* state and covariance estimates

$$\hat{\mathbf{x}}(t_0) = \hat{\mathbf{x}}_0 \tag{3.2a}$$

$$P_0 = E\{\tilde{\mathbf{x}}(t_0)\tilde{\mathbf{x}}^T(t_0)\} \tag{3.2b}$$

The gain is found by determining an expression for the *a posteriori* state estimate from the *a priori* estimates:

$$\hat{\mathbf{x}}_k^+ = \hat{\mathbf{x}}_k^- + K_k\left[\tilde{\mathbf{y}}_k - H_k\left(\hat{\mathbf{x}}_k^-\right)\right] \tag{3.3}$$

The gain of Eq. (3.3), K_k, is defined to be a scaling factor that minimizes the *a posteriori* covariance. This is done by taking expression of Eq. (3.3) and substituting it into the expression for the covariance, Eq. (3.2b), evaluated at t_k. Taking the derivative of the trace of this matrix with respect to the Kalman gain, K, setting the result equal to zero, and solving for K will yield an expression for the gain that minimizes the covariance. This is defined by Eq. (3.4).

$$K_k = P_k^- H_k^T(\hat{\mathbf{x}}_k^-)\left[H_k(\hat{\mathbf{x}}_k^-)P_k^- H_k^T(\hat{\mathbf{x}}_k^-) + R_k\right]^{-1} \tag{3.4}$$

The measurement basis function, H_k, is simply defined as the coefficient matrix that picks up the terms that build the measurement function. The update step for the states is defined in Eq. (3.3); the update for the covariance is defined by Eq. (3.5).

$$P_k^+ = \left[I - K_k H_k((\hat{\mathbf{x}}_k^-))\right] P_k^- \tag{3.5}$$

Finally, the propagation of the states and covariances follows Eq. (3.6):

$$\hat{\mathbf{x}}_{k+1}^- = \Phi_k \hat{\mathbf{x}}_k^+ \tag{3.6a}$$

$$P_{k+1}^- 1 = \Phi_k P_k^+ \Phi_k^T + \Upsilon_k Q_k \Upsilon_k^T \tag{3.6b}$$

III.B. Continuous Discrete Kalman Filter

There are situations in which the dynamics are not given in terms of a state-transition matrix, but rather they are given as linear differential equations. The algorithm for these scenarios is very much the same as that of Section III.A, with the following exceptions: the dynamics are no longer governed by Eq. (3.1a), but are defined by Eq. (3.7); the propagation of the states and covariance follow Eq. (3.8), rather than Eq. (3.6).

$$\dot{\mathbf{x}}(t) = F(t)\mathbf{x}(t) + G(t)\mathbf{w}(t) \tag{3.7}$$

$$\dot{\hat{\mathbf{x}}}(t) = F(t)\hat{\mathbf{x}} \tag{3.8a}$$

$$\dot{P}(t) = F(t)P(t) + P(t)F^T(t) + G(t)Q(t)G^T(t) \tag{3.8b}$$

III.C. The Measurement Basis Function

The coefficient matrix, H, has been assumed to be coefficient throughout the previous two sections. This applies for linear systems with linear measurements. However, there are scenarios wherein these measurements are not linear. This section looks at these situations and how the Kalman filter is adjusted to account for the nonlinearity.

It is important to ensure observability over the course of the entire time span. This is dependent on the selection of an appropriate observation vector. For this thesis, the spacecraft estimation problem, the measurement function is as follows:

$$\tilde{\mathbf{y}} = \begin{bmatrix} \delta x \\ \delta y \\ \delta z \end{bmatrix} \tag{3.9}$$

As in Chapter II, the triplet $(\delta x, \delta y, \delta z)$ represents coordinates in the LVLH frame. The measurement coefficient matrix, H, is simply:

$$H = \begin{bmatrix} 1 & 0 & 0 & 0 & 0 & 0 \\ 0 & 1 & 0 & 0 & 0 & 0 \\ 0 & 0 & 1 & 0 & 0 & 0 \end{bmatrix} \tag{3.10}$$

This type of measurement represents a vector position; that is to say, on board the chief spacecraft there are sensors that making specific measurements that are converted into the component position. A second type of measurement takes the information directly from the sensors; no longer are the azimuth, elevation, and scalar range utilized to build the three coordinates. This measurement follows the

form of Eq. (3.11):

$$\tilde{\mathbf{y}} = \begin{bmatrix} \alpha \\ \epsilon \\ \rho \end{bmatrix}_{LVLH} \tag{3.11}$$

where ρ is the scalar position, Eq. (3.12a), α is the azimuth, Eq. (3.12b), and ϵ is the elevation, Eq. (3.12c).

$$\rho = \sqrt{\delta x^2 + \delta y^2 + \delta z^2} \tag{3.12a}$$

$$\alpha = \arctan \frac{\delta y}{\delta x} \tag{3.12b}$$

$$\epsilon = \arcsin \frac{\delta z}{\rho} \tag{3.12c}$$

It is immediately evident that the measurements presented in Eq. (3.12) are not linear and do not follow the form of Eq. (3.10). There is a class of the Kalman filter, the extended Kalman filter, that linearizes the nonlinear dynamics, or the nonlinear measurements about a reference point. It does so by expanding the dynamics/measurements in a Taylor's Series, and neglecting all but the first terms. What is left is that shown in Eq. (3.13), in which the measurements are now represented by the expression $\tilde{\mathbf{y}}_k = \mathbf{h}(\mathbf{x}_k)$.

$$H_k\left(\hat{\mathbf{x}}_k^-\right) \equiv \frac{\partial \mathbf{h}}{\partial \mathbf{x}}|_{\hat{\mathbf{x}}_k^-} \tag{3.13}$$

Applying Eq. (3.13) to Eqs. (3.11) and (3.12) yields the measurement basis function shown in Appendix A.

A portion of this thesis focuses on the propagation of the GA-STM. Measurements for this scenario are made in the LVLH frame as well, however propagation occurs in the curvilinear frame. Thus, the measurements become nonlinear functions of the curvilinear coordinates, and an altered version of the operation of Eq. (3.13) is necessary. The equation takes the form of Eq. (3.14):

$$H = \frac{\partial h}{\partial x_{LVLH}}|_{\hat{\mathbf{x}}^-_{LVLH}} \frac{\partial x_{LVLH}}{\partial x_{CURV}}|_{\hat{\mathbf{x}}^-_{CURV}} \tag{3.14}$$

The first part of the above equation is measurement specific; if the measurements are defined by Eq. (3.9), the first part of Eq. (3.14) is defined by Eq. (3.10). If the measurements are defined by Eq. (3.12), the first part is defined in Appendix A.

The second part of Eq. (3.14) is defined as the partial derivatives, with respect to the curvilinear coordinates, of Eq. (2.31) and Eq. (2.32) of Chapter II. This expands out to the H matrix of Appendix A. This type of expansion is important for large relative orbits. While this thesis utilizes the full expansion for smaller reference orbits in addition to the larger ones, it can be shown that for very small relative orbits, the second part of Eq. (3.14) does not affect the behavior of the H matrix. This is due to the fact that for smaller orbits, the curvilinear frame and the LVLH frame can be approximated as the same reference frame. For larger orbits, this assumption no longer is valid.

CHAPTER IV

ESTIMATION MODELS

The governing equations of motion for two satellites orbiting the Earth in close proximity are presented in Chapter II, specifically Section II.D. Additionally the procedure to estimate the relative states was presented in Chapter III. It is the focus of this chapter to apply these equations and models to a specific set of problems. Section IV.A presents the preliminaries for the estimation problems. The remainder of the chapter deals with the analysis of two reference orbits.

The focus of this chapter will be a highlight of the key results. A number of scenarios were run; these results can be found in tabulated form in Appendix B.

IV.A. Preliminaries

The initial conditions for the orbit propagation are defined in the proceeding sections; each scenario was propagated for two orbits of the chief. With a constant semi-major axis of $a = 7100$ km, the orbital period is 5952.8 seconds (or 1.6538 hours). This chapter presents several permutations of the initial conditions and the estimator properties. These are as follows:

- Two reference orbits are analyzed: mean circular ($\bar{e} = 0$) and elliptic ($\bar{e} = 0.005$)
- For each of the reference orbits, four relative orbit geometries are analyzed
  - Relative orbit size: $\rho = 1$ km, relative orbit phase angle: $\alpha = 0^\circ$

  - Relative orbit size: $\rho = 10$ km, relative orbit phase angle: $\alpha = 0°$
  - Relative orbit size: $\rho = 1$ km, relative orbit phase angle: $\alpha = 90°$
  - Relative orbit size: $\rho = 10$ km, relative orbit phase angle: $\alpha = 90°$
- For each of the relative orbits three propagation models are utilized:
  - Gim-Alfriend State Transition Matrix
  - J_2-Linearized differential equations for circular orbits
  - Clohessy-Wiltshire equations of motion
- For each of the propagation models, two measurement types are utilized:
  - Linear: $[\delta x\, \delta y\, \delta z]^T$
  - Nonlinear: $[\alpha\, \epsilon\, \rho]^T$
- For each of the two measurement types, two sampling times are analyzed:
  - $dt = 1$ second
  - $dt = 10$ seconds

The Kalman filter estimator is outlined in Chapter III. For both the discrete and the continuous-discrete forms of the estimator, several variables need to be initialized. The transition matrix of Eq. (3.1) is dependent on the propagation model utilized: if the GA-STM is the model of choice, the transition matrix Φ_k is defined by Eq. (2.44); if the CW equations are the model of choice, the transition matrix is defined by $e^{A(t-t_0)}$ where A is defined by Eq. (2.65). Given a continuous-time system, such as the J_2-Linearized equations of motion, the coefficient matrix of Eq. (3.7) is defined

by Eq. (2.54). For the purposes of this analysis, the coefficients Υ_k and $G(t)$ are assumed to be equivalent, and are define to be a six-dimension identity matrix.

The initial state estimation error is assumed to be %1 of the nominal values, and the initial covariance is defined as:

$$P_0 = \begin{bmatrix} \mathbf{P}_{0,A} & \mathbf{0}_{3x3} \\ \mathbf{0}_{3x3} & \mathbf{P}_{0,B} \end{bmatrix} \tag{4.1}$$

where

$$\mathbf{P}_{0,A} = diag(\left[(\frac{0.01}{n})^2 \ (\frac{0.01}{n})^2 \ (\frac{0.01}{n})^2\right]) \ m^2 \tag{4.2}$$

$$\mathbf{P}_{0,B} = diag(\left[(0.01)^2 \ (0.01)^2 \ (0.01)^2\right]) \ m^2/sec^2 \tag{4.3}$$

where n is the mean motion of the chief. This type of analysis was not incorporated into this thesis.

Mitchell [26] in her thesis, referring to the work of Alfriend et al [27], presented an in-depth analysis of the covariance matrix, and the conditions that would ensure zero error in the semi-major axis state estimate. The two requirements that ensure this estimate are as follows:

$$\rho_{x\dot{y}} = -1 \tag{4.4}$$

$$\sigma_{\dot{y}} = 2n\sigma_x \tag{4.5}$$

where $\rho_{x\dot{y}}$ is the cross-correlation coefficient, and $\sigma_{\dot{y}}$ is the correlation of the along-track velocity.

It is shown purely as a reference for an additional approach to the initialization of the covariance.

This covariance was utilized in all cases analyzed. The measurement error covariance is defined as

$$R_k = \begin{bmatrix} \rho \cdot 1 \times 10^{-10}\ m^2 \\ \rho \cdot 1 \times 10^{-10}\ m^2 \\ \rho \cdot 1 \times 10^{-10}\ m^2 \end{bmatrix} \tag{4.6}$$

if the measurements are linear (the vector components). This is based upon a 1 cm error in each of the axes, totaling $\rho \cdot \sqrt{3}$ cm in range, ρ. The components are scaled by the size of the relative orbit, ρ. Given a larger relative orbit, the noise on the components would be scaled accordingly. If the measurements are non-linear (azimuth, elevation, and range), the measurement error covariance is:

$$R_k = \begin{bmatrix} 7.6154 \times 10^{-7}\ rad^2 \\ 7.6154 \times 10^{-7}\ rad^2 \\ \rho \cdot 1 \times 10^{-10}\ m^2 \end{bmatrix} \tag{4.7}$$

This is based upon a 1 cm error in the range measurements (once again, scaled by the relative orbit size) and 0.05° in the angular measurements.

Process noise covariance, Q, is chosen to ensure proper convergence of the error residual (the difference between the filtered state and the true state). Hablani [28] showed that for sampling times much smaller than the orbital period (such as those at the focus of this work), the covariance matrix can be modeled as follows:

$$Q = \begin{bmatrix} \sigma_{wx}^2\left(\frac{T^3}{3}\right) & 0 & 0 & \sigma_{wx}^2\left(\frac{T^2}{2}\right) & 0 & 0 \\ 0 & \sigma_{wy}^2\left(\frac{T^3}{3}\right) & 0 & 0 & \sigma_{wy}^2\left(\frac{T^2}{2}\right) & 0 \\ 0 & 0 & \sigma_{wz}^2\left(\frac{T^3}{3}\right) & 0 & 0 & \sigma_{wz}^2\left(\frac{T^2}{2}\right) \\ 0 & 0 & 0 & \sigma_{wx}^2 T & 0 & 0 \\ 0 & 0 & 0 & 0 & \sigma_{wy}^2 T & 0 \\ 0 & 0 & 0 & 0 & 0 & \sigma_{wz}^2 T \end{bmatrix} \tag{4.8}$$

To simplify the analysis, $\sigma_{wx} = \sigma_{wy} = \sigma_{wz}$, thus creating one variable with which the covariance could be tuned. The value of this parameter is case specific and was tuned to ensure the error residual fell between the three-sigma bounds, as determined by the covariance.

The initial conditions for the drag model are given in Table IV.1:

Table IV.1. Initial conditions for the drag model.

Parameter	Chief	Deputy
Satellite Mass (kg)	1	0.1
Satellite Reference Area (m^2)	1	0.1
Coefficient of Drag	2.1	2.1

The value for the density of air at the altitude is assumed to be 2.36×10^{-14} kg/m^3.

IV.B. Reference Orbits

Two inertial reference orbits were analyzed in this thesis: a mean circular orbit ($\bar{e} = 0$) and a elliptic orbit ($\bar{e} = 0.005$).

IV.B.1. Mean Circular Orbit

The first scenario has the chief orbiting the Earth in an orbit with a mean eccentricity of 0. The remainder of the initial, mean orbital elements are provided in Table IV.2:

Table IV.2. Mean orbital elements for the cheif in an orbit with mean eccentricity of 0.

Mean Classical Elements		Mean Non-Singular Elements	
Element	Value	Element	Value
a (km)	7100	a (km)	7100
e	0	θ (deg)	0
i (deg)	70	i (deg)	70
Ω (deg)	45	q_1	0
ω (deg)	0	q_2	0
M_0 (deg)	0	Ω (deg)	45

The short period, long period, and secular effects can be included in both the classical and non-singular elements. These are the osculating elements of Table IV.3:

Table IV.3. Osculating orbital elements for the cheif in an orbit with mean eccentricity of 0.

Osculating Classical Elements		Osculating Non-Singular Elements	
Element	Value	Element	Value
a (km)	7105.57	a (km)	7105.57
e	7.8726×10^{-4}	θ (deg)	0
i (deg)	70.0003	i (deg)	70.0003
Ω (deg)	45	q_1	7.8726×10^{-4}
ω (deg)	0	q_2	0
M_0 (deg)	0	Ω (deg)	45

The osculating elements can be converted into the Cartesian position and veloc-

ity, which become the initial conditions for the integration of the perturbed, two-body equations of motion, given in Table IV.4:

Table IV.4. Initial Carteisan position and velocity for the chief in a mean circular orbit.

State	Value
X (km)	5023.5585
Y (km)	5023.5585
Z (km)	0
V_X (km/sec)	-1.8109
V_Y (km/sec)	1.8109
V_Z (km/sec)	7.0411

Figure IV.1 shows the inertial trajectory of the chief that is obtained through numerical integration of the perturbed two-body equations of motion:

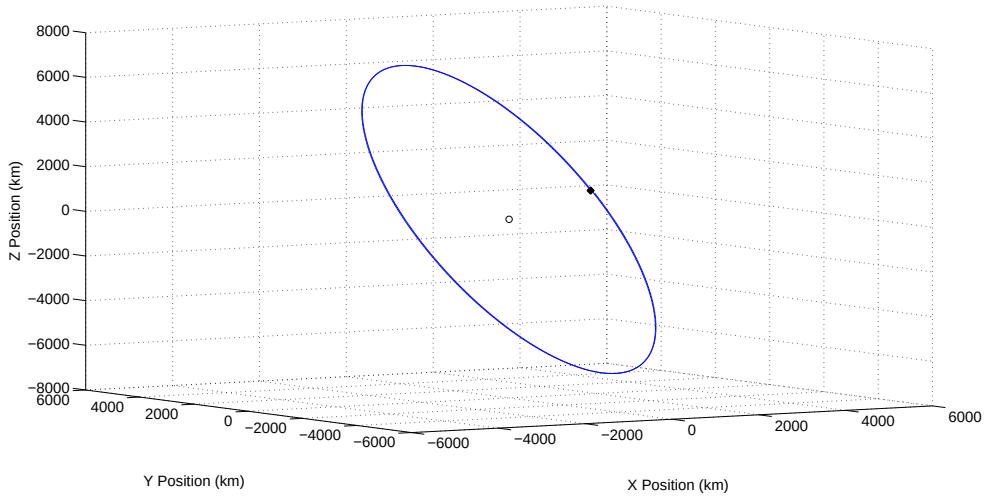

Figure IV.1. Inertial frame trajectory of the chief along a mean, circular orbit.

IV.B.2. Elliptic Orbit

In the second scenario, the chief is assumed to be orbiting the Earth in a slightly elliptic orbit, with a mean eccentricity of 0.005. The remainder of the initial, mean orbital elements are provided in Table IV.5:

Table IV.5. Mean orbital elements for the cheif in an orbit with mean eccentricity of 0.

Mean Classical Elements		Mean Non-Singular Elements	
Element	Value	Element	Value
a (km)	7100	a (km)	7100
e	0.005	θ (deg)	0
i (deg)	70	i (deg)	70
Ω (deg)	45	q_1	0.005
ω (deg)	0	q_2	0
M_0 (deg)	0	Ω (deg)	45

The short period, long period, and secular effects can be included in both the classical and non-singular elements. These are the osculating elements of Table IV.6:

Table IV.6. Osculating orbital elements for the cheif in an orbit with mean eccentricity of 0.005.

Osculating Classical Elements		Osculating Non-Singular Elements	
Element	Value	Element	Value
a (km)	7105.57	a (km)	7105.57
e	5.7969×10^{-3}	θ (deg)	0
i (deg)	70.0003	i (deg)	70.0003
Ω (deg)	45	q_1	5.7949×10^{-3}
ω (deg)	0	q_2	0
M_0 (deg)	0	Ω (deg)	45

The osculating elements can be converted into the Cartesian position and veloc-

ity, which become the initial conditions for the integration of the perturbed, two-body equations of motion, given in Table IV.7:

Table IV.7. Initial Carteisan position and velocity for the chief in a elliptic orbit.

State	Value
X (km)	4998.4531
Y (km)	4998.4531
Z (km)	0
V_X (km/sec)	-1.8200
V_Y (km/sec)	1.8200
V_Z (km/sec)	7.0765

IV.C. Modeling Error

Three separate models were utilized to propagate the *a posteriori* state estimates; as previously defined, these are the Gim-Alfriend State Transition Matrix (GA-STM), the J_2-Linearized Equations of Motion, and the Clohessy-Wiltshire (CW) Equations of Motion. The truth model from whence the estimates are built, comes from the integration of the perturbed two-body equations of motion, which includes the effects of drag as well as the J_2, J_3, J_4, J_5 and J_6 perturbations. There are inherent errors between the propagation models and the truth model. This section details some of these differences. As previously mentioned, Appendix B presents the entirety of the raw data in tabular form. Appendix B provides the error statistics, as well as the covariance models utilized, allowing reproduction of the graphical response.

IV.C.1. GA-STM Modeling Error

The GA-STM, as defined in Chapter II, includes the first order J_2 effects ($O(J_2^2)$ are neglected). Thus it becomes an accurate predictor of the true behavior for small relative orbital element differences. Additionally, the GA-STM has not been developed for a specific set of initial conditions. Unlike the other propagation models (which are only valid for specific orbits, e.g. circular or mean circular), the GA-STM is valid for any elliptic orbit; however, like the other propagation models, the GA-STM does not account for higher order perturbations, nonlinearities, drag, and any other disturbing accelerations. The only perturbation included is the first order J_2 effect.

Given an arbitrary relative orbit of relative size, $\rho = 1$ km, and phase angle $\alpha = 0°$, there exists a certain level of error between the propagated states (the GA-STM), and the truth (the results from numerical integration), in the absence of any noise. Figures IV.2 and IV.3 present the position and velocity errors, respectively, given a mean, circular reference orbit.

Given a non-circular reference orbit, the modeling error takes the form of Figure IV.4, which presents the position errors, and Figure IV.5, which presents the velocity errors. A comparison of Figures IV.2 through IV.4 shows the exemplification of the previous statement: the GA-STM holds for any valid orbit. Given a slight eccentricity, the GA-STM still predicts to within half a meter the position. The velocity shows a slight degradation in model accuracy, as the slight increase in eccentricity begins to compounds the unaccounted-for perturbations.

The power of the GA-STM lies in the fact that no integration is required. For

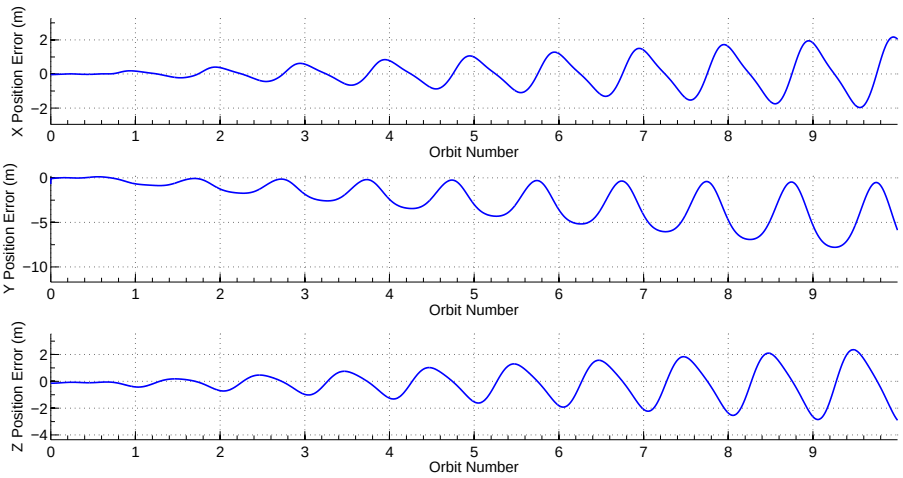

Figure IV.2. Position model error between GA-STM and perturbed two body; relative orbit: 1 km, relative orbit phase: 0°; mean circular reference orbit.

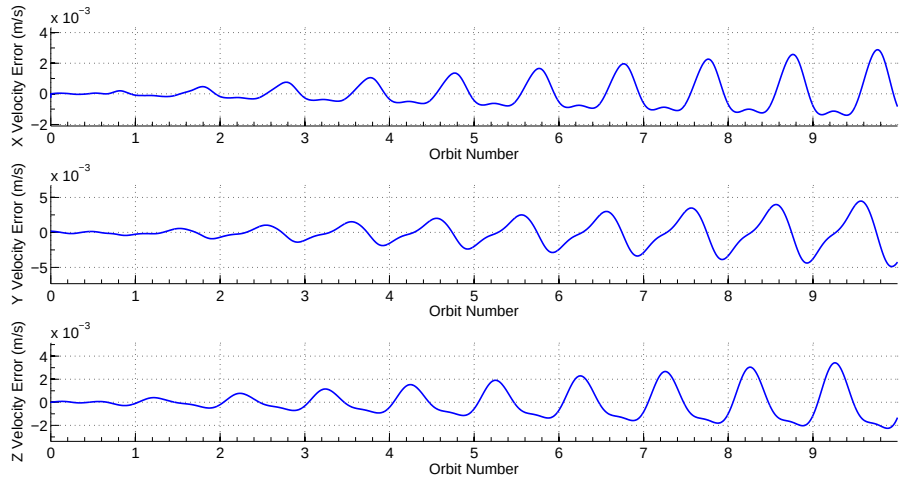

Figure IV.3. Velocity model error between GA-STM and perturbed two body; relative orbit: 1 km, relative orbit phase: 0°; mean circular reference orbit.

the reference and relative orbits described, with a time step of $dt = 1$ second for two orbits, the GA-STM propagation takes approximately one-third as long as the

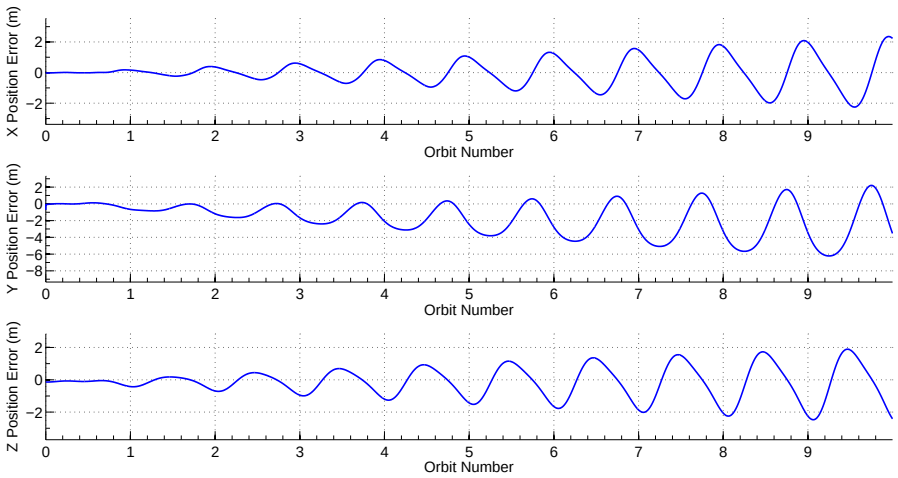

Figure IV.4. Position model error between GA-STM and perturbed two body; relative orbit: 1 km, relative orbit phase: 0°; elliptic reference orbit.

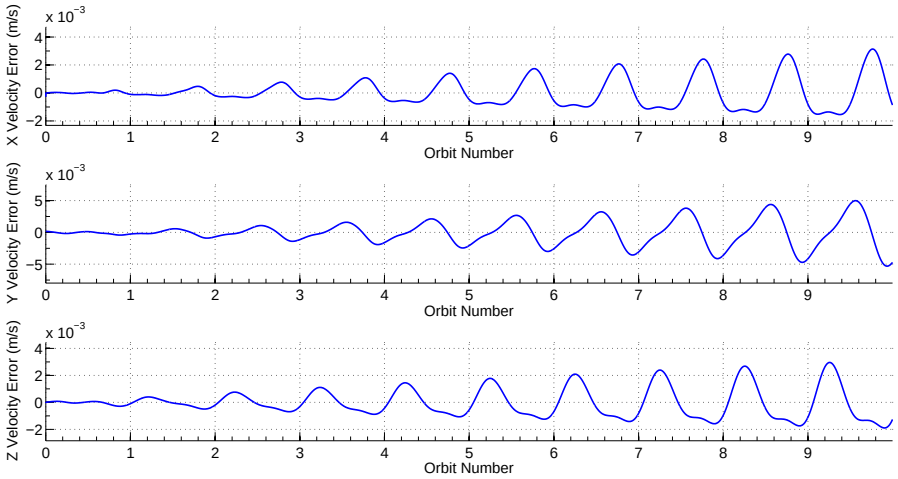

Figure IV.5. Velocity model error between GA-STM and perturbed two body; relative orbit: 1 km, relative orbit phase: 0°; elliptic reference orbit.

numerical integration using a 4^{th} order Runga-Kutta routine [1]. Figures such as IV.2

[1]This is being run on an Intel Core i5-2450M CPU running at 2.50 GHZ, with 4.00 GB memory on a Windows 7 64-bit operating system

and IV.3 have been created for every permutation of the initial conditions presented above. These can be found in Appendix B.

IV.C.2. J_2-Linearized Equations of Motion

As presented in Chapter II, the J_2-Linearized equations of motion are a set of linear differential equations that describe the relative position and velocity in the LVLH frame. These equations, however, are valid only for circular orbits. Figures IV.6 and IV.7 show the model error for a mean, circular reference orbit. The relative orbit is of the same size and phase as that of the previous section. Given a non-circular reference orbit, the modeling error takes the form of Figures IV.8 and IV.9.

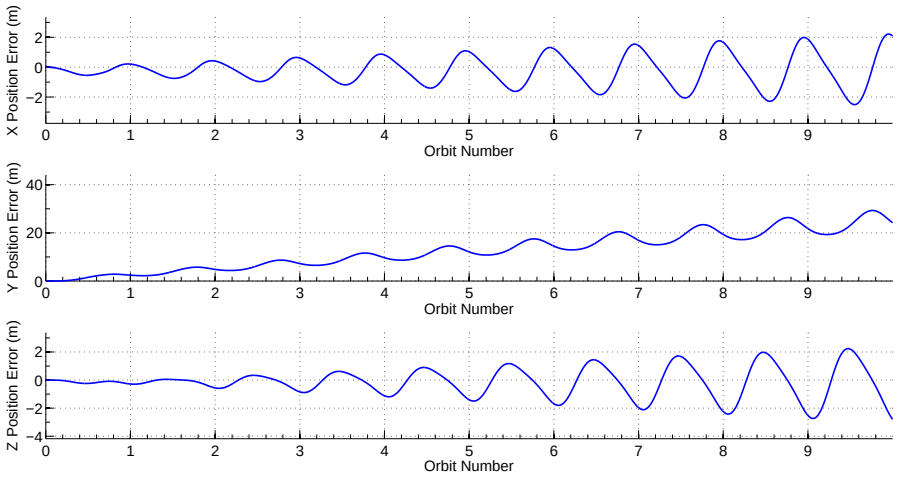

Figure IV.6. Position model error between J_2-Linearized EOM and perturbed two body; relative orbit: 1 km, relative orbit phase: 0°; mean circular reference orbit.

The accuracy of the J_2-Linearized EOM is slightly degraded in the presence of eccentricity (Figures IV.8 and IV.9). However, for a circular orbit, with minor

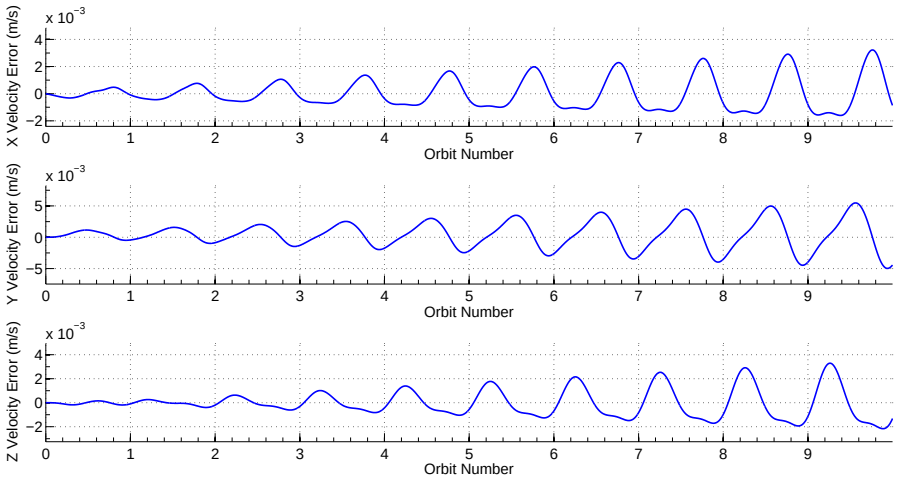

Figure IV.7. Velocity model error between J_2-Linearized EOM and perturbed two body; relative orbit: 1 km, relative orbit phase: $0°$; mean circular reference orbit.

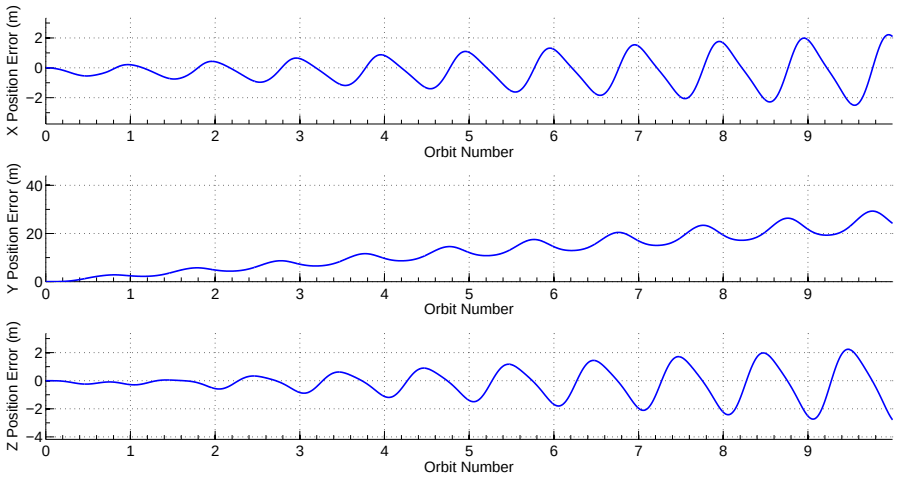

Figure IV.8. Position model error between J_2-Linearized EOM and perturbed two body; relative orbit: 1 km, relative orbit phase: $0°$; elliptic reference orbit.

exceptions, the linearized equations of motion perform quite well.

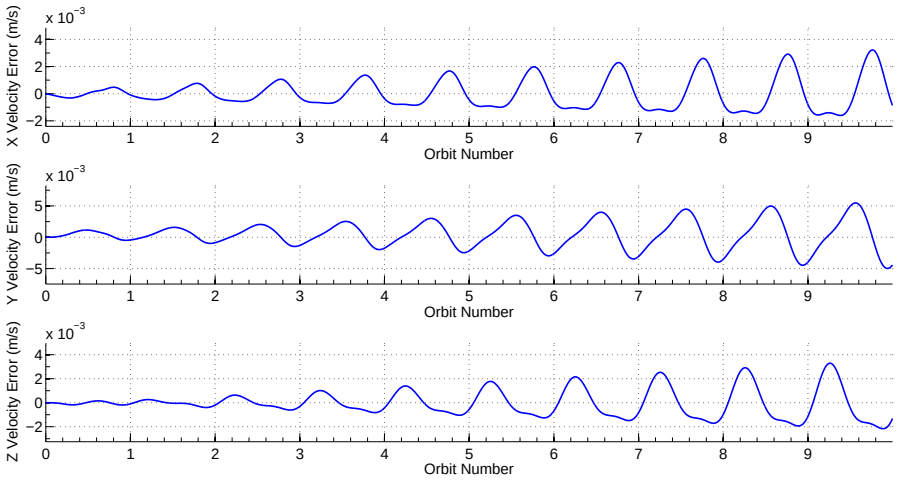

Figure IV.9. Velocity model error between J_2-Linearized EOM and perturbed two body; relative orbit: 1 km, relative orbit phase: 0°; elliptic reference orbit.

IV.C.3. CW Equations of Motion

The primary advantage to the CW equations is the fact that they have a known solution - no numerical integration is required. There is large error that is introduced through the omission of nonlinearities and the J_2 effects as well as higher order gravitational perturbations. This is shown by the larger position and velocity errors that are introduced in Figures IV.10 and IV.11.

The drift that is present in the y-position of Figure IV.10 is a direct result of the neglecting of J_2. When compared against the computational requirements of the GA-STM, the CW equations perform remarkably well, taking approximately one-tenth the time to complete the two-orbit propagation as the GA-STM does.

It is important to note that the differences in the model error for a circular reference orbit and the model error for an elliptical reference orbit are minimal. The position model error resulting from an elliptic reference orbit is shown in Figure IV.12,

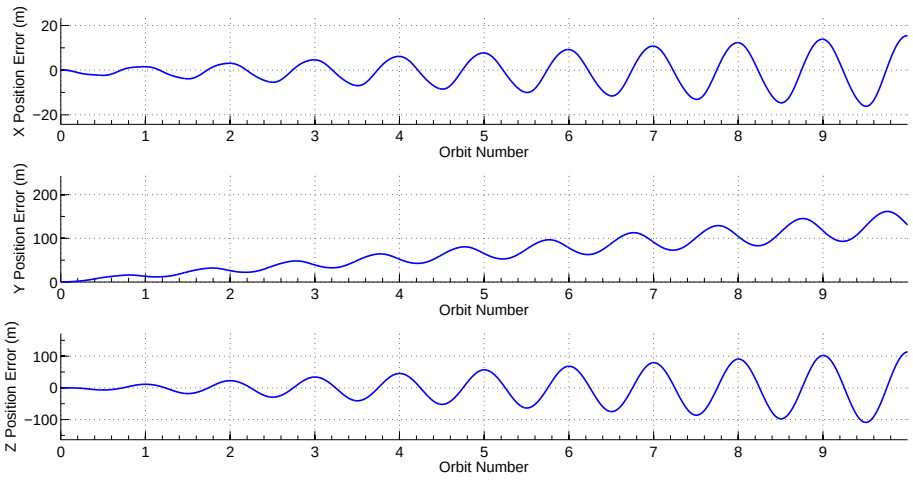

Figure IV.10. Position model error between CW EOM and perturbed two body; relative orbit: 1 km, relative orbit phase: 0°; mean circular reference orbit.

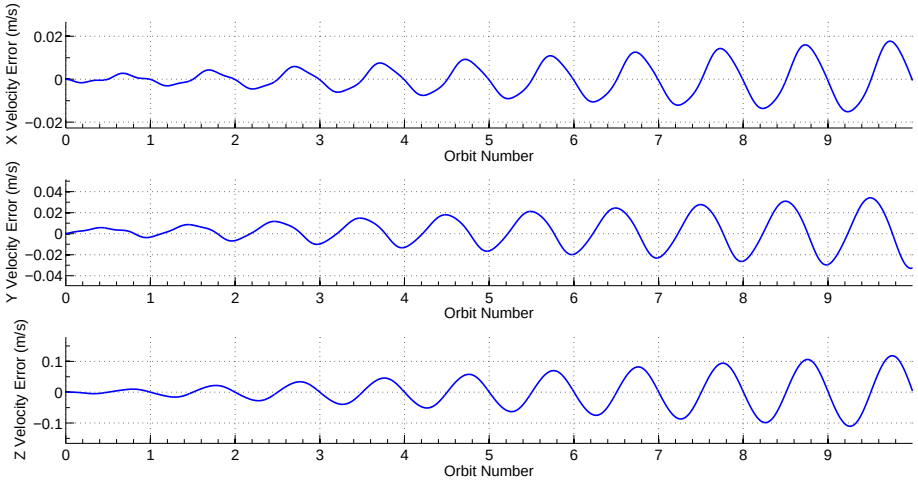

Figure IV.11. Velocity model error between CW EOM and perturbed two body; relative orbit: 1 km, relative orbit phase: 0°; mean circular reference orbit.

and the velocity error is shown in Figure IV.13. The eccentricity is very small. As the eccentricity increases (for instance, to approximately 0.05), the accuracy of the model degrades, and a more pronounced difference in the two plots can be observed.

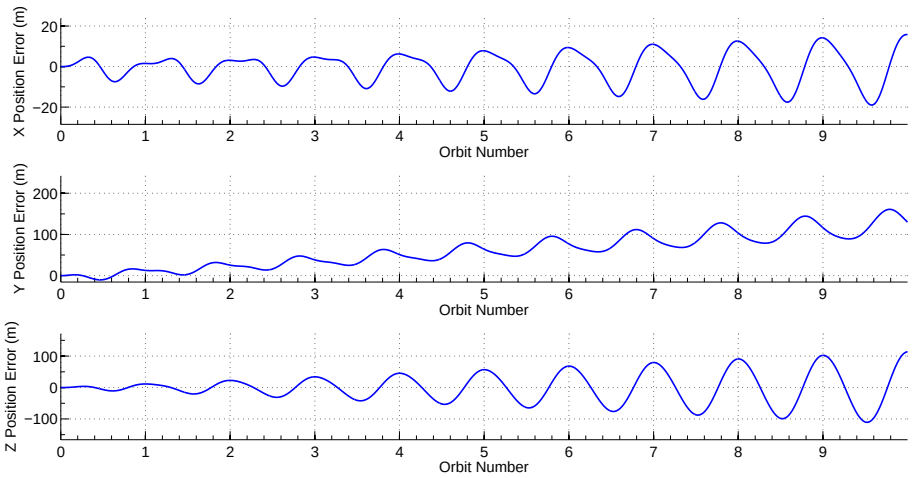

Figure IV.12. Position model error between CW and perturbed two body; relative orbit: 1 km, relative orbit phase: 0°; elliptic reference orbit.

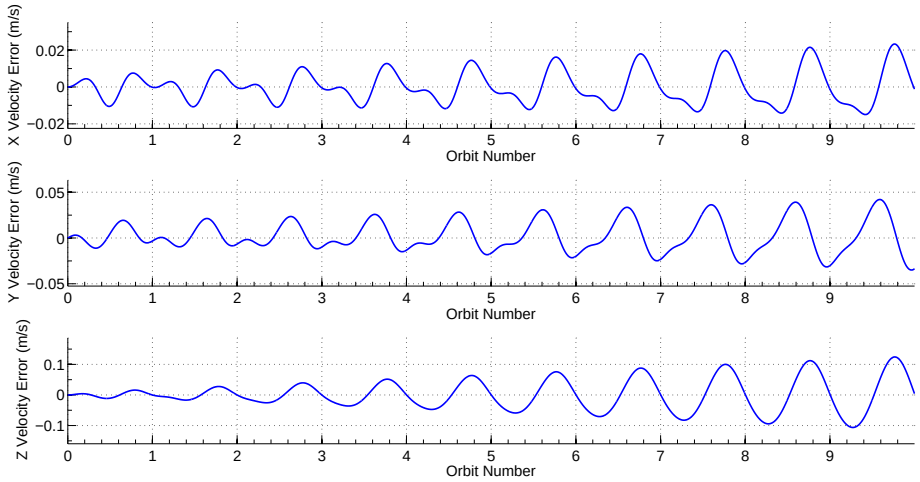

Figure IV.13. Velocity model error between CW and perturbed two body; relative orbit: 1 km, relative orbit phase: 0°; elliptic reference orbit.

IV.C.4. Unmodeled Relative Accelerations

It is possible to look at the acceleration error present from the unmodeled perturbations (J_3 through J_6, as well as drag). Figure IV.14 presents all the perturbing

accelerations included in the integration of the perturbed two-body equations of motion, in the ECI frame. These are the disturbances that the estimators are attempting to accommodate and account for.

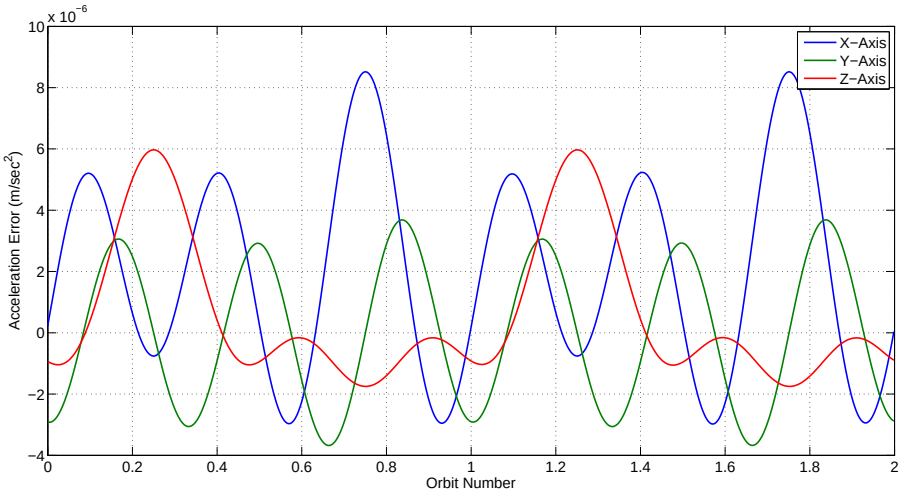

Figure IV.14. The relative disturbing perturbations, given a circular reference orbit.

The results of Figure IV.14 are obtained by subtracting the difference in the accelerations (the two-body acceleration as well as the J_2 perturbation) of the chief and the deputy, from the accelerations coming from the CW equations; in other words, the results are the the difference in the right hand side of Eq. (2.43) and the component-wise right hand side of Eq. (2.63), where in the non-acceleration level terms (all but the second derivative) are brought to the right hand side of the equation.

IV.C.5. Velocity Level Errors

It is extremely important to minimize errors in the velocity state estimate. Large errors in these states can compound into very large estimates in the position states. How and Tillerson [15] showed that a 2 mm/s in-track velocity error results in approximately a 1.2 m in-track position error after 200 seconds of a LEO. Eq. 4.9 provides a metric by which this drift can be quantified.

$$y_{drift}(t) = -3\dot{y}(0)t \tag{4.9}$$

It is also possible to look at the cross-track error. Looking at the duty-cycle of the impulse control system shown in Figure IV.15, it is evident that a small error in the cross-track velocity control impulse (0.7 mm/s) can compound into a large cross-track position error (7 cm), given an impulse frequency of 200 seconds, as per the work of Delpech et al [13].

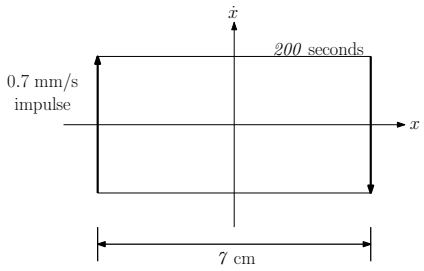

Figure IV.15. Limit cycle for cross-track velocity and position control.

IV.D. Results

Three sets of results are presented in this section: the first is a comparison of modeling techniques; the second set presents an evaluation of the effects of nonlinearities; finally, the third set looks at the effect of the sampling time. The analysis was performed for 2 orbits of the chief around the Earth.

IV.D.1. Model Comparison

As presented in Chapter II, several models were analyzed. The results in Table IV.8 are obtained for a 1 km, $\alpha = 0$, circular reference orbit, with linear measurements coming every one second. Shown are the sum of the absolute value of the mean and the standard deviation for the error residual between the truth (the integration of the perturbed two-body) and the model based on 100 Monte Carlo simulations. The bias dynamic's initial conditions were assumed to be 0.

Table IV.8. Model error comparison for linear measurements model with 1 Hz update frequency.

State	GA-STM	GA (no J2)	CW	CW w/ bias
δx (m)	1.32e-3	1.73e-3	2.84e-3	2.37e-3
δy (m)	3.23e-3	3.41e-3	3.46e-3	3.98e-3
δz (m)	1.76e-3	2.05e-3	2.04e-3	1.86e-3
δv_x (m/sec)	2.23e-5	2.34e-5	1.28e-4	7.39e-5
δv_y (m/sec)	2.76e-5	3.26e-5	5.50e-5	7.54e-5
δv_z (m/sec)	3.25e-5	3.41e-5	5.93e-5	4.09e-5

It is immediately evident that the GA-STM, whether propagated with the J2 parameter or without, is the superior propagation tool, providing the most accurate

results (the least mean and standard deviation of the error residual). Appendix B presents the remainder of the propagation results for the other permutations of the orbital parameters outline in Section IV.A. The advantages of the GA-STM are not significant for this specific orbit, and this specific sampling frequency. Table IV.8 shows that for the 1 km relative orbit, there is only a slight degradation when moving from the highly accurate GA-STM to the simplified CW equations. However, for situations with larger nonlinear effects, the CW results show greater inaccuracy. This is the focus of the next sections. Several observations can be made on the trends of Table IV.8. The neglecting of the J_2 parameter in the GA-STM only slightly worsens the state estimates; for the most part, the position and velocity error residuals are comparable. There is an obvious loss in the accuracy as the omission of the J_2 term introduces another source of error when compared to the truth (the integration using $J_2 - J_6$ effect. The CW equations, which inherently introduce a source of error as they do not account for the nonlinearities or the other perturbations present, show an obvious worsening in the accuracy of the results. However, the along-track and the cross track position estimates show comparable results to the GA-STM, with J_2 set to 0. The CW equations with the bias terms show an improvement upon the estimates obtained from the CW equations alone in the radial and cross-track state estimates. The along-track position and velocity estimates however show a slight degradation when utilizing the additional bias term.

Table IV.9. Effect of nonlinearity for a circular reference orbit; nonlinear measurement model, 1 Hz sampling frequency.

	$\rho = 1$ km			$\rho = 10$ km		
State	GA-STM	CW	CW w/ Bias	GA-STM	CW	CW w/ Bias
δx (m)	0.036	0.118	0.083	0.881	1.59	0.872
δy (m)	0.043	0.050	0.049	0.684	0.49	0.548
δz (m)	0.045	0.065	0.072	0.616	0.55	0.814
δv_x (m/sec)	1.24e-4	8.11e-4	5.26e-4	2.69e-3	1.13e-2	5.83e-3
δv_y (m/sec)	1.34e-4	2.92e-4	3.22e-4	2.54e-3	3.26e-3	4.02e-3
δv_z (m/sec)	1.65e-4	2.83e-4	4.81e-4	3.68e-3	3.56e-3	5.74e-3

IV.D.2. Nonlinear Effects

Several of the more simplified models neglect nonlinearities in the analysis. This section of results looks at the effects of this omission on the accuracy of the results. Table IV.9 shows the comparison of the results for a 1km vs a 10 km relative orbits with a 0° phase angle, given nonlinear measurements made every 1 second. As previous, the values shown are the sums of the absolute value of the mean and the standard deviation of the error residual.

In addition to the sum of absolute value of the mean and the standard deviation, the error residual plots can be analyzed as well. The visual representation of the above tabulated data ensures that the residual remains between the three-sigma bounds, and that the residual contains no extemporaneous data. Figures IV.16 and IV.17 present the error residual plots for a circular reference orbit with a 1 km relative orbit with nonlinear measurements made every 1 second.

The above residual plots can be compared to those of Figures IV.18 and IV.19. The trends shown in Table IV.9 are demonstrated in this comparison. While the

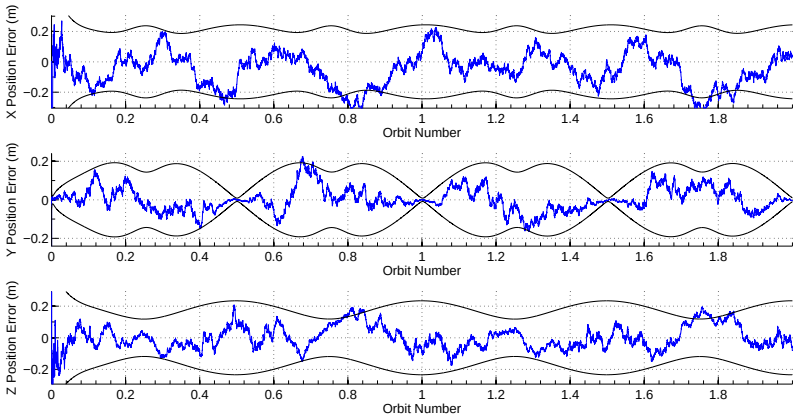

Figure IV.16. CW estimation of position error for a circular orbit reference orbit, and a 1 km relative orbit.

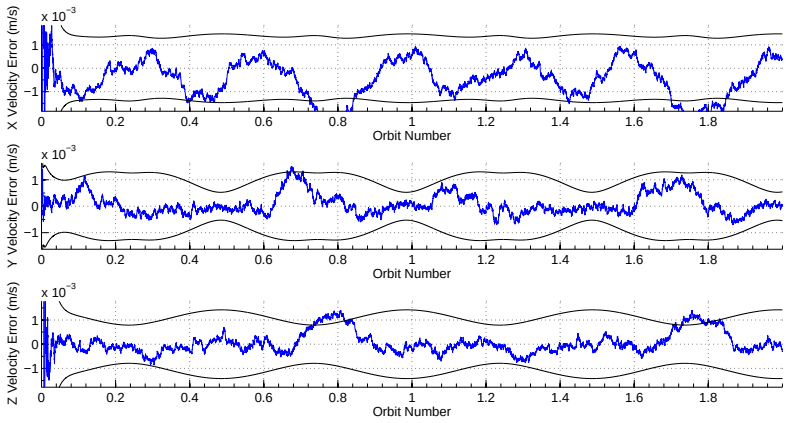

Figure IV.17. CW estimation of velocity error for a circular orbit reference orbit, and a 1 km relative orbit.

covariance shows a similar trend, the magnitude of both the covariance and the error residuals are smaller when utilizing the GA-STM as the propagation model, by approximately 50%. Radial position and velocity estimates have improved, however, the along-track and corss track errors have increased.

An elliptic reference orbit increases the nonlinearity in the system. The eccen-

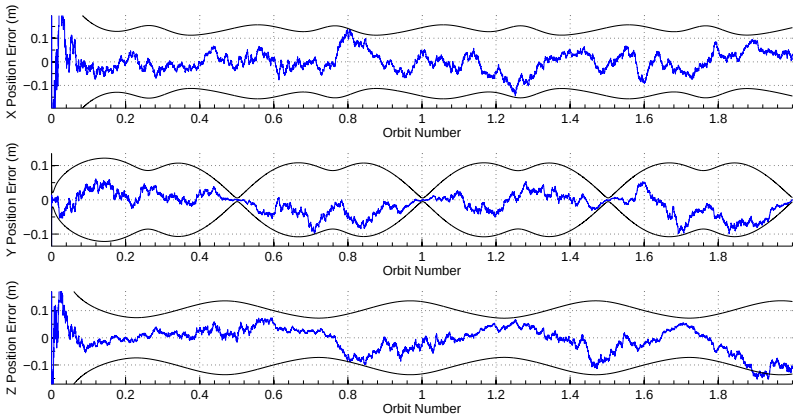

Figure IV.18. GA-STM estimation of position error for a circular orbit reference orbit, and a 1 km relative orbit.

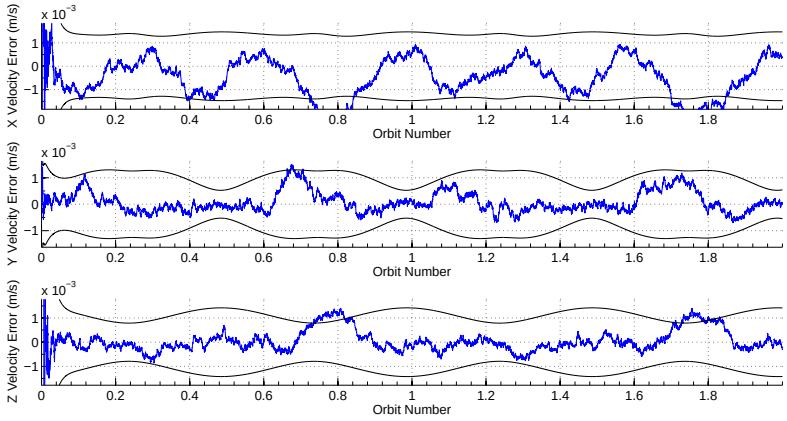

Figure IV.19. GA-STM estimation of velocity error for a circular orbit reference orbit, and a 1 km relative orbit.

tricy utilized in this analysis of 0.005 is still very small, and nearly circular; however, a comparison of Tables IV.9 and IV.10 shows that the error has increased by an order of magnitude when utilizing the CW equations with bias - for the 1 km relative orbit, the radial position and velocity estimates and the cross-track position all demonstrate error residuals that have doubled in magnitude. For the 10 km relative

orbit, the CW equations with bias again show a degradation in the error residual characteristics for the radial and the cross-track position estimates. Table IV.10 presents the data for a 1 and 10 km relative orbit, with an elliptic reference orbit.

Table IV.10. Effect of nonlinearity for an elliptic reference orbit; nonlinear measurements, 1 Hz sampling frequency.

	$\rho = 1$ km			$\rho = 10$ km		
State	GA-STM	CW	CW w/ Bias	GA-STM	CW	CW w/ Bias
δx (m)	0.042	0.112	0.134	0.868	1.598	1.194
δy (m)	0.048	0.109	0.079	0.451	1.009	0.751
δz (m)	0.057	0.101	0.121	0.799	1.168	1.066
δv_x (m/sec)	1.07e-4	9.17e-4	1.01e-3	2.47e-3	1.23e-2	7.82e-3
δv_y (m/sec)	1.35e-4	6.82e-4	6.33e-4	2.09e-3	6.55e-3	5.90e-3
δv_z (m/sec)	1.65e-4	4.91e-4	9.14e-4	3.36e-3	5.78e-3	7.01e-3

A comparison of Tables IV.9 and IV.10 shows that the increase in the eccentricity does show a slight decrease in the accuracy of the CW equations and the CW equations with the bias terms. The GA-STM does not show any adverse affects as a result of the increase in eccentricity. The CW equations show a doubling of the error in the along- and cross-track position and velocity estimates, while the radial position and velocity estimates only show a slight worsening of the accuracy. For the larger relative orbit, again there is minimal difference in the GA-STM state estimates. And again, the radial position and velocity estimates from the CW equations shows only a slight degradation. The state estimates for the along-track and cross-track position and velocity however show a great deal of error, again, almost twice as large as for the circular reference orbit case.

As with the circular orbit case, the error residual plots can be analyzed for consistency. The first two plots (Figures IV.20 and IV.21) are the position and velocity estimates utilizing the CW equations as the propagation tool. The next two figures (Figures IV.22 and IV.23) are the estimates using the GA-STM as the propagation tool.

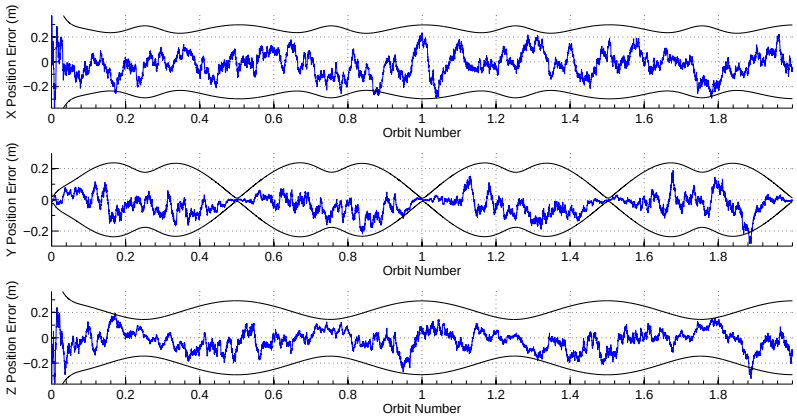

Figure IV.20. CW estimation of position error for e = 0.005 orbit reference orbit, and a 1 km relative orbit.

Comparing the error residual plots above, it can be seen that there is limited difference given the slight increase in the eccentricity. If the eccentricity of the reference orbit were to be increased to 0.05, the error residual plot for the CW propagation would exhibit the behavior of Figures IV.24 and IV.25. There is a clear difference between these plots and those of Figures IV.20 and IV.21. Table IV.11 presents the sums of the absolute value of the mean and the standard deviation for this higher eccentricity orbit. The CW equations, as mentioned before, were not derived for elliptic orbits, and the simplifying assumptions that went into their development precludes them use as an accurate propagation technique when the

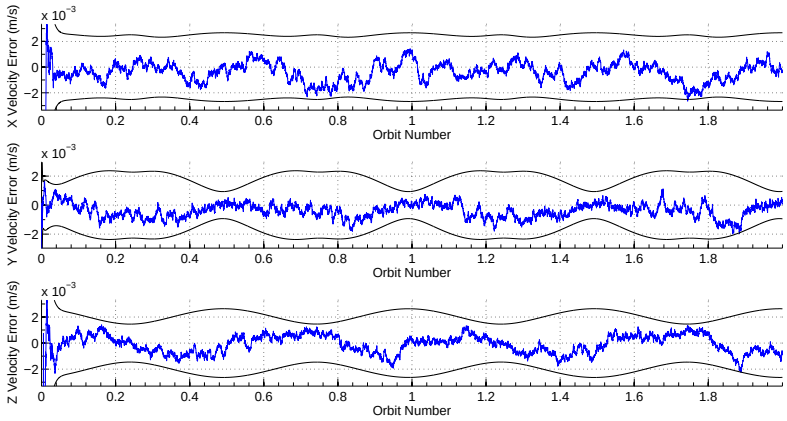

Figure IV.21. CW estimation of velocity error for e = 0.005 orbit reference orbit, and a 1 km relative orbit.

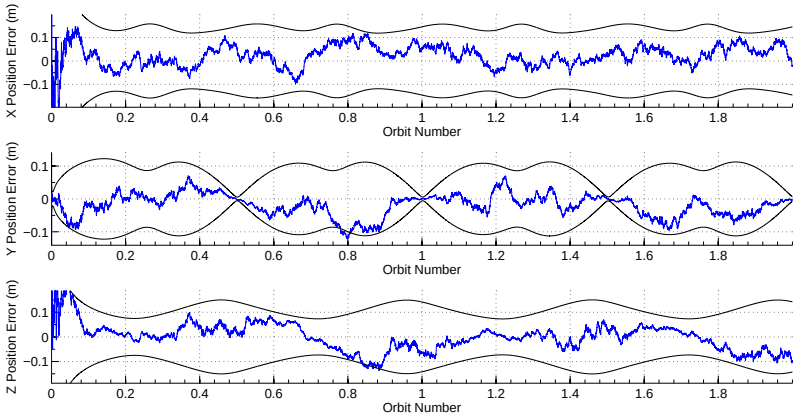

Figure IV.22. GA-STM estimation of position error for e = 0.005 orbit reference orbit, and a 1 km relative orbit.

reference orbit has ellipticity.

Comparing Table IV.11 to Table IV.9 shows immediately the effect of an increase in the eccentricity; the radial position error has tripled, the along-track error estimate has increased by a factor of 8, and the cross-track estimate has increased by a factor of 4. Likewise the radial velocity estimate has tripled, the along-track

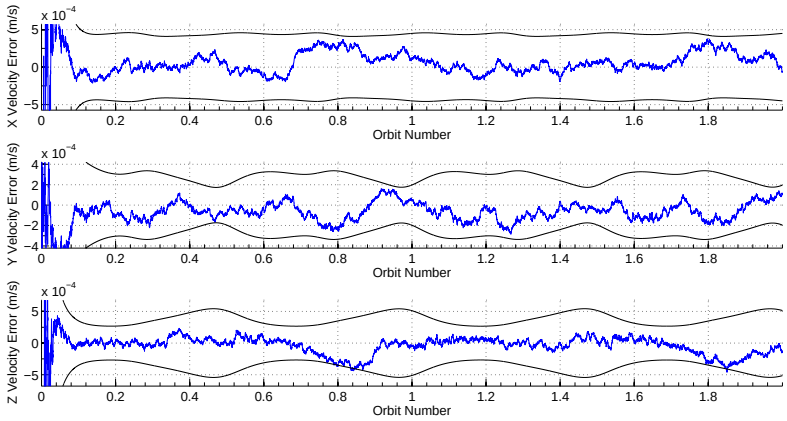

Figure IV.23. GA-STM estimation of velocity error for e = 0.005 orbit reference orbit, and a 1 km relative orbit.

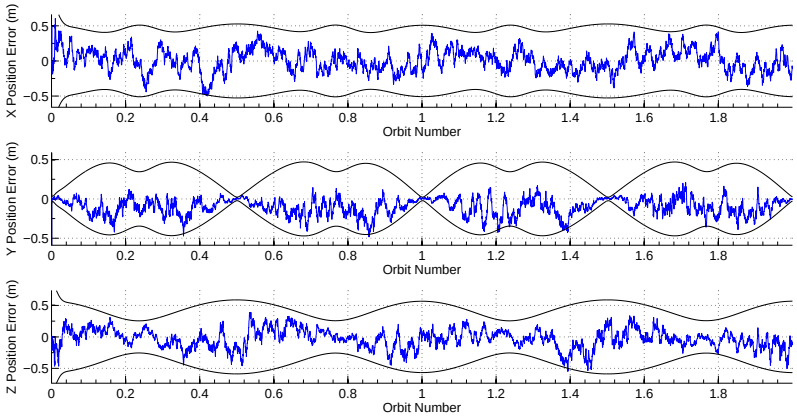

Figure IV.24. CW estimation of position error for e = 0.05 orbit reference orbit, and a 1 km relative orbit.

velocity estimate has increased by a factor of 30, and the cross-track by a factor of 7. As mentioned several times, the CW equations were not derived for elliptic orbits. While a slightly elliptic orbit may not exhibit a large loss in accuracy, larger eccentricities do demonstrate the pitfalls of using the CW equations.

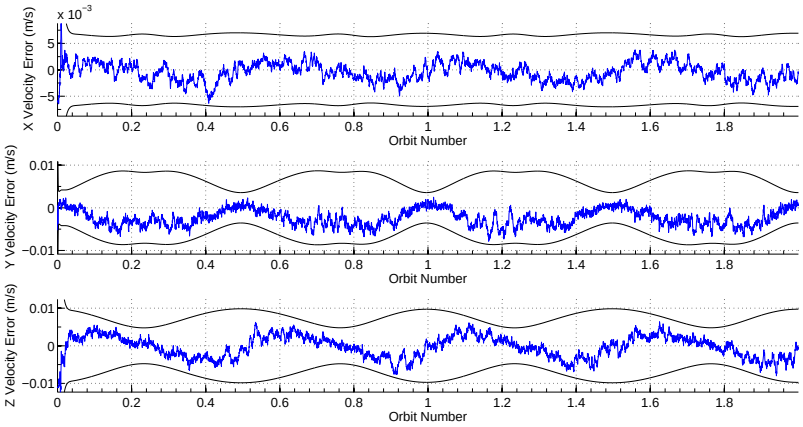

Figure IV.25. CW estimation of velocity error for e = 0.05 orbit reference orbit, and a 1 km relative orbit.

Table IV.11. Error residual for $e = 0.05$ reference orbit.

State	Residual Error
x (m)	0.319
y (m)	0.427
z (m)	0.209
v_x (m/s)	0.003
v_y (m/s)	0.009
v_z (m/s)	0.002

IV.D.3. Sampling Time Comparison

This section of results look at a comparison of the results given two different sampling times: 1 second sampling times, and 10 second sampling times. A comparison of the GA-STM and the CW equations for these two sampling times is shown in Table IV.12.

The key observation to note from the above table is at a higher sampling frequency, the accuracy of the model becomes irrelevant. If measurements could be made every 0.01 seconds, the GA-STM and the CW equations would show compa-

Table IV.12. Comparison of error residuals with varying sample times; linear measurements for a 1 km relative orbit with $\alpha = 0$.

	GA-STM		CW	
State	1 second	10 seconds	1 second	10 seconds
δx (m)	1.32e-3	4.24e-3	2.84e-3	9.09e-3
δy (m)	3.23e-3	2.02e-3	3.46e-3	2.11e-2
δz (m)	1.76e-3	5.29e-3	2.04e-3	5.44e-3
δv_x (m/sec)	2.23e-5	1.95e-5	1.28e-4	2.28e-4
δv_y (m/sec)	2.76e-5	3.23e-5	5.50e-5	6.76e-5
δv_z (m/sec)	3.25e-5	7.32e-5	5.93e-5	1.16e-4

rable error residuals. At the higher sampling frequency, the accuracy of the model becomes more important. This is a straight forward and logical conclusion from the results; the estimator attempts to track the measurements that are coming from the truth model. As the estimator runs, it is correcting itself to account for the errors in the propagation model and in what it believes to be the truth. If the estimator is correcting every 1 second or less, the accuracy of the propagation model will have less of an effect on the error residual. However, if the estimator is correcting every 10 seconds, the effect of the simplifications becomes more apparent, and the error residual begins to degrade.

IV.D.4. J_2-Linear State Transition Matrix

One of the models presented is that of the state transition matrix that is build through the J_2-linearized equations of motion. For a 1 km relative orbit with a 0° phase angle ,given linear measurements from a 100 simulation Monte Carlo analysis, the results of Table IV.13 presents the results for 1 second and 10 second time steps, given both circular and elliptic reference orbits. As with the previous results, the

values shown are the combination of the absolute value of the mean and the standard deviation.

Table IV.13. J_2-Linearized State Transition Matrix simulation results.

State	Circular		Elliptic	
	1 second	10 seconds	1 second	10 seconds
δx (m)	1.9e-3	5.3e-3	2.6e-3	6.6e-3
δy (m)	2.9e-3	1.9e-2	6.0e-3	2.9e-2
δz (m)	2.0e-3	5.7e-3	1.9e-3	5.8e-3
δv_x (m/sce)	3.03e-5	5.76e-5	9.11e-5	1.39e-4
δv_y (m/sec)	2.05e-5	2.13e-5	2.99e-4	4.95e-4
δv_z (m/sec)	3.33e-5	7.2e-5	3.46e-5	7.93e-5

The first column of Table IV.13 compares with Table IV.8. It is evident that this STM provides a much better estimate for the position and velocity, improving upon the accuracy of the GA-STM in the along-track state estimates. However, in the radial and the cross-track estimates, both the position and the velocity error residuals are worse than those obtained from the GA-STM. The J_2-linearized STM does perform much better than the CW equations, and the CW equations with the linear bias term (the exception to this is the cross-track position estimate for the CW w/ bias, which exhibits a slightly smaller error residual than the same estimate from the linearized STM). The second column of Table IV.13 compares with the second and the fourth columns of Table IV.12. As before, the linearized STM provides a better estimate for the position and velocity than the CW equations, but not as good as the estimates using the GA-STM. The only exception again is the along-track position and velocity estimates; the J_2-linear STM provides a better estimate for these two states than the GA-STM. The use of the J_2-linearized equations in the

state transition matrix form, though highly constrained in their possible application, prove to be an accurate propagation technique. The resulting error characteristics are comparable to the error characteristics of the GA-STM, however, the equations lose some of their accuracy when applied to an elliptic orbit.

IV.E. Generalizations

Presented previously were the estimated relative position and velocity for specific cases, and a comparison of results for a unique set of conditions. This section looks at the dependence on the individual variables, by observing the residual error characteristics versus various values of the variable. Four variables are analyzed in this section: the time step, the relative orbit size, the relative orbit phase angle, and the noise level. In each of these cases, only one variable is altered at a time. For instance, when looking at the dependence on the time step, the relative orbit remains unchanged, and the measurement noise is constant. To show these trends, the CW equations are utilized and the analysis is performed for a circular orbit with linear measurements. In each of the scenarios presented, the results are shown and labeled in terms of "Radial", "Along-Track", and "Cross-Track" position or velocity; these correspond to, respectively, the x-direction, y-direction, and the z-direction.

IV.E.1. Error Characteristics vs. Time Step

The first scenario that was analyzed was that of a sampling frequency sweep, from once a second to once every 10 seconds (1 Hz to 0.1 Hz), at increments of 1 second). Measurement noise was held constant at 0.01 m (1 cm) for linear measure-

ments, while the relative orbit was held constant at $\rho = 1km$ and $\alpha = 0$.

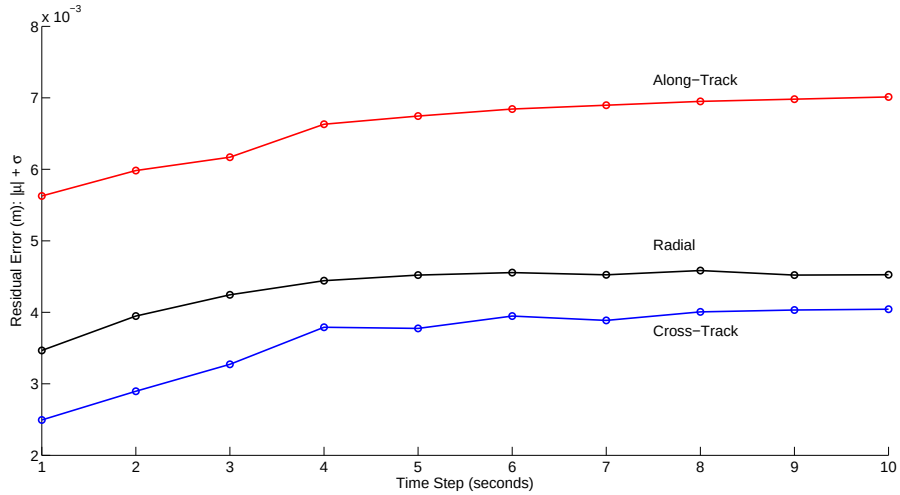

Figure IV.26. Dependence of the position error residual magnitude on the sampling frequency.

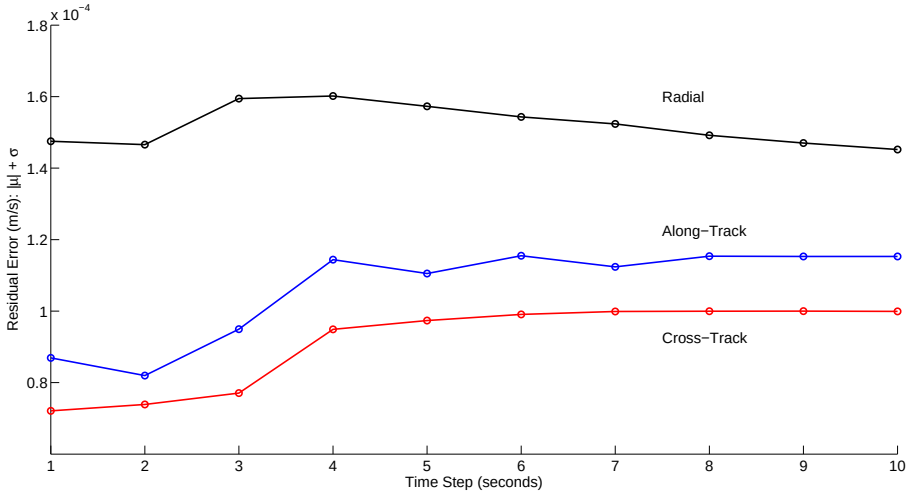

Figure IV.27. Dependence of the velocity error residual magnitude on the sampling frequency.

As mentioned before, the sampling frequency has a large impact on the error

residual, especially when dealing with the CW equations. The larger the sampling frequency, the greater the error residual. Figures IV.26 and IV.27 show this trend. An interesting trend to note is the leveling off of the error residual as the time step increases. At sampling times of 9 seconds and 10 seconds, it appears that the error residual has reached steady state, in all 6 state estimates. The along-track position estimation error is larger than the cross-track and the radial position estimates; however, the radial velocity error residuals are the larger of the three state estimates.

IV.E.2. Error Characteristics vs. Relative Orbit Size

If instead of varying the sampling time, the relative orbit size is varied from 1 km to 10 km, with a constant sampling time of 1 second, the characteristics follow the linear patterns of Figures IV.28 and IV.29. This is again an expected trend. As the relative orbit size increases, the nonlinear effects as well as the measurement noise increases, as it is being scaled by the size of the orbit. Thus an increase in the relative orbit size not only affects the initial conditions and the states, but indirectly affects the state estimates through the measurement noise. In this scenario, α was help constant, $\alpha = 0$, with linear measurements and measurement noise was set at 0.01 m (1 cm).

Both plots exhibit linear trends in the error residuals. Table IV.14 present the slope of the "best-fit" line and the y-intercept of the lines. This type of relationship is extremely useful; if given a comparable set of initial conditions and a specific relative orbit size, rather than running several estimators, it is possible to look at the results presented in this section, namely the summary table, and determine the residual

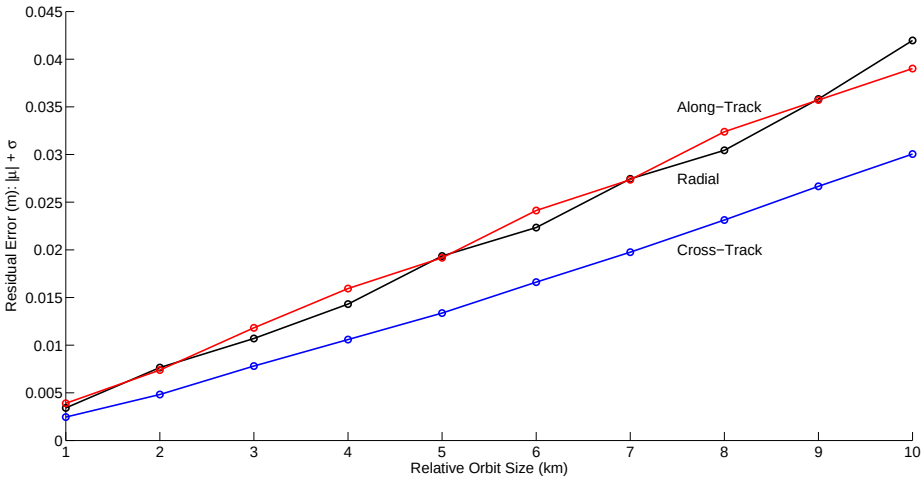

Figure IV.28. Dependence of the position error residual magnitude on the relative orbit size.

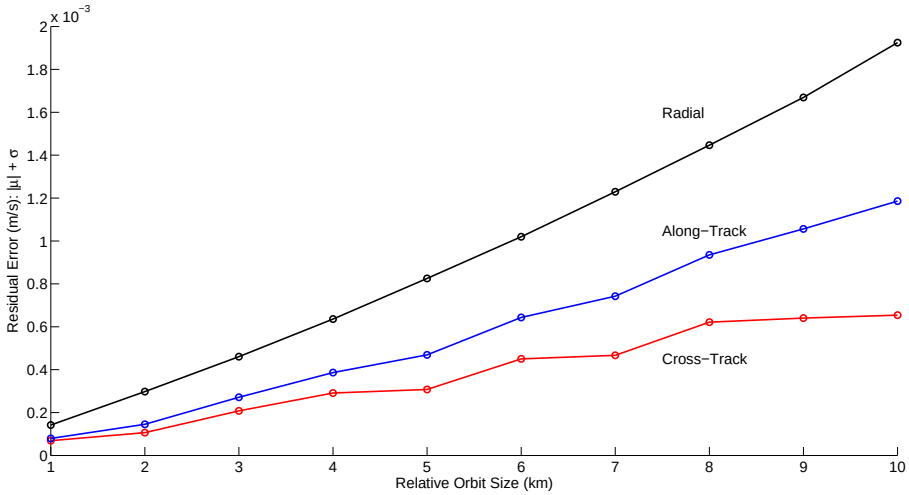

Figure IV.29. Dependence of the velocity error residual magnitude on the relative orbit size.

error after estimation.

Table IV.14. Slope and y-intercept for "best-fit" line for residual error's dependence on the relative orbit size.

State	Slope	Y-Intercept
x	0.0043 m/km	0.0034 m
y	0.0039 m/km	0.0039 m
z	0.0031 m/km	0.0025 m
v_x	1.98e-4 m/s/km	1.42e-4 m/s
v_y	6.50e-5 m/s/km	6.92e-5 m/s
v_z	1.23e-4 m/s/km	7.95e-5 m/s

IV.E.3. Error Characteristics vs. Relative Orbit Phase Angle

This set of iterations keeps the sampling time fixed at 1 second intervals, with a relative orbit of 1 km, and linear measurements with measurement noise of 1 cm. The phase angle is varied between 0° and 90°. These phase angles are defined by Figure II.3.

Figures IV.30 and IV.31 show the dependence on the phase angle. Figure IV.30 shows a unique trend. The x-position residual error appears to peak around $40 - 45°$, while the y-position residual and the z-position residual trend downwards and upwards, respectively. Their point of intersection appears to coincide with the peak of the x-position error residual, implying that the best estimate for the position occurs at this $40 - 45°$ phase angle.

Further analysis using Eq. (5.62) of [20], reproduced in Eq. (4.10) of this thesis, shows that the instantaneous error due to nonlinear effects in the along-track direction demonstrated in Figure IV.30 corresponds to the trend demonstrated by the plot obtained from the periodic portion of the equation.

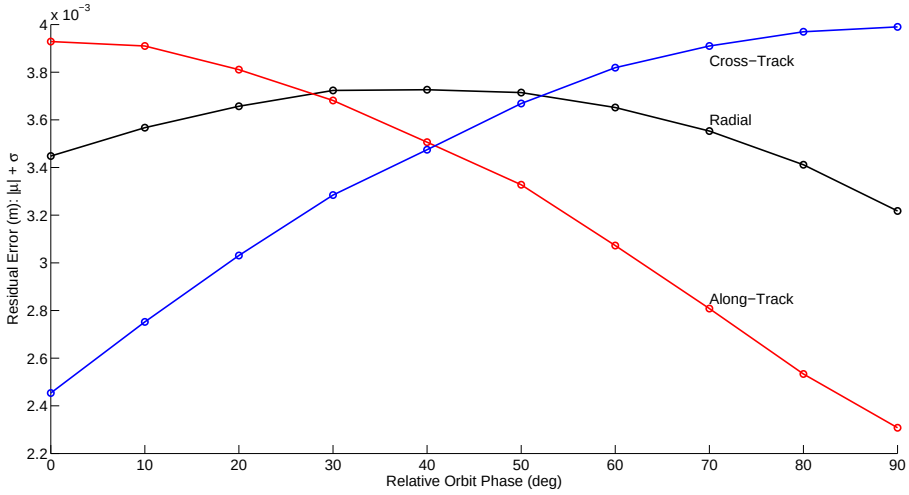

Figure IV.30. Dependence of the position error residual magnitude on the relative orbit phase angle.

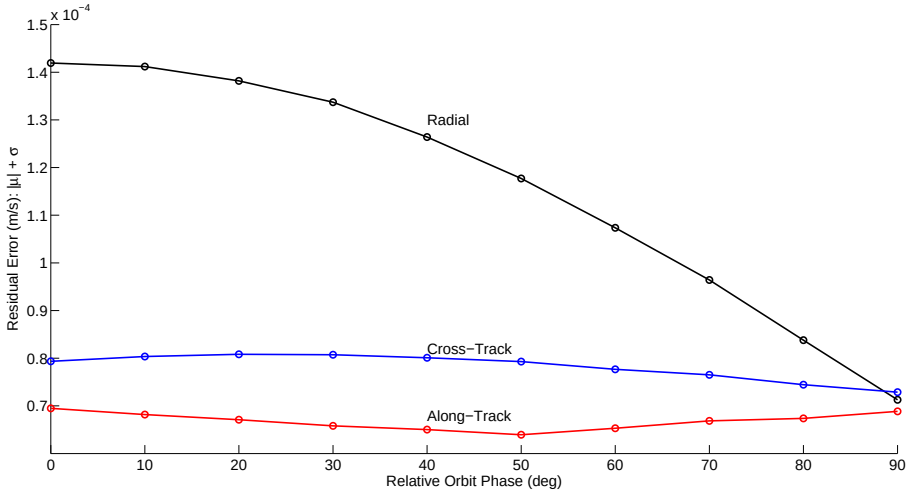

Figure IV.31. Dependence of the velocity error residual magnitude on the relative orbit phase angle.

$$\dot{y}(0) + 2nx(0) = -\frac{9n\rho^2}{8a_0}\left(2 + \cos 2\alpha\right) \tag{4.10}$$

This results also shows that J_2 does not affect along-track as much as the non-

linearity of the system does. Additionally, there is again a correlation between the radial velocity error residual and the along-track error residual. In this set of trials, the two estimates follow the same trend.

IV.E.4. Error Characteristics vs. Measurement Noise

The final set of iterations keeps the properties of the relative orbit constant, and looks to vary the measurement noise. That is to say, this section looks at the effect of having less accurate range sensors. The relative orbit was held constant at $\rho = 1$ km and $\alpha = 0$, with linear measurements and a sampling frequency of 1 Hz. The results of Figures IV.32 and IV.33 again show an expected trend. As the measurement noise increases, the error residual worsens. There is generally a linear relationship for the position estimates. The velocity estimates on the other hand, exhibit a nonlinear behavior; there appears to be a quadratic behavior to the state estimates, with a slight jump in the along-track and cross-track estimates. Additionally, the radial position and velocity estimates exhibit larger and faster growth than the along- and cross-track position and velocity estimates, both of which are comparable.

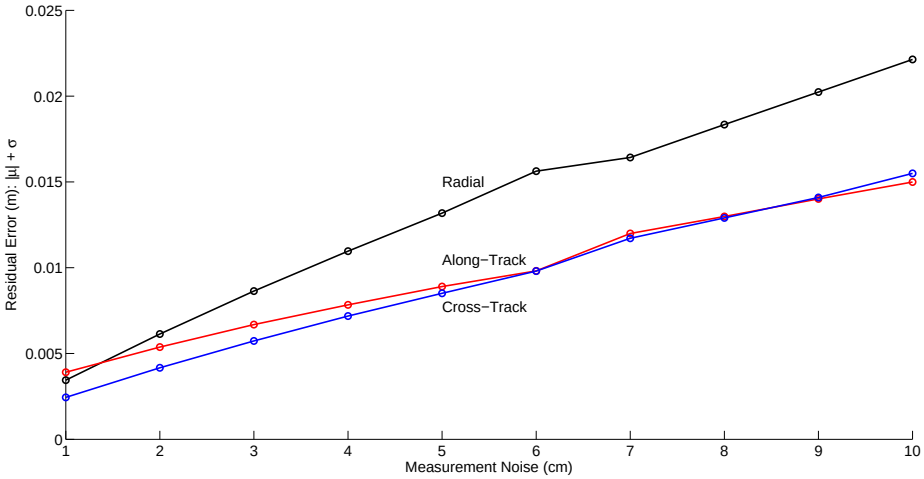

Figure IV.32. Dependence of the position error residual magnitude on the measurement noise.

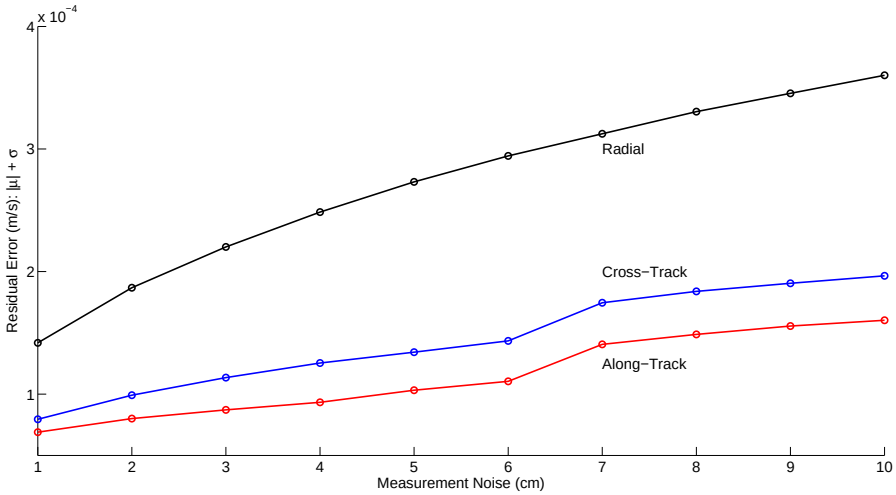

Figure IV.33. Dependence of the velocity error residual magnitude on the measurement noise.

CHAPTER V

SUMMARY

The goal of this thesis was to compare relative orbit propagation techniques when applied to the estimation of the relative position and velocity. Several scenarios were analyzed. Based upon these results, several observations can be made:

- The majority of the work of this thesis confirms the belief that the GA-STM is the most robust and accurate of the estimation models. The GA-STM has been derived to hold valid for any elliptcal orbit and includes the first order J_2 effect; while the other propagation models were derived under more restrictive assumptions. However, for a specific orbit and time step (circular reference orbit, 1 km relative orbit, 1 second linear measurements), it was shown that the error residuals from the state estimates propagated using the CW equations were comparable to the results obtained from propagation using the GA-STM.

- Part of this thesis addressed the possibility of including a drift term in the CW equations that would account for dynamics of the unmodeled nonlinearities. This inclusion did not consistently improve the response; along-track position and velocity estimates for a 1 km relative orbit, given linear measurements, were worse than their counterparts for the straight CW equations. Given a nonlinear measurement, the CW equations with bias terms only improved upon the radial position and velocity, while the along-track and cross-track position and velocity showed significant increases in the error residual. Similar trends

were shown with an elliptic reference orbit.

- The linearized J_2-STM model also improves upon the CW results greatly. It also shows improvement on the along-track position and velocity estimates when compared to the GA-STM at small time steps. At larger time steps, the linearized STM also shows significant improvement upon the CW equations, and again shows improvement upon the along-track estimates when compared to the GA-STM.

- An attempt to quantify the results in terms of the relative orbit size and phase angle, the sampling time, and the measurement noise provided the expected results. As the sampling time and measurement noise increases, the error residuals increase as well. With the phase angle, the minimal error in each of the 6 relative states occurred at approximately 45°. A linear dependence on the relative orbit size was shown, and, for each state, slope and y-intercept values were determined.

- As the frequency of the updates increases (the sampling time decreases), the accuracy of the model is less important. If measurements were to be obtained every 0.01 seconds, the GA-STM and the CW equations would yield similar error residuals; however, if the sampling time were to be every 60 seconds, the CW equations would exhibit a much larger error than the GA-STM. The estimator attempts to track the measurements. Thus, with a frequent updates, the estimator can correct often, adjusting to account for the unmodeled non-linearities. With less frequent updates, the estimator has to account for larger

drifts in the states between estimates.

- Larger relative orbits introduce additional errors, specifically in the radial velocity.

V.A. Future Work

This scope of this work was limited to the linear Kalman filter and the extended Kalman filter. Additionally, it was limited to two sets of reference orbits, a few sets of relative orbits, and two types of measurements. For a better understanding of how a model would behave, several other orbits would need to be analyzed. This includes larger orbits ($\tilde{1}$00 km), at various other phase angles. Additionally, this thesis looked at one general set of conditions (with the exception of the slight addition of eccentricity); for a more complete look at the system and a better understanding of the responses, it would be beneficial to look at varying inclinations, varying semimajor axes, and changing the overall orientation of the either the reference orbit or the relative orbit (or both). This would be a logical and straightforward extension of this work.

Additionally, there are several types of measurement functions that exist aside from the two explored here. Namely, there is an increasing focus on the idea of angles-only navigation, wherein azimuth and elevation are the only two angles utilized to estimate position and velocity. Much work has been done to look at the possibilities of angles-only with the linear equations of motion; however, with application to the GA-STM and the propagation of the curvilinear states, there is still room for exploration.

This thesis touched on generalizing the results obtained, with the goal of building a metric by which one could potentially develop an understanding of when one model is better and more applicable than another. These generalizations were developed for a 10-point mesh per variable; likewise, they were developed by holding several variables constant, and only changing one. To expand these generalizations, it would become necessary to vary all parameters and obtain a surface plot of the error residual response. Given this three-dimensional representation of the error residuals, it would become easy to determine where one model excels, and where it lacks.

REFERENCES

[1] Battin, R. H., *An Introduction to the Mathematics and Methods of Astrodynamics, Revised Edition*, American Institude of Aeronautics and Astronautics, Inc., Reston, VA, 1999.

[2] Hacker, B. C. and Grimwood, J. M., *On the Shoulders of Tians: A History of Project Gemini*, The NASA Historical Series, Washington, D.C., 1977, NASA SP-4203.

[3] Parkinson, B. W. and Pilker Jr., J. J., *Global Positioning System: Theory and Applications, Volume 2*, American Institute of Aeronautics and Astronautics, Cambridge, Massachusetts, 1996.

[4] Curtis, S., "The Magnetospheric Multiscale Mission: Resolving Fundamental Processes in Space Plasmas," *Report of the NASA Science and Technology Definition Team for the Magnetospheric Multiscale (MMS) Mission*, 1999, Goddard Space Flight Center.

[5] Escobal, P., *Methods of Orbit Determination*, John Wiley & Sons, Inc., New York, New York, 1975.

[6] Markley, F., "Autonomous Navigation Using Landmark and Intersatellite Data," *AIAA/AAS Astrodynamics Conference*, August 20-22 1984, Seattle, Washington.

[7] Yim, J. R., *Autonomous Spacecraft Orbit Navigation*, Ph.d. dissertation, Texas A&M University, December 2002.

[8] Schmidt, J. and Lovell, T. A., "Estimating Geometric Aspects of Relative Satellite Motion Using Angles-Only Measurements," *AIAA/AAS Astrodynamics Specialist Conference*, August 2008, Honolulu, Hawaii.

[9] Griffith, E. and Kumar, K., "On the Observability of Nonlinear Systems: 1," *Journal of Mathematical Analysis and Applications*, Vol. 35, No. 1, 1971, pp. 135–147.

[10] Woffinden, D. C. and Geller, D. K., "Observability Criteria for Angles-Only Navigation," *IEEE Transactions on Aerospace and Electronic Systems*, Vol. 45, No. 3, 2009, pp. 1194–1208.

[11] Kim, S.-G., Crassidis, J. L., Cheng, Y., Fosbury, A. M., and Junkins, J. L., "Kalman Filtering for Relative Spacecraft Attitude and Position Estimation," *AIAA Guidance, Navigation, and Control Conference and Exhibit*, August 15-18 2005, San Francisco, California.

[12] Fritz, M. P., *A Comparative Study of Kalman Filter Implementations for Relative GPS Navigation*, Master's thesis, Texas A&M University, December 2009.

[13] Delpech, M., Berges, J., Djalal, S., Guidotti, P., and Christy, J., "Preliminary Results of the Vision Based Rendezvous and Formation Flying Experiments Performed During the Prisma Extended Mission," *IAA-AIAA Dynamics and Controls of Space Systems*, December 2007, AAS 12-388.

[14] Fian-feng, L., Si-yuan, R., and Nai-gang, C., "The determination of relative orbit for formation flying subject to J2," *Aircraft Eingeering and Aerospace Technology: An International Journal*, Vol. 80, No. 5, 2008, pp. 549–552.

[15] How, J. P. and Tillerson, R. M., "Analysis of the impact of sensor noise on formation flying control," *AAS/AIAA Space Flight Mechanics Meeting*, February 2001, Santa Barbara, CA.

[16] Alfriend, K. and Yan, H., "Evaluation and Comparison of Relative Motion Theories," *Journal of Guidance, Control, and Dynamics*, Vol. 28, No. 2, 2005, pp. 254–261.

[17] Hintz, G. R., "Survey of Orbit Element Sets," *Journal of Guidance, Control, and Dynamics*, Vol. 31, No. 3, 2008, pp. 785–790.

[18] Sengupta, P., Vadali, S. R., and Alfriend, K. T., "Averaged Relative Motion and Applications to Formation Flying Near Perturbed Orbits," *Journal of Guidance, Control, and Dynamics*, Vol. 31, No. 2, 2008, pp. 258–272.

[19] Sengupta, P. and Vadali, S. R., "Relative Motion and the Geometry of Formations in Keplerian Ellipc Orbits," *Journal of Guidance, Control, and Dynamics*, Vol. 30, No. 4, 2007, pp. 953–964.

[20] Alfriend, K. T., Vadali, S. R., Gurfil, P., How, J. P., and Breger, L. S., *Spacecraft Formation Flying*, Addison-Wesley, Burlington, MA, 2010.

[21] Schaub, H. and Junkins, J. L., *Analytical Mechanics of Space Systems*, American Institute of Aeronautics and Astronautics, Reston, VA, 1st ed., 2003.

[22] Bate, R. R., Mueller, D. D., and White, J. E., *Fundamentals of Astrodynamics*, Dover, Mineola, New York, 1st ed., 1971.

[23] Gim, D.-W. and Alfriend, K. T., "State Transition Matrix of Relative Motion for the Perturbed Noncircular Reference Orbit," *Journal of Guidance, Control, and Dynamics*, Vol. 26, No. 6, 2003, pp. 956–971.

[24] Vadali, S. R., "Model for Linearized Satellite Relative Motion About a J_2-Perturbed Mean Circular Orbit," *Journal of Guidance, Control, and Dynamics*, Vol. 32, No. 5, 2009, pp. 1687–1691.

[25] Crassidis, J. L. and Junkins, J. L., *Optimal Estimation of Dynamic Systems*, Chapman & Hall/CRC Press, Boca Raton, FL, 1st ed., 2004.

[26] Mithcell, M. L., *CDGPS-Based Relative Navigation for Multiple Spacecraft*, Master's thesis, Massachusetts Institute of Technology, June 2004.

[27] Mitchell, M., Breger, L., How, J. P., and Alfriend, K. T., "Effects of Navigation Filter Properties on Formation Flying Control," *AIAA Guidance, Navigation, and Control Conference and Exhibit*, August 2004, Providence, Rhode Island.

[28] Hablani, H. B., Tapper, M. L., and Dana-Bashian, D. J., "Guidance and Relative Navigation for Autonomous Rendezvous in a Circular Orbit," *Journal of Guidance, Control, and Dynamics*, Vol. 25, No. 3, 2002, pp. 553–562.

APPENDIX A

MEASUREMENT COEFFICIENT MATRIX

The measurement coefficient matrix for the curvilinear coordinate system, when given vector-style measurements, is defined by:

$$H = \frac{\partial h}{\partial x_{LVLH}}|_{\hat{\mathbf{x}}^-_{LVLH}} \frac{\partial x_{LVLH}}{\partial x_{CURV}}|_{\hat{\mathbf{x}}^-_{CURV}} \tag{A.1}$$

Let the first half of the measurement coefficient matrix of Eq. (A.1) be defined by h_x, and the second half of the equation be defined as h_c. For the simple, vector measurement case, h_x is defined by:

$$h_x = \begin{bmatrix} 1 & 0 & 0 & 0 & 0 & 0 \\ 0 & 0 & 1 & 0 & 0 & 0 \\ 0 & 0 & 0 & 0 & 1 & 0 \end{bmatrix} \tag{A.2}$$

For the purposes of this section, the ordering of the variables has changed. Rather than being ordered in the typical $[xyzv_xv_yv_z]^T$ format, the variables are ordered $[xv_xyv_yzv_z]^T$. This is due to the fact that the GA-STM propagates the latter format of the variables.

For the more complex measurements, the matrix h_x is defined as:

$$h_x(1,1) = -\frac{\delta y}{\delta x^2 + \delta y^2} \tag{A.3}$$

$$h_x(1,2) = 0 \tag{A.4}$$

$$h_x(1,3) = \frac{\delta x}{\delta x^2 + \delta y^2} \tag{A.5}$$

$$h_x(1,4) = 0 \tag{A.6}$$

$$h_x(1,5) = 0 \tag{A.7}$$

$$h_x(1,6) = 0 \tag{A.8}$$

$$h_x(2,1) = -\frac{\delta x \delta z}{\sqrt{\delta x^2 + \delta y^2}\,(\delta x^2 + \delta y^2 + \delta z^2)} \tag{A.9}$$

$$h_x(2,2) = 0 \tag{A.10}$$

$$h_x(2,3) = -\frac{\delta y \delta z}{\sqrt{\delta x^2 + \delta y^2}\,(\delta x^2 + \delta y^2 + \delta z^2)} \tag{A.11}$$

$$h_x(2,4) = 0 \tag{A.12}$$

$$h_x(2,5) = \frac{\sqrt{\delta x^2 + \delta y^2}}{\delta x^2 + \delta y^2 + \delta z^2} \tag{A.13}$$

$$h_x(2,6) = 0 \tag{A.14}$$

$$h_x(3,1) = \frac{\delta x}{\sqrt{\delta x^2 + \delta y^2 + \delta z^2}} \tag{A.15}$$

$$h_x(3,2) = 0 \tag{A.16}$$

$$h_x(3,3) = \frac{\delta y}{\sqrt{\delta x^2 + \delta y^2 + \delta z^2}} \tag{A.17}$$

$$h_x(3,4) = 0 \tag{A.18}$$

$$h_x(3,5) = \frac{\delta z}{\sqrt{\delta x^2 + \delta y^2 + \delta z^2}} \tag{A.19}$$

$$h_x(3,6) = 0 \tag{A.20}$$

The second half of Eq. (A.1), h_c, is defined as the partial derivatives of the curvilinear-to-LVLH frame transformations, given in Section II.B.4.b. This is defined as:

$$h_c(1,1) = \cos\frac{z_c}{R_c+x_c}\cos\frac{y_c}{R_c} + \frac{z_c \sin\frac{z_c}{R_c+x_c}\cos\frac{y_c}{R_c}}{R_c+x_c} \tag{A.21}$$

$$h_c(1,2) = 0 \tag{A.22}$$

$$h_c(1,3) = -\frac{\cos\frac{z_c}{R_c+x_c}\sin\frac{y_c}{R_c}}{R_c} \tag{A.23}$$

$$h_c(1,4) = 0 \tag{A.24}$$

$$h_c(1,5) = -\sin\frac{z_c}{R_c+x_c}\cos\frac{y_c}{R_c} \tag{A.25}$$

$$h_c(1,6) = 0 \tag{A.26}$$

$$\begin{aligned} h_c(2,1) =& \frac{\sin\frac{z_c}{R_c+x_c}\cos\frac{y_c}{R_c}\left(v_{z,c}\left(R_c+x_c\right) - \dot{R}_c v_{x,c} z_c\right)}{\left(R_c+x_c\right)^2} \\ &- \frac{\cos\frac{z_c}{R_c+x_c}\sin\frac{y_c}{R_c}\left(R_c + v_{y,c} - \dot{R}_c y_c\right)}{R_c^2} \\ &- \frac{v_{z_c}\sin\frac{z_c}{R_c+x_c}\cos\frac{y_c}{R_c}}{R_c+x_c} \\ &+ \frac{z_c\cos\frac{z_c}{R_c+x_c}\cos\frac{y_c}{R_c}\left(v_{z,c}\left(R_c+x_c\right) - \dot{R}_c v_{x,c} z_c\right)}{\left(R_c+x_c\right)^3} \\ &+ \frac{z_c\sin\frac{z_c}{R_c+x_c}\cos y_c R_c\left(\dot{R}_c + v_{x,c}\right)}{\left(R_c+x_c\right)^2} \\ &- \frac{z_c\sin\frac{z_c}{R_c+x_c}\sin\frac{y_c}{R_c}\left(R_c + v_{y,c} - \dot{R}_c y_c\right)}{R_c^2\left(R_c+x_c\right)} \end{aligned} \tag{A.27}$$

$$h_c(2,2) = \frac{\cos\frac{z_c}{R_c+x_c}\cos\frac{y_c}{R_c} + \dot{R}_c z_c \sin\frac{z_c}{R_c+x_c}\cos\frac{y_c}{R_c}}{R_c+x_c} \tag{A.28}$$

$$
\begin{aligned}
h_c(2,3) =& \frac{\dot{R}_c \cos\frac{z_c}{R_c+x_c} \sin\frac{y_c}{R_c} (R_c + x_c)}{R_c^2} \\
& - \frac{\cos\frac{z_c}{R_c+x_c} \cos\frac{y_c}{R_c} (R_c + x_c) \left(R_c + v_{y,c} - \dot{R}_c y_c\right)}{Rc^3} \\
& - \frac{\cos\frac{z_c}{R_c+x_c} \sin\frac{y_c}{R_c} \left(\dot{R}_c + v_{x,c}\right)}{R_c} \\
& + \frac{\sin\frac{z_c}{R_c+x_c} \sin\frac{y_c}{R_c} \left(v_{z,c} (R_c + x_c) - \dot{R}_c v_{x,c} z_c\right)}{R_c (R_c + x_c)}
\end{aligned} \tag{A.29}
$$

$$
h_c(2,4) = -\frac{\cos\frac{z_c}{R_c+x_c} \sin\frac{y_c}{R_c} (R_c + x_c)}{R_c^2} \tag{A.30}
$$

$$
\begin{aligned}
h_c(2,5) =& \frac{\sin\frac{z_c}{R_c+x_c} \sin\frac{y_c}{R_c} \left(R_c + v_{y,c} - \dot{R}_c y_c\right)}{R_c^2} \\
& - \frac{\cos\frac{z_c}{R_c+x_c} \cos\frac{y_c}{R_c} \left(v_{z,c} (R_c + x_c) - \dot{R}_c v_{x,c} z_c\right)}{(R_c + x_c)^2} \\
& - \frac{\sin\frac{z_c}{R_c+x_c} \cos\frac{y_c}{R_c} \left(\dot{R}_c + v_{x,c}\right)}{R_c + x_c} \\
& + \frac{\dot{R}_c v_{x,c} \sin\frac{z_c}{R_c+x_c} \cos\frac{yc}{R_c}}{R_c + x_c}
\end{aligned} \tag{A.31}
$$

$$
h_c(2,6) = -sin\frac{z_c}{R_c + x_c} \cos\frac{y_c}{R_c} \tag{A.32}
$$

$$
h_c(3,1) = \cos\frac{z_c}{R_c + x_c} \sin\frac{y_c}{R_c} + \frac{z_c \sin\frac{z_c}{R_c+x_c} \sin\frac{y_c}{R_c}}{R_c + x_c} \tag{A.33}
$$

$$
h_c(3,2) = 0 \tag{A.34}
$$

$$
h_c(3,3) = \frac{\cos\frac{z_c}{R_c+x_c} \cos\frac{y_c}{R_c}}{R_c} \tag{A.35}
$$

$$
h_c(3,4) = 0 \tag{A.36}
$$

$$
h_c(3,5) = -\sin\frac{z_c}{R_c + x_c} \sin\frac{y_c}{R_c} \tag{A.37}
$$

$$
h_c(3,6) = 0 \tag{A.38}
$$

$$
\begin{aligned}
h_c(4,1) =& \frac{\cos\frac{z_c}{R_c+x_c}\cos\frac{y_c}{R_c}\left(R_c + v_{y,c} - \dot{R}_c y_c\right)}{R_c^2} \\
&- \frac{v_{z,c}\sin\frac{z_c}{R_c+x_c}\sin y_c R_c}{R_c + x_c} \\
&+ \frac{\sin\frac{z_c}{R_c+x_c}\sin\frac{y_c}{R_c}\left(v_{z,c}\left(R_c + x_c\right) - \dot{R}c v_{x,c} z_c\right)}{\left(R_c + x_c\right)^2} \\
&+ \frac{z_c\cos\frac{z_c}{R_c+x_c}\sin\frac{y_c}{R_c}\left(v_{z,c}\left(R_c + x_c\right) - \dot{R}c v_{x,c} z_c\right)}{\left(R_c + x_c\right)^3} \\
&+ \frac{z_c\sin\frac{z_c}{R_c+x_c}\sin\frac{y_c}{R_c}\left(\dot{R}_c + v_{x,c}\right)}{\left(R_c + x_c\right)^2} \\
&+ \frac{z_c\sin\frac{z_c}{R_c+x_c}\cos\frac{y_c}{R_c}\left(R_c + v_{y,c} - \dot{R}_c * y_c\right)}{R_c^2\left(R_c + x_c\right)}
\end{aligned} \tag{A.39}
$$

$$
h_c(4,2) = \frac{\cos\frac{z_c}{R_c+x_c}\sin\frac{y_c}{R_c} + \dot{R}_c z_c\sin\frac{z_c}{R_c+x_c}\sin\frac{y_c}{R_c}}{R_c + x_c} \tag{A.40}
$$

$$
\begin{aligned}
h_c(4,3) =& \frac{\cos\frac{z_c}{R_c+x_c}\cos\frac{y_c}{R_c}\left(\dot{R}_c + v_{x,c}\right)}{R_c} \\
&- \frac{\dot{R}_c\cos\frac{z_c}{R_c+x_c}\cos y_c R_c\left(R_c + x_c\right)}{R_c^2} \\
&- \frac{\cos\frac{z_c}{R_c+x_c}\sin\frac{y_c}{R_c}\left(R_c + x_c\right)\left(R_c + v_{y,c} - \dot{R}_c y_c\right)}{R_c^3} \\
&- \frac{\sin\frac{z_c}{R_c+x_c}\cos\frac{y_c}{R_c}\left(v_{z,c}\left(R_c + x_c\right) - dot R_c v_{x,c} z_c\right)}{R_c\left(R_c + x_c\right)}
\end{aligned} \tag{A.41}
$$

$$
h_c(4,4) = \frac{\cos\frac{z_c}{R_c+x_c}\cos\frac{y_c}{R_c}\left(R_c + x_c\right)}{R_c^2} \tag{A.42}
$$

$$
\begin{aligned}
h_c(4,5) =& \frac{\dot{R}_c v_{x,c} \sin \frac{z_c}{R_c+x_c} \sin y_c R_c}{R_c + x_c} \\
&- \frac{\cos \frac{z_c}{R_c+x_c} \sin \frac{y_c}{R_c} \left(v_{z,c} \left(R_c + x_c \right) - \dot{R}_c v_{x,c} z_c \right)}{\left(R_c + x_c \right)^2} \\
&- \frac{\sin \frac{z_c}{R_c+x_c} \sin y_c R_c \left(\dot{R}_c + v_{x,c} \right)}{R_c + x_c} \\
&- \frac{\sin \frac{z_c}{R_c+x_c} \cos \frac{y_c}{R_c} \left(R_c + v_{y,c} - \dot{R}_c y_c \right)}{R_c^2}
\end{aligned} \tag{A.43}
$$

$$
h_c(4,6) = -\sin \frac{z_c}{R_c + x_c} \sin \frac{y_c}{R_c} \tag{A.44}
$$

$$
h_c(5,1) = \sin \frac{z_c}{R_c + x_c} - \frac{z_c \cos \frac{z_c}{R_c+x_c}}{R_c + x_c} \tag{A.45}
$$

$$
h_c(5,2) = 0 \tag{A.46}
$$

$$
h_c(5,3) = 0 \tag{A.47}
$$

$$
h_c(5,4) = 0 \tag{A.48}
$$

$$
h_c(5,5) = \cos \frac{z_c}{R_c + x_c} \tag{A.49}
$$

$$
h_c(5,6) = 0 \tag{A.50}
$$

$$
\begin{aligned}
h_c(6,1) =& \frac{v_{z,c} \cos \frac{z_c}{R_c+x_c}}{R_c + x_c} \\
&- \frac{\cos \frac{z_c}{R_c+x_c} \left(v_{z,c} \left(R_c + x_c \right) - \dot{R}_c v_{x,c} z_c \right)}{\left(R_c + x_c \right)^2} \\
&+ \frac{z_c \sin \frac{z_c}{R_c+x_c} \left(v_{z,c} \left(R_c + x_c \right) - \dot{R}_c v_{x,c} z_c \right)}{\left(R_c + x_c \right)^3} \\
&- \frac{z_c \cos \frac{z_c}{R_c+x_c} \left(\dot{R}_c + v_{x,c} \right)}{\left(R_c + x_c \right)^2}
\end{aligned} \tag{A.51}
$$

$$h_c(6,2) = sin\frac{z_c}{R_c + x_c} - \frac{\dot{R}_c z_c \cos\frac{z_c}{R_c+x_c}}{R_c + x_c} \tag{A.52}$$

$$h_c(6,3) = 0 \tag{A.53}$$

$$h_c(6,4) = 0 \tag{A.54}$$

$$\begin{aligned} h_c(6,5) =& \frac{\cos\frac{z_c}{R_c+x_c}\left(\dot{R}_c + v_{x,c}\right)}{R_c + x_c} \\ & - \frac{\sin\frac{z_c}{R_c+x_c}\left(v_{z,c}\left(R_c + x_c\right) - \dot{R}_c v_{x,c} z_c\right)}{\left(R_c + x_c\right)^2} \\ & - \frac{\dot{R}_c v_{x,c}\cos\frac{z_c}{R_c+x_c}}{R_c + x_c} \end{aligned} \tag{A.55}$$

$$h_c(6,6) = \cos\frac{z_c}{R_c} \tag{A.56}$$

APPENDIX B

ERROR RESIDUAL TABLES

Included in this appendix are the error tables from Chapter IV. All units, unless otherwise specified, are in meters and meters per second. These are results for single-run cases.

B.1. Initial Conditions and Error Residuals - Circular Reference Orbit

B.1.a. Relative Orbit: $\rho = 1km$, $\alpha = 0^\circ$

Table B.1. Initial conditions for deputy with 1 km relative orbit with 0° phase; circular chief reference orbit.

ECI		LVLH	
State	Value	State	Value
X (km)	4998.2119	δx (km)	-6.0259×10^{-4}
Y (km)	4998.2119	δy (km)	0.9976
Z (km)	0.0009	δz (km)	4.1720×10^{-4}
V_X (km/sec)	-1.8197	δv_x (km/sec)	5.3206×10^{-4}
V_Y (km/sec)	1.8190	δv_y (km/sec)	5.2234×10^{-7}
V_Z (km/sec)	7.0768	δv_z (km/sec)	1.0600×10^{-3}

Curvilienear	
State	Value
x (km)	-5.6473×10^{-4}
y (km)	0.9975
z (km)	2.7685×10^{-4}
v_x (km/sec)	5.3206×10^{-4}
v_y (km/sec)	6.1005×10^{-7}
v_z (km/sec)	1.0600×10^{-3}

Table B.2. Modeling error between GA-STM and perturbed two-body; relative orbit of $\rho = 1$ km and $\alpha = 0°$; circular reference orbit

State	Mean	Standard Deviation
δx	0.029745	0.147548
δy	-0.333901	0.369456
δz	-0.129907	0.196872
δv_x	$3.464821e-005$	$1.573987e-004$
δv_y	$-1.064337e-004$	$3.374763e-004$
δv_z	$-4.802574e-005$	$2.218489e-004$

Table B.3. Error residual for: 1 km relative orbit, 0° phase angle, $\bar{e} = 0$ reference orbit. Propagation model: GA-STM. Measurement model: Linear

dt	Statistic	δx	δy	δz
1 sec	μ	0.000363	-0.000067	-0.000708
	σ	0.001620	0.001821	0.001416
10 sec	μ	0.001036	0.000362	-0.002558
	σ	0.004730	0.003980	0.003943
dt	Statistic	δv_x	δv_y	δv_z
1 sec	μ	$7.986813e-006$	$-3.670513e-006$	$-1.563298e-005$
	σ	7.794986×10^{-5}	4.473023×10^{-5}	1.942406×10^{-4}
10 sec	μ	$1.684686e-005$	$-1.343235e-006$	$-2.981766e-005$
	σ	$2.934031e-005$	$7.209716e-005$	$1.953058e-005$

Table B.4. Error residual for: 1 km relative orbit, 0° phase angle, $\bar{e} = 0$ reference orbit. Propagation model: GA-STM. Measurement model: Non-Linear

dt	Statistic	δx	δy	δz
1 sec	μ	0.001253	-0.013613	-0.008246
	σ	0.047042	0.032131	0.047974
10 sec	μ	-0.022943	-0.016644	-0.027538
	σ	0.092732	0.072275	0.084472
dt	Statistic	δv_x	δv_y	δv_z
1 sec	μ	$5.535794e-005$	$-4.931108e-005$	$-3.029934e-005$
	σ	$2.900229e-004$	$1.053572e-004$	$2.150018e-004$
10 sec	μ	$-7.603912e-006$	$-3.766455e-005$	$-5.467049e-005$
	σ	$1.528389e-004$	$1.728552e-004$	$1.614413e-004$

Table B.5. Modeling error between the J_2-Linearized equations of motion and the perturbed two-body; relative orbit of $\rho = 1$km and $\alpha = 0°$; circular reference orbit

State	Mean	Standard Deviation
δx	-0.220703	0.324916
δy	2.722549	1.734952
δz	-0.132952	0.131615
δv_x	$3.564918e-005$	$3.450283e-004$
δv_y	$4.060536e-004$	$6.978693e-004$
δv_z	$-4.798618e-005$	$1.604517e-004$

Table B.6. Error residual for: 1 km relative orbit, 0° phase angle, $\bar{e} = 0$ reference orbit. Propagation model: J_2-Linearized. Measurement model: Linear

dt	Statistic	δx	δy	δz
1 sec	μ	-0.000629	0.000235	-0.000698
	σ	0.001420	0.001545	0.001570
10 sec	μ	-0.001942	0.000216	-0.002903
	σ	0.003374	0.003511	0.003775
dt	Statistic	δv_x	δv_y	δv_z
1 sec	μ	$-1.403311e-005$	$-6.211790e-006$	$-1.534985e-005$
	σ	$1.631107e-005$	$2.004718e-005$	$2.036868e-005$
10 sec	μ	$-2.462893e-005$	$-2.609128e-006$	$-2.975492e-005$
	σ	$2.725964e-005$	$2.899793e-005$	$3.129807e-005$

Table B.7. Error residual for: 1 km relative orbit, 0° phase angle, $\bar{e} = 0$ reference orbit. Propagation model: J_2-Linearized. Measurement model: Non-Linear

dt	Statistic	δx	δy	δz
1 sec	μ	-0.018103	-0.003173	-0.010942
	σ	0.048332	0.026851	0.038740
10 sec	μ	0.021267	-0.009283	-0.038905
	σ	0.066534	0.050009	0.060099
dt	Statistic	δv_x	δv_y	δv_z
1 sec	μ	$-5.769413e-005$	$2.359537e-006$	$1.000834e-005$
	σ	$1.801142e-004$	$8.316709e-005$	$1.616629e-004$
10 sec	μ	$-4.471887e-005$	$-3.156457e-006$	$-5.150514e-005$
	σ	$2.682871e-004$	$1.206881e-004$	$1.427727e-004$

Table B.8. Modeling error between CW and perturbed two-body; relative orbit of $\rho = 1$km and $\alpha = 0°$; circular reference orbit

State	Mean	Standard Deviation
δx	-0.650082	1.904236
δy	15.737374	9.317589
δz	-0.361614	9.838643
δv_x	$2.652322e-004$	$1.932428e-003$
δv_y	$2.216568e-003$	$3.998678e-003$
δv_z	$1.948760e-003$	$1.001992e-002$

Table B.9. Error residual for: 1 km relative orbit, 0° phase angle, $\bar{e} = 0$ reference orbit. Propagation model: CW. Measurement model: Linear

dt	Statistic	δx	δy	δz
1 sec	μ	-0.001261	0.000108	-0.000172
	σ	0.002602	0.002558	0.002621
10 sec	μ	-0.004146	0.000537	-0.000450
	σ	0.007688	0.007188	0.007429
dt	Statistic	δv_x	δv_y	δv_z
1 sec	μ	$-7.647549e-005$	$-6.018014e-006$	$-1.234428e-005$
	σ	$1.118230e-004$	$1.014085e-004$	$1.102017e-004$
10 sec	μ	$-1.407224e-004$	$-4.227964e-006$	$-1.912617e-005$
	σ	$2.058341e-004$	$1.787121e-004$	$1.998546e-004$

Table B.10. Error residual for: 1 km relative orbit, 0° phase angle, $\bar{e} = 0$ reference orbit. Propagation model: CW. Measurement model: Non-Linear

dt	Statistic	δx	δy	δz
1 sec	μ	-0.051695	0.002037	0.000482
	σ	0.112889	0.061255	0.073499
10 sec	μ	-0.043711	-0.016356	-0.006144
	σ	0.183923	0.138122	0.150941
dt	Statistic	δv_x	δv_y	δv_z
1 sec	μ	$-4.872630e-004$	$8.060793e-005$	$5.237349e-005$
	σ	$8.024549e-004$	$3.953561e-004$	$4.382347e-004$
10 sec	μ	$-5.508102e-004$	$7.747328e-005$	$6.926679e-005$
	σ	$1.009123e-003$	$6.225567e-004$	$5.745424e-004$

B.1.b. Relative Orbit: $\rho = 10km$, $\alpha = 0^\circ$

Table B.11. Initial conditions for deputy with 10 km relative orbit with 0° phase; circular chief reference orbit.

ECI		LVLH	
State	Value	State	Value
X (km)	5021.1461	δx (km)	-0.0091
Y (km)	5025.95805	δy (km)	10.0006
Z (km)	0.0094	δz (km)	0.0169
V_X (km/sec)	-1.8077	δv_x (km/sec)	0.0053
V_Y (km/sec)	1.8002	δv_y (km/sec)	3.3499×10^{-6}
V_Z (km/sec)	7.0447	δv_z (km/sec)	0.0105

Curvilienear	
State	Value
x (km)	-0.0056
y (km)	9.9998
z (km)	0.0028
v_x (km/sec)	5.6018×10^{-3}
v_y (km/sec)	5.9113×10^{-6}
v_z (km/sec)	1.0547×10^{-2}

Table B.12. Modeling error between GA-STM and perturbed two-body; relative orbit of $\rho = 10$km and $\alpha = 0^\circ$; circular reference orbit

State	Mean	Standard Deviation
δx	-1.236554	1.763392
δy	-3.659232	7.084113
δz	-10.731026	3.218904
δv_x	$3.187220e-004$	$2.756631e-003$
δv_y	$-1.423097e-003$	$1.170533e-002$
δv_z	$-5.104712e-004$	$5.950203e-003$

Table B.13. Error residual for: 10 km relative orbit, 0° phase angle, $\bar{e} = 0$ reference orbit. Propagation model: GA-STM. Measurement model: Linear

dt	Statistic	δx	δy	δz
1 sec	μ	0.005672	0.000473	−0.011330
	σ	0.024243	0.027077	0.021450
10 sec	μ	0.010871	0.002471	−0.038263
	σ	0.062958	0.066580	0.054388
dt	Statistic	δv_x	δv_y	δv_z
1 sec	μ	$2.999059e-004$	$-4.684873e-005$	$-5.696282e-004$
	σ	$8.043173e-004$	$1.145579e-003$	$5.296239e-004$
10 sec	μ	$4.354623e-004$	$7.006158e-005$	$-1.077756e-003$
	σ	$1.247971e-003$	$1.504874e-003$	$8.490590e-004$

Table B.14. Error residual for: 10 km relative orbit, 0° phase angle, $\bar{e} = 0$ reference orbit. Propagation model: GA-STM. Measurement model: Non-Linear

dt	Statistic	δx	δy	δz
1 sec	μ	0.230804	−0.074406	−0.253443
	σ	0.903527	0.499510	0.784032
10 sec	μ	0.851294	−0.903939	−0.695842
	σ	1.513914	1.150472	1.456146
dt	Statistic	δv_x	δv_y	δv_z
1 sec	μ	$1.637466e-003$	$-8.718546e-004$	$-1.457724e-003$
	σ	$7.133899e-003$	$3.632868e-003$	$6.076547e-003$
10 sec	μ	$3.725981e-003$	$-2.658541e-003$	$-2.651687e-003$
	σ	$6.609900e-003$	$4.478203e-003$	$4.533118e-003$

Table B.15. Modeling error between the J_2-Linearized equations of motion and the perturbed two-body; relative orbit of $\rho = 10$km and $\alpha = 0°$; circular reference orbit

State	Mean	Standard Deviation
δx	−26.479752	20.929401
δy	301.369319	186.207200
δz	−11.031234	8.922400
δv_x	$4.002694e-004$	$2.252785e-002$
δv_y	$5.013619e-002$	$4.462548e-002$
δv_z	$-4.483295e-004$	$1.073072e-002$

Table B.16. Error residual for: 10 km relative orbit, 0° phase angle, $\bar{e} = 0$ reference orbit. Propagation model: J_2-Linearized. Measurement model: Linear

dt	Statistic	δx	δy	δz
1 sec	μ	-0.007056	0.001030	-0.006070
	σ	0.022745	0.019064	0.023028
10 sec	μ	-0.024715	0.001926	-0.014618
	σ	0.059144	0.053213	0.053938
dt	Statistic	δv_x	δv_y	δv_z
1 sec	μ	$-5.261307e-004$	$-5.946554e-005$	$-3.716831e-004$
	σ	$6.306963e-004$	$4.941854e-004$	$6.818912e-004$
10 sec	μ	$-9.915022e-004$	$4.381480e-005$	$-7.432959e-004$
	σ	$8.901508e-004$	$8.425772e-004$	$9.376266e-004$

Table B.17. Error residual for: 10 km relative orbit, 0° phase angle, $\bar{e} = 0$ reference orbit. Propagation model: J_2-Linearized. Measurement model: Non-Linear

dt	Statistic	δx	δy	δz
1 sec	μ	-0.543103	-0.058405	0.211959
	σ	0.713336	0.484039	0.703372
10 sec	μ	-0.694700	0.007061	-0.144683
	σ	1.768765	1.031954	1.288470
dt	Statistic	δv_x	δv_y	δv_z
1 sec	μ	$-4.106643e-003$	$5.980668e-004$	$8.399766e-004$
	σ	$6.181341e-003$	$2.675201e-003$	$5.319758e-003$
10 sec	μ	$-5.094280e-003$	$1.651805e-003$	$9.247792e-004$
	σ	$4.179357e-003$	$2.630190e-003$	$2.107552e-003$

Table B.18. Modeling error between CW and perturbed two-body; relative orbit of $\rho = 10$km and $\alpha = 0°$; circular reference orbit

State	Mean	Standard Deviation
δx	-30.762277	35.738600
δy	431.763233	260.952045
δz	-13.308565	106.327775
δv_x	$2.696093e-003$	$3.773043e-002$
δv_y	$6.823887e-002$	$7.518289e-002$
δv_z	$1.949321e-002$	$1.090106e-001$

Table B.19. Error residual for: 10 km relative orbit, 0° phase angle, $\bar{e} = 0$ reference orbit. Propagation model: CW. Measurement model: Linear

dt	Statistic	δx	δy	δz
1 sec	μ	-0.011288	-0.000134	-0.007032
	σ	0.027009	0.024642	0.026322
10 sec	μ	-0.051005	0.006009	-0.025028
	σ	0.071209	0.069892	0.075982
dt	Statistic	δv_x	δv_y	δv_z
1 sec	μ	$-1.050177e-003$	$-5.011670e-005$	$-4.437754e-004$
	σ	$1.106264e-003$	$9.458800e-004$	$1.143502e-003$
10 sec	μ	$-1.992767e-003$	$1.737409e-005$	$-8.343255e-004$
	σ	$1.819244e-003$	$1.634439e-003$	$2.067983e-003$

Table B.20. Error residual for: 10 km relative orbit, 0° phase angle, $\bar{e} = 0$ reference orbit. Propagation model: CW. Measurement model: Non-Linear

dt	Statistic	δx	δy	δz
1 sec	μ	-0.140818	0.007550	-0.339664
	σ	1.109895	0.651074	0.949882
10 sec	μ	-0.513574	-0.026531	0.207313
	2.175367	1.195098	1.422107	
dt	Statistic	δv_x	δv_y	δv_z
1 sec	μ	$-3.167926e-003$	$3.682476e-004$	$-2.281238e-003$
	σ	$9.276300e-003$	$4.697967e-003$	$8.419250e-003$
10 sec	μ	$-5.706535e-003$	$3.433047e-004$	$-5.738162e-004$
	σ	$1.102854e-002$	$6.021099e-003$	$6.234892e-003$

Table B.21. Initial conditions for deputy with 1 km relative orbit with 90° phase; circular chief reference orbit.

ECI		LVLH	
State	Value	State	Value
X (km)	5024.5770	δx (km)	0.4999
Y (km)	5023.2472	δy (km)	2.809×10^{-4}
Z (km)	0.0003	δz (km)	1.0061
V_X (km/sec)	-1.8108	δv_x (km/sec)	-3.2308×10^{-7}
V_Y (km/sec)	1.8108	δv_y (km/sec)	-1.0551×10^{-3}
V_Z (km/sec)	7.0407	δv_z (km/sec)	-1.7525×10^{-7}

Curvilienear	
State	Value
x (km)	0.5001
y (km)	2.8094×10^{-4}
z (km)	1.0005
v_x (km/sec)	-2.9615×10^{-7}
v_y (km/sec)	-1.0552×10^{-3}
v_z (km/sec)	-1.4816×10^{-7}

Table B.22. Modeling error between GA-STM and perturbed two-body; relative orbit of $\rho = 1$km and $\alpha = 90^\circ$; circular reference orbit

State	Mean	Standard Deviation
δx	0.033223	0.151415
δy	-0.167376	0.406641
δz	-0.095175	0.257601
δv_x	$2.039095e-005$	$1.614446e-004$
δv_y	$-2.619227e-005$	$3.032075e-004$
δv_z	$6.312562e-006$	$2.949614e-004$

Table B.23. Error residual for: 1 km relative orbit, 90° phase angle, $\bar{e} = 0$ reference orbit. Propagation model: GA-STM. Measurement model: Linear

dt	Statistic	δx	δy	δz
1 sec	μ	-0.000001	0.000222	-0.000117
	σ	0.001631	0.001654	0.001402
10 sec	μ	0.000057	0.000233	-0.000611
	σ	0.003736	0.003880	0.003744
dt	Statistic	δv_x	δv_y	δv_z
1 sec	μ	$-2.067273e-006$	$1.295251e-006$	$-1.222253e-005$
	σ	$2.726419e-005$	$6.676868e-005$	$1.880382e-005$
10 sec	μ	$-6.055879e-006$	$-2.321664e-006$	$-1.394400e-005$
	σ	$3.793865e-005$	$6.690438e-005$	$2.931752e-005$

Table B.24. Error residual for: 1 km relative orbit, 90° phase angle, $\bar{e} = 0$ reference orbit. Propagation model: GA-STM. Measurement model: Non-Linear

dt	Statistic	δx	δy	δz
1 sec	μ	-0.003077	0.001811	-0.011872
	σ	0.047380	0.025289	0.027970
10 sec	μ	0.052887	-0.025251	-0.004627
	σ	0.097024	0.051323	0.046328
dt	Statistic	δv_x	δv_y	δv_z
1 sec	μ	$-6.850547e-006$	$2.485177e-005$	$-2.658645e-005$
	σ	$1.884310e-004$	$1.304004e-004$	$8.468600e-005$
10 sec	μ	$5.023630e-005$	$-4.838870e-005$	$9.374473e-006$
	σ	$1.601237e-004$	$1.610035e-004$	$6.619067e-005$

Table B.25. Modeling error between the J_2-Linearized equations of motion and the perturbed two-body; relative orbit of $\rho = 1$km and $\alpha = 90°$; circular reference orbit

State	Mean	Standard Deviation
δx	-0.002646	0.151203
δy	0.905969	0.473157
δz	-0.096198	0.247437
δv_x	$2.123337e-005$	$1.571845e-004$
δv_y	$1.406956e-004$	$2.729356e-004$
δv_z	$7.175977e-006$	$2.831686e-004$

Table B.26. Error residual for: 1 km relative orbit, 90° phase angle, $\bar{e} = 0$ reference orbit. Propagation model: J_2-Linearized. Measurement model: Linear

dt	Statistic	δx	δy	δz
1 sec	μ	-0.000825	0.000214	-0.000318
	σ	0.001401	0.001283	0.001466
10 sec	μ	-0.002801	0.001195	-0.000620
	σ	0.003684	0.003297	0.003313
dt	Statistic	δv_x	δv_y	δv_z
1 sec	μ	$-2.013438e-005$	$5.014621e-006$	$-1.153913e-005$
	σ	$1.899454e-005$	$1.458866e-005$	$1.836024e-005$
10 sec	μ	$-3.678204e-005$	$1.203491e-005$	$-1.393971e-005$
	σ	$3.049448e-005$	$2.480582e-005$	$2.902344e-005$

Table B.27. Error residual for: 1 km relative orbit, 90° phase angle, $\bar{e} = 0$ reference orbit. Propagation model: J_2-Linearized. Measurement model: Non-Linear

dt	Statistic	δx	δy	δz
1 sec	μ	-0.023366	0.001092	0.000038
	σ	0.040117	0.033137	0.036485
10 sec	μ	0.001624	0.009091	-0.030050
	σ	0.095641	0.054584	0.051472
dt	Statistic	δv_x	δv_y	δv_z
1 sec	μ	$-9.353650e-005$	$1.852746e-005$	$-6.766732e-006$
	σ	$1.820739e-004$	$1.418677e-004$	$1.076438e-004$
10 sec	μ	$-9.963335e-005$	$8.199188e-005$	$-1.209056e-005$
	σ	$1.585303e-004$	$1.542257e-004$	$7.224507e-005$

Table B.28. Modeling error between CW and perturbed two-body; relative orbit of $\rho = 1$km and $\alpha = 90°$; circular reference orbit

State	Mean	Standard Deviation
δx	0.769914	1.226258
δy	-3.469577	3.850248
δz	0.616570	3.412411
δv_x	$2.544061e-005$	$1.330818e-003$
δv_y	$-1.199619e-003$	$2.517359e-003$
δv_z	$1.132183e-005$	$3.716147e-003$

Table B.29. Error residual for: 1 km relative orbit, 90° phase angle, $\bar{e} = 0$ reference orbit. Propagation model: CW. Measurement model: Linear

dt	Statistic	δx	δy	δz
1 sec	μ	-0.000029	-0.000171	-0.000223
	σ	0.002755	0.002678	0.002380
10 sec	μ	-0.000321	0.000292	-0.000149
	σ	0.008841	0.007344	0.006439
dt	Statistic	δv_x	δv_y	δv_z
1 sec	μ	$-7.193808e-006$	$7.427813e-007$	$-9.727839e-006$
	σ	$1.219228e-004$	$1.064342e-004$	$7.151868e-005$
10 sec	μ	$-1.517542e-005$	$5.754299e-006$	$-6.341160e-007$
	σ	$2.268755e-004$	$1.918272e-004$	$1.224050e-004$

Table B.30. Error residual for: 1 km relative orbit, 90° phase angle, $\bar{e} = 0$ reference orbit. Propagation model: CW. Measurement model: Non-Linear

dt	Statistic	δx	δy	δz
1 sec	μ	-0.001245	-0.001628	0.006041
	σ	0.094995	0.056648	0.070012
10 sec	μ	0.008575	-0.006691	0.026621
	σ	0.238281	0.145623	0.206309
dt	Statistic	δv_x	δv_y	δv_z
1 sec	μ	$-1.486027e-005$	$1.414605e-005$	$1.627585e-006$
	σ	$7.209943e-004$	$4.313475e-004$	$4.378929e-004$
10 sec	μ	$1.520295e-005$	$2.393731e-005$	$5.077642e-005$
	σ	$1.175914e-003$	$5.847234e-004$	$6.468532e-004$

B.1.c. Relative Orbit: $\rho = 1km$, $\alpha = 90^\circ$

B.1.d. Relative Orbit: $\rho = 10km$, $\alpha = 90^\circ$

Table B.31. Initial conditions for deputy with 10 km relative orbit with 90° phase; circular chief reference orbit.

ECI		LVLH	
State	Value	State	Value
X (km)	5033.7423	δx (km)	4.9936
Y (km)	5020.4368	δy (km)	0.0028×10^{-3}
Z (km)	0.0034	δz (km)	10.0124
V_X (km/sec)	-1.8097	δv_x (km/sec)	-5.6514×10^{-6}
V_Y (km/sec)	1.8097	δv_y (km/sec)	-1.0542×10^{-2}
V_Z (km/sec)	7.0362	δv_z (km/sec)	-4.1926×10^{-6}

Curvilienear	
State	Value
x (km)	5.0006
y (km)	2.8094×10^{-3}
z (km)	10.0054
v_x (km/sec)	-2.9615×10^{-6}
v_y (km/sec)	-1.0552×10^{-2}
v_z (km/sec)	-1.4816×10^{-6}

Table B.32. Modeling error between GA-STM and perturbed two-body; relative orbit of $\rho = 10$km and $\alpha = 90^\circ$; circular reference orbit

State	Mean	Standard Deviation
δx	-1.292365	3.081460
δy	-6.330458	8.353629
δz	-10.529506	4.776192
δv_x	$1.706895e-004$	$4.077421e-003$
δv_y	$6.208117e-005$	$1.293057e-002$
δv_z	$4.336092e-005$	$7.085720e-003$

Table B.33. Error residual for: 10 km relative orbit, 90° phase angle, $\bar{e} = 0$ reference orbit. Propagation model: GA-STM. Measurement model: Linear

dt	Statistic	δx	δy	δz
1 sec	μ	0.001706	−0.000376	−0.011881
	σ	0.024165	0.023954	0.019240
10 sec	0.017762	−0.000515	−0.035338	
	σ	0.070474	0.062422	0.052490
dt	Statistic	δv_x	δv_y	δv_z
1 sec	μ	$1.521272e-004$	$-5.374601e-006$	$-5.808590e-004$
	σ	$7.866040e-004$	$1.023691e-003$	$4.333517e-004$
10 sec	μ	$3.312648e-004$	$-1.671068e-004$	$-9.622794e-004$
	σ	$1.403054e-003$	$1.409578e-003$	$7.619059e-004$

Table B.34. Error residual for: 10 km relative orbit, 90° phase angle, $\bar{e} = 0$ reference orbit. Propagation model: GA-STM. Measurement model: Non-Linear

dt	Statistic	δx	δy	δz
1 sec	μ	0.450555	−0.056456	−0.296088
	σ	1.055363	0.557116	0.663784
10 sec	μ	0.385891	−0.324338	−0.410057
	σ	1.981225	1.101810	1.570150
dt	Statistic	δv_x	δv_y	δv_z
1 sec	μ	$2.750838e-003$	$-8.513248e-004$	$-2.347168e-003$
	σ	$5.641082e-003$	$3.007319e-003$	$2.443253e-003$
10 sec	μ	$2.551704e-003$	$-1.204788e-003$	$-2.737177e-003$
	$7.908975e-003$	$4.369946e-003$	$3.953881e-003$	

Table B.35. Modeling error between the J_2-Linearized equations of motion and the perturbed two-body; relative orbit of $\rho = 10$km and $\alpha = 90°$; circular reference orbit

State	Mean	Standard Deviation
δx	-4.902357	3.462278
δy	100.633407	57.016754
δz	-10.669594	6.079705
δv_x	$2.390370e-004$	$4.335621e-003$
δv_y	$1.679880e-002$	$8.635674e-003$
δv_z	$1.331595e-004$	$8.179971e-003$

Table B.36. Error residual for: 10 km relative orbit, 90° phase angle, $\bar{e} = 0$ reference orbit. Propagation model: J_2-Linearized. Measurement model: Linear

dt	Statistic	δx	δy	δz
1 sec	μ	-0.019382	0.001801	-0.011317
	σ	0.019310	0.020072	0.019918
10 sec	μ	-0.015817	-0.003977	-0.032823
	σ	0.079040	0.052256	0.051052
dt	Statistic	δv_x	δv_y	δv_z
1 sec	μ	$-8.362233e-004$	$5.283444e-005$	$-5.711004e-004$
	σ	$4.031743e-004$	$4.611425e-004$	$4.413948e-004$
10 sec	μ	$-6.592507e-004$	$7.792457e-007$	$-9.613604e-004$
	σ	$1.891603e-003$	$7.849378e-004$	$7.522149e-004$

Table B.37. Error residual for: 10 km relative orbit, 90° phase angle, $\bar{e} = 0$ reference orbit. Propagation model: J_2-Linearized. Measurement model: Non-Linear

dt	Statistic	δx	δy	δz
1 sec	μ	-0.436373	-0.192583	-0.001222
	σ	0.798018	0.555670	0.667879
10 sec	μ	-0.830671	0.023664	-0.593514
	σ	1.619583	0.965204	1.175207
dt	Statistic	δv_x	δv_y	δv_z
1 sec	μ	$-4.116423e-003$	$5.519611e-004$	$-3.009203e-004$
	σ	$3.630932e-003$	$2.602218e-003$	$1.683058e-003$
10 sec	μ	$-6.448447e-003$	$1.564816e-003$	$-6.410965e-004$
	σ	$4.244546e-003$	$2.856543e-003$	$2.256513e-003$

Table B.38. Modeling error between CW and perturbed two-body; relative orbit of $\rho = 10$km and $\alpha = 90°$; circular reference orbit

State	Mean	Standard Deviation
δx	2.819847	11.773094
δy	56.990967	32.679625
δz	-3.536302	34.847831
δv_x	$2.800168e-004$	$1.264890e-002$
δv_y	$3.404709e-003$	$2.612385e-002$
δv_z	$1.613660e-004$	$3.752304e-002$

Table B.39. Error residual for: 10 km relative orbit, 90° phase angle, $\bar{e} = 0$ reference orbit. Propagation model: CW. Measurement model: Linear

dt	Statistic	δx	δy	δz
1 sec	μ	-0.009062	0.001276	-0.005763
	σ	0.026789	0.026846	0.023728
10 sec	μ	-0.010135	0.001786	-0.004808
	σ	0.027853	0.026362	0.023917
dt	Statistic	δv_x	δv_y	δv_z
1 sec	μ	$-5.584365e-004$	$2.804250e-005$	$-4.066521e-004$
	σ	$1.220251e-003$	$1.076441e-003$	$7.722111e-004$
10 sec	μ	$-5.568480e-004$	$2.368310e-005$	$-4.073551e-004$
	σ	$2.273240e-003$	$1.967757e-003$	$1.175918e-003$

Table B.40. Error residual for: 10 km relative orbit, 90° phase angle, $\bar{e} = 0$ reference orbit. Propagation model: CW. Measurement model: Non-Linear

dt	Statistic	δx	δy	δz
1 sec	μ	-0.127070	0.022757	-0.026280
	σ	0.974522	0.610364	0.776712
10 sec	μ	-0.470571	-0.259075	-0.062967
	σ	1.984426	1.245561	1.742832
dt	Statistic	δv_x	δv_y	δv_z
1 sec	μ	$-1.830396e-004$	$2.286657e-004$	$-3.719814e-004$
	σ	$9.460907e-003$	$5.146418e-003$	$5.153006e-003$
10 sec	μ	$-1.858951e-003$	$-3.236596e-005$	$-1.007831e-003$
	σ	$1.125262e-002$	$5.580259e-003$	$6.260802e-003$

B.2. Initial Conditions and Error Residuals - Elliptic Reference Orbit

B.2.a. Relative Orbit: $\rho = 1km$, $\alpha = 0^\circ$

Table B.41. Initial conditions for deputy with 1 km relative orbit with 0° phase; elliptic chief reference orbit.

ECI		LVLH	
State	Value	State	Value
X (km)	4998.2119	δx (km)	-6.0259×10^{-3}
Y (km)	4998.6935	δy (km)	0.9976
Z (km)	0.0009	δz (km)	4.1719×10^{-4}
V_X (km/sec)	-1.8197	δv_x (km/sec)	5.3206×10^{-4}
V_Y (km/sec)	1.8189	δv_y (km/sec)	5.2234×10^{-7}
V_Z (km/sec)	7.0768	δv_z (km/sec)	1.0600×10^{-3}

Curvilienear	
State	Value
x (km)	-5.6473×10^{-4}
y (km)	0.9975
z (km)	2.7685×10^{-4}
v_x (km/sec)	5.3206×10^{-4}
v_y (km/sec)	6.1005×10^{-7}
v_z (km/sec)	1.0600×10^{-3}

Table B.42. Modeling error between GA-STM and perturbed two-body; relative orbit of $\rho = 1$km and $\alpha = 0^\circ$; elliptic reference orbit

State	Mean	Standard Deviation
δx	0.027768	0.146869
δy	-0.312546	0.359329
δz	-0.130458	0.194886
δv_x	$3.376795e-005$	$1.582881e-004$
δv_y	$-1.072113e-004$	$3.373908e-004$
δv_z	$-4.759682e-005$	$2.205767e-004$

Table B.43. Error residual for: 1 km relative orbit, 0° phase angle, $\bar{e} = 0.005$ reference orbit. Propagation model: GA-STM. Measurement model: Linear

dt	Statistic	δx	δy	δz
1 sec	μ	0.000319	−0.000035	−0.000593
	σ	0.001774	0.001768	0.001521
10 sec	μ	0.000023	0.000222	−0.000857
	σ	0.011601	0.003999	0.004343
dt	Statistic	δv_x	δv_y	δv_z
1 sec	μ	$8.865136e-006$	$-1.060277e-005$	$-1.734113e-005$
	σ	$3.286246e-005$	$7.345447e-005$	$2.093744e-005$
10 sec	μ	$1.109360e-005$	$-6.228877e-006$	$-2.542477e-005$
	σ	$4.977971e-005$	$7.759032e-005$	$3.158889e-005$

Table B.44. Error residual for: 1 km relative orbit, 0° phase angle, $\bar{e} = 0.005$ reference orbit. Propagation model: GA-STM. Measurement model: Non-Linear

dt	Statistic	δx	δy	δz
1 sec	μ	0.023478	−0.019317	−0.001666
	σ	0.042853	0.034165	0.052968
10 sec	μ	0.055201	−0.024063	−0.025875
	σ	0.092312	0.057761	0.074640
dt	Statistic	δv_x	δv_y	δv_z
1 sec	μ	$6.196576e-005$	$-7.117789e-005$	$-3.812294e-005$
	σ	$1.712185e-004$	$1.028609e-004$	$1.418589e-004$
10 sec	μ	$1.119012e-004$	$-9.382118e-005$	$-1.001621e-004$
	σ	$1.893450e-004$	$1.385939e-004$	$1.499819e-004$

Table B.45. Modeling error between the J_2-Linearized equations of motion and the perturbed two-body; relative orbit of $\rho = 1$km and $\alpha = 0°$; elliptic reference orbit

State	Mean	Standard Deviation
δx	−91.739891	55.865759
δy	592.528926	564.482498
δz	−0.126642	0.520866
δv_x	$-7.679293e-003$	$3.031822e-002$
δv_y	$1.438019e-001$	$9.707654e-002$
δv_z	$9.282159e-005$	$5.280476e-004$

Table B.46. Error residual for: 1 km relative orbit, 0° phase angle, $\bar{e} = 0.005$ reference orbit. Propagation model: J_2-Linearized. Measurement model: Linear

dt	Statistic	δx	δy	δz
1 sec	μ	-0.000103	-0.002941	-0.000590
	σ	0.003595	0.002584	0.001471
10 sec	μ	-0.001248	-0.005674	-0.001552
	σ	0.009347	0.008117	0.003794
dt	Statistic	δv_x	δv_y	δv_z
1 sec	μ	$-9.678977e-006$	$-2.211496e-004$	$-1.317785e-005$
	σ	$2.191005e-004$	$9.137944e-005$	$1.941931e-005$
10 sec	μ	$-4.182367e-005$	$-2.987491e-004$	$-2.467303e-005$
	σ	$3.358062e-004$	$2.067879e-004$	$2.913686e-005$

Table B.47. Error residual for: 1 km relative orbit, 0° phase angle, $\bar{e} = 0.005$ reference orbit. Propagation model: J_2-Linearized. Measurement model: Non-Linear

dt	Statistic	δx	δy	δz
1 sec	μ	-0.005416	-0.036612	-0.005720
	σ	0.097696	0.049134	0.046269
10 sec	μ	-0.033984	-0.120442	-0.039936
	σ	0.257913	0.117257	0.090188
dt	Statistic	δv_x	δv_y	δv_z
1 sec	μ	$-5.904200e-005$	$-6.529977e-004$	$-4.668211e-005$
	σ	$1.492247e-003$	$4.147249e-004$	$1.770776e-004$
10 sec	μ	$-4.981289e-004$	$-1.105239e-003$	$-7.419521e-005$
	σ	$2.299451e-003$	$6.975550e-004$	$1.355012e-004$

Table B.48. Modeling error between CW and perturbed two-body; relative orbit of $\rho = 1$km and $\alpha = 0°$; elliptic reference orbit

State	Mean	Standard Deviation
δx	-0.623975	3.943600
δy	9.137396	11.501167
δz	-0.431079	10.368287
δv_x	$2.631920e-004$	$5.536557e-003$
δv_y	$2.154444e-003$	$9.694093e-003$
δv_z	$1.940280e-003$	$1.199186e-002$

Table B.49. Error residual for: 1 km relative orbit, 0° phase angle, $\bar{e} = 0.005$ reference orbit. Propagation model: CW. Measurement model: Linear

dt	Statistic	δx	δy	δz
1 sec	μ	-0.000871	-0.000057	-0.000168
	σ	0.002844	0.003118	0.003410
10 sec	μ	-0.003712	-0.000018	-0.001180
	σ	0.008381	0.008933	0.010771
dt	Statistic	δv_x	δv_y	δv_z
1 sec	μ	$-6.486166e-005$	$-7.991480e-006$	$-1.230429e-005$
	σ	$1.265648e-004$	$1.503892e-004$	$1.929378e-004$
10 sec	μ	$-1.294619e-004$	$-1.813353e-005$	$-4.737999e-005$
	σ	$2.272812e-004$	$2.608617e-004$	$3.600815e-004$

Table B.50. Error residual for: 1 km relative orbit, 0° phase angle, $\bar{e} = 0.005$ reference orbit. Propagation model: CW. Measurement model: Non-Linear

dt	Statistic	δx	δy	δz
1 sec	μ	-0.023143	-0.032144	-0.022040
	σ	0.094259	0.059263	0.077395
10 sec	μ	-0.129542	-0.106579	-0.054867
	σ	0.227665	0.149757	0.195572
dt	Statistic	δv_x	δv_y	δv_z
1 sec	μ	$-3.832112e-004$	$-3.895435e-004$	$-9.080534e-005$
	σ	$7.366880e-004$	$4.966045e-004$	$6.958326e-004$
10 sec	μ	$-8.254954e-004$	$-6.002246e-004$	$-2.966352e-004$
	σ	$1.261801e-003$	$7.466313e-004$	$1.138792e-003$

B.2.b. Relative Orbit: $\rho = 10km$, $\alpha = 0^\circ$

Table B.51. Initial conditions for deputy with 10 km relative orbit with 0° phase; elliptic chief reference orbit.

ECI		LVLH	
State	Value	State	Value
X (km)	4996.0467	δx (km)	-9.2134×10^{-3}
Y (km)	5000.8466	δy (km)	9.9755
Z (km)	0.0094	δz (km)	1.6803×10^{-2}
V_X (km/sec)	-1.8167	δv_x (km/sec)	5.3234×10^{-3}
V_Y (km/sec)	1.80924	δv_y (km/sec)	-3.1387×10^{-6}
V_Z (km/sec)	7.0801	δv_z (km/sec)	1.0600×10^{-2}

Curvilienear	
State	Value
x (km)	-5.6473×10^{-3}
y (km)	9.9747
z (km)	2.7685×10^{-3}
v_x (km/sec)	5.3206×10^{-3}
v_y (km/sec)	6.1005×10^{-6}
v_z (km/sec)	1.0600×10^{-2}

Table B.52. Modeling error between GA-STM and perturbed two-body; relative orbit of $\rho = 10$km and $\alpha = 0^\circ$; elliptic reference orbit

State	Mean	Standard Deviation
δx	-1.256323	1.769558
δy	-3.446169	7.011660
δz	-10.738550	3.195679
δv_x	$3.093199e-004$	$2.756031e-003$
δv_y	$-1.432736e-003$	$1.172683e-002$
δv_z	$-5.068954e-004$	$5.949502e-003$

Table B.53. Error residual for: 10 km relative orbit, 0° phase angle, $\bar{e} = 0.005$ reference orbit. Propagation model: GA-STM. Measurement model: Linear

dt	Statistic	δx	δy	δz
1 sec	μ	0.007251	−0.000881	−0.019475
	σ	0.026154	0.024893	0.021543
10 sec	μ	0.011022	−0.000015	−0.040896
	σ	0.061584	0.067323	0.053590
dt	Statistic	δv_x	δv_y	δv_z
1 sec	μ	$3.542295e-004$	$-1.139926e-004$	$-8.608073e-004$
	σ	$9.315093e-004$	$1.115615e-003$	$6.410595e-004$
10 sec	μ	$4.398333e-004$	$1.687630e-005$	$-1.089857e-003$
	σ	$1.238453e-003$	$1.503824e-003$	$8.595091e-004$

Table B.54. Error residual for: 10 km relative orbit, 0° phase angle, $\bar{e} = 0.005$ reference orbit. Propagation model: GA-STM. Measurement model: Non-Linear

dt	Statistic	δx	δy	δz
1 sec	μ	0.308332	−0.122878	−0.142209
	σ	0.817719	0.520089	0.815799
10 sec	μ	0.927438	−0.947109	−0.718113
	σ	2.302100	1.173841	1.768700
dt	Statistic	δv_x	δv_y	δv_z
1 sec	μ	$1.663865e-003$	$-6.912682e-004$	$-1.890734e-003$
	σ	$6.823732e-003$	$3.546370e-003$	$6.899020e-003$
10 sec	μ	$3.994269e-003$	$-2.937052e-003$	$-2.741338e-003$
	σ	$7.474267e-003$	$4.654918e-003$	$5.031537e-003$

Table B.55. Modeling error between the J_2-Linearized equations of motion and the perturbed two-body; relative orbit of $\rho = 10$km and $\alpha = 0°$; elliptic reference orbit

State	Mean	Standard Deviation
δx	−936.732874	567.598924
δy	6182.515142	5801.094853
δz	−11.077200	14.041850
δv_x	$-7.245634e-002$	$3.278817e-001$
δv_y	$1.475635e+000$	$9.971733e-001$
δv_z	$9.542157e-004$	$1.555951e-002$

Table B.56. Error residual for: 10 km relative orbit, 0° phase angle, $\bar{e} = 0.005$ reference orbit. Propagation model: J_2-Linearized. Measurement model: Linear

dt	Statistic	δx	δy	δz
1 sec	μ	-0.007906	-0.010993	-0.004696
	σ	0.035999	0.031032	0.023091
10 sec	μ	-0.019167	-0.048902	-0.016970
	σ	0.093425	0.086043	0.060148
dt	Statistic	δv_x	δv_y	δv_z
1 sec	μ	$-4.746823e-004$	$-1.510878e-003$	$-3.753249e-004$
	σ	$2.189175e-003$	$1.496308e-003$	$6.653742e-004$
10 sec	μ	$-9.694622e-004$	$-2.934127e-003$	$-7.425320e-004$
	σ	$3.397434e-003$	$2.154042e-003$	$9.804921e-004$

Table B.57. Error residual for: 10 km relative orbit, 0° phase angle, $\bar{e} = 0.005$ reference orbit. Propagation model: J_2-Linearized. Measurement model: Non-Linear

dt	Statistic	δx	δy	δz
1 sec	μ	-0.051002	-0.442190	-0.322953
	σ	1.229454	0.575372	0.757068
10 sec	μ	-0.577577	-1.652276	-0.731853
	σ	3.072318	1.504103	1.425691
dt	Statistic	δv_x	δv_y	δv_z
1 sec	μ	$-1.595720e-003$	$-6.825102e-003$	$-2.790956e-003$
	σ	$1.368215e-002$	$5.066223e-003$	$6.777535e-003$
10 sec	μ	$-4.981787e-003$	$-1.272618e-002$	$-3.741488e-003$
	σ	$2.199903e-002$	$8.153928e-003$	$4.301108e-003$

Table B.58. Modeling error between CW and perturbed two-body; relative orbit of $\rho = 10$km and $\alpha = 0°$; elliptic reference orbit

State	Mean	Standard Deviation
δx	-30.548821	49.695970
δy	366.217878	270.383086
δz	-14.004604	111.258673
δv_x	$2.675734e-003$	$6.418287e-002$
δv_y	$6.769410e-002$	$1.160662e-001$
δv_z	$1.940760e-002$	$1.273889e-001$

Table B.59. Error residual for: 10 km relative orbit, 0° phase angle, $\bar{e} = 0.005$ reference orbit. Propagation model: CW. Measurement model: Linear

dt	Statistic	δx	δy	δz
1 sec	μ	-0.011754	0.000767	-0.006957
	σ	0.028971	0.028142	0.033964
10 sec	μ	-0.050686	0.003189	-0.024473
	σ	0.076512	0.086551	0.107683
dt	Statistic	δv_x	δv_y	δv_z
1 sec	μ	$-1.048372e-003$	$-6.617143e-005$	$-3.957036e-004$
	σ	$1.234261e-003$	$1.465526e-003$	$1.945273e-003$
10 sec	μ	$-2.080303e-003$	$-1.063641e-004$	$-1.022958e-003$
	σ	$2.186841e-003$	$2.539293e-003$	$3.603605e-003$

Table B.60. Error residual for: 10 km relative orbit, 0° phase angle, $\bar{e} = 0.005$ reference orbit. Propagation model: CW. Measurement model: Non-Linear

dt	Statistic	δx	δy	δz
1 sec	μ	-0.380165	-0.502558	-0.102029
	σ	1.230743	0.734710	1.091325
10 sec	μ	-0.673317	-0.644796	-0.320268
	σ	2.130496	1.671687	1.777621
dt	Statistic	δv_x	δv_y	δv_z
1 sec	μ	$-6.742306e-003$	$-4.365760e-003$	$-1.345403e-003$
	σ	$8.181886e-003$	$5.720807e-003$	$8.166244e-003$
10 sec	μ	$-8.562993e-003$	$-5.574054e-003$	$-2.226047e-003$
	σ	$1.131679e-002$	$8.355503e-003$	$1.026629e-002$

Table B.61. Initial conditions for deputy with 1 km relative orbit with 90° phase; elliptic chief reference orbit.

ECI		LVLH	
State	Value	State	Value
X (km)	4999.4682	δx (km)	0.4999
Y (km)	4998.1452	δy (km)	2.8176×10^{-4}
Z (km)	0.0003	δz (km)	0.9956
V_X (km/sec)	-1.8199	δv_x (km/sec)	-3.2641×10^{-7}
V_Y (km/sec)	1.8199	δv_y (km/sec)	-1.6300×10^{-3}
V_Z (km/sec)	7.0759	δv_z (km/sec)	-1.7855×10^{-7}

Curvilienear	
State	Value
x (km)	0.5000
y (km)	2.8186×10^{-4}
z (km)	0.9955
v_x (km/sec)	-3.0113×10^{-7}
v_y (km/sec)	-1.0631×10^{-3}
v_z (km/sec)	-1.15132×10^{-7}

Table B.62. Modeling error between GA-STM and perturbed two-body; relative orbit of $\rho = 1$km and $\alpha = 90^\circ$; elliptic reference orbit

State	Mean	Standard Deviation
δx	0.031191	0.149424
δy	-0.152339	0.401669
δz	-0.095394	0.256312
δv_x	$1.963970e-005$	$1.604237e-004$
δv_y	$-2.359521e-005$	$3.003953e-004$
δv_z	$6.299505e-006$	$2.935183e-004$

Table B.63. Error residual for: 1 km relative orbit, 90° phase angle, $\bar{e} = 0.005$ reference orbit. Propagation model: GA-STM. Measurement model: Linear

dt	Statistic	δx	δy	δz
1 sec	μ	-0.000102	0.000055	-0.000230
	σ	0.001503	0.001636	0.001326
10 sec	μ	-0.000772	0.000069	-0.001106
	σ	0.004458	0.004242	0.004719
dt	Statistic	δv_x	δv_y	δv_z
1 sec	μ	$-1.796297e-006$	$1.431656e-006$	$-1.165103e-005$
	σ	$2.243598e-005$	$7.141893e-005$	$1.809759e-005$
10 sec	μ	$-6.947720e-006$	$9.411961e-006$	$-3.012855e-005$
	σ	$5.915202e-005$	$7.775761e-005$	$5.773451e-005$

Table B.64. Error residual for: 1 km relative orbit, 90° phase angle, $\bar{e} = 0.005$ reference orbit. Propagation model: GA-STM. Measurement model: Non-Linear

dt	Statistic	δx	δy	δz
1 sec	μ	-0.003318	0.000696	-0.018590
	σ	0.049181	0.028219	0.032950
10 sec	μ	0.057316	0.024243	-0.023659
	σ	0.101897	0.048338	0.051580
dt	Statistic	δv_x	δv_y	δv_z
1 sec	μ	$-1.760738e-005$	$1.990119e-005$	$-2.842648e-005$
	σ	$1.520169e-004$	$1.096176e-004$	$7.894020e-005$
10 sec	μ	$7.728346e-005$	$-2.774781e-005$	$-3.513419e-005$
	σ	$1.712975e-004$	$1.400157e-004$	$7.501844e-005$

Table B.65. Modeling error between the J_2-Linearized equations of motion and the perturbed two-body; relative orbit of $\rho = 1$km and $\alpha = 90°$; elliptic reference orbit

State	Mean	Standard Deviation
δx	2.454331	2.224253
δy	-23.852501	14.331417
δz	-0.089374	0.170038
δv_x	$-3.690634e-004$	$4.013043e-003$
δv_y	$-3.740335e-003$	$3.952968e-003$
δv_z	$5.150715e-006$	$1.902456e-004$

Table B.66. Error residual for: 1 km relative orbit, 90° phase angle, $\bar{e} = 0.005$ reference orbit. Propagation model: J_2-Linearized. Measurement model: Linear

dt	Statistic	δx	δy	δz
1 sec	μ	-0.000143	0.000004	-0.000291
	σ	0.003176	0.002509	0.001401
10 sec	μ	-0.000545	-0.000223	-0.000385
	σ	0.009607	0.006551	0.003619
dt	Statistic	δv_x	δv_y	δv_z
1 sec	μ	$-7.356517e-006$	$1.383870e-006$	$-1.288680e-005$
	σ	$1.980480e-004$	$8.538296e-005$	$1.678143e-005$
10 sec	μ	$-3.149110e-005$	$-7.171094e-006$	$-1.500139e-005$
	σ	$3.599455e-004$	$1.410654e-004$	$2.541006e-005$

Table B.67. Error residual for: 1 km relative orbit, 90° phase angle, $\bar{e} = 0.005$ reference orbit. Propagation model: J_2-Linearized. Measurement model: Non-Linear

dt	Statistic	δx	δy	δz
1 sec	μ	0.008705	-0.006288	-0.015520
	σ	0.091931	0.051521	0.042749
10 sec	μ	0.044089	0.012464	-0.038563
	σ	0.197384	0.093802	0.085596
dt	Statistic	δv_x	δv_y	δv_z
1 sec	μ	$-2.328667e-005$	$-5.896051e-007$	$-2.128092e-005$
	σ	$8.503617e-004$	$3.654419e-004$	$1.037323e-004$
10 sec	μ	$-1.703542e-004$	$7.259629e-008$	$-4.943242e-005$
	σ	$1.373996e-003$	$5.797260e-004$	$1.428413e-004$

Table B.68. Modeling error between CW and perturbed two-body; relative orbit of $\rho = 1$km and $\alpha = 90°$; elliptic reference orbit

State	Mean	Standard Deviation
δx	-12.089317	10.517729
δy	141.785705	87.819595
δz	8.271056	4.917958
δv_x	$3.918501e-005$	$1.176059e-002$
δv_y	$2.319308e-002$	$2.349275e-002$
δv_z	$-2.580996e-005$	$6.584313e-003$

Table B.69. Error residual for: 1 km relative orbit, 90° phase angle, $\bar{e} = 0.005$ reference orbit. Propagation model: CW. Measurement model: Linear

dt	Statistic	δx	δy	δz
1 sec	μ	-0.001659	0.000083	0.001667
	σ	0.002848	0.002882	0.003042
10 sec	μ	-0.006954	0.001336	0.006837
	σ	0.007616	0.009174	0.008788
dt	Statistic	δv_x	δv_y	δv_z
1 sec	μ	$-1.765994e-004$	$4.672859e-006$	$1.612156e-004$
	σ	$1.367084e-004$	$1.492351e-004$	$1.730769e-004$
10 sec	μ	$-3.582602e-004$	$3.791235e-005$	$3.269646e-004$
	σ	$2.271281e-004$	$2.626512e-004$	$2.992953e-004$

Table B.70. Error residual for: 1 km relative orbit, 0° phase angle, $\bar{e} = 0.005$ reference orbit. Propagation model: CW. Measurement model: Non-Linear

dt	Statistic	δx	δy	δz
1 sec	μ	-0.108364	0.022370	0.030628
	σ	0.096483	0.057104	0.080829
10 sec	μ	-0.266010	0.077273	0.114359
	σ	0.237205	0.133075	0.195030
dt	Statistic	δv_x	δv_y	δv_z
1 sec	μ	$-1.658909e-003$	$2.854547e-004$	$6.115941e-004$
	σ	$8.760043e-004$	$5.219082e-004$	$6.894489e-004$
10 sec	μ	$-2.451299e-003$	$7.005840e-004$	$1.026959e-003$
	σ	$1.227823e-003$	$8.034105e-004$	$1.096024e-003$

B.2.c. Relative Orbit: $\rho = 1km$, $\alpha = 90^\circ$

B.2.d. Relative Orbit: $\rho = 10km$, $\alpha = 90^\circ$

Table B.71. Initial conditions for deputy with 10 km relative orbit with 90° phase; elliptic chief reference orbit.

ECI		LVLH	
State	Value	State	Value
X (km)	5008.6035	δx (km)	4.9934
Y (km)	4995.3645	δy (km)	2.8230×10^{-3}
Z (km)	0.003408	δz (km)	9.9624
V_X (km/sec)	-1.8188	δv_x (km/sec)	-5.6844×10^{-6}
V_Y (km/sec)	1.8188	δv_y (km/sec)	-1.0622×10^{-2}
V_Z (km/sec)	7.0715	δv_z (km/sec)	-4.2378×10^{-6}

Curvilienear	
State	Value
x (km)	5.0004
y (km)	2.8186×10^{-3}
z (km)	9.9554
v_x (km/sec)	-3.0113×10^{-6}
v_y (km/sec)	-1.0631×10^{-2}
v_z (km/sec)	-1.5132×10^{-6}

Table B.72. Modeling error between GA-STM and perturbed two-body; relative orbit of $\rho = 10$km and $\alpha = 90^\circ$; elliptic reference orbit

State	Mean	Standard Deviation
δx	-1.312869	3.056272
δy	-6.173595	8.327437
δz	-10.531213	4.766223
δv_x	$1.635761e-004$	$4.053784e-003$
δv_y	$9.122874e-005$	$1.290686e-002$
δv_z	$4.352623e-005$	$7.077544e-003$

Table B.73. Error residual for: 10 km relative orbit, 90° phase angle, $\bar{e} = 0.005$ reference orbit. Propagation model: GA-STM. Measurement model: Linear

dt	Statistic	δx	δy	δz
1 sec	μ	0.003885	0.000850	−0.010267
	σ	0.024069	0.023691	0.020717
10 sec	μ	0.001367	−0.000622	−0.036558
	σ	0.063605	0.068874	0.049270
dt	Statistic	δv_x	δv_y	δv_z
1 sec	μ	$1.490338e-004$	$-4.367000e-006$	$-5.793802e-004$
	σ	$7.584092e-004$	$1.034270e-003$	$4.487596e-004$
10 sec	μ	$2.227145e-004$	$-1.635198e-004$	$-9.637903e-004$
	σ	$1.216757e-003$	$1.423150e-003$	$7.119638e-004$

Table B.74. Error residual for: 10 km relative orbit, 90° phase angle, $\bar{e} = 0.005$ reference orbit. Propagation model: GA-STM. Measurement model: Non-Linear

dt	Statistic	δx	δy	δz
1 sec	μ	0.194549	−0.127496	−0.313389
	σ	0.822223	0.534399	0.595864
10 sec	μ	0.090254	−0.533570	0.476440
	σ	1.719909	1.067152	1.442136
dt	Statistic	δv_x	δv_y	δv_z
1 sec	μ	$2.219007e-003$	$-3.807889e-004$	$-1.986774e-003$
	σ	$5.049032e-003$	$4.537669e-003$	$2.459052e-003$
10 sec	μ	$1.136684e-003$	$-1.902466e-003$	$-5.347285e-004$
	σ	$7.054728e-003$	$3.277827e-003$	$4.247779e-003$

Table B.75. Modeling error between the J_2-Linearized equations of motion and the perturbed two-body; relative orbit of $\rho = 10$km and $\alpha = 90°$; elliptic reference orbit

State	Mean	Standard Deviation
δx	21.829526	17.907685
δy	-155.658660	94.763717
δz	-10.653384	5.853946
δv_x	$-2.128387e-003$	$3.630485e-002$
δv_y	$-2.560027e-002$	$2.611602e-002$
δv_z	$1.114231e-004$	$7.871415e-003$

Table B.76. Error residual for: 10 km relative orbit, 90° phase angle, $\bar{e} = 0.005$ reference orbit. Propagation model: J_2-Linearized. Measurement model: Linear

dt	Statistic	δx	δy	δz
1 sec	μ	-0.002195	0.000446	-0.011472
	σ	0.033022	0.026020	0.020818
10 sec	μ	-0.012608	-0.002770	-0.017403
	σ	0.094617	0.077379	0.055030
dt	Statistic	δv_x	δv_y	δv_z
1 sec	μ	$-3.373895e-004$	$1.855865e-005$	$-5.736364e-004$
	σ	$2.050789e-003$	$1.027508e-003$	$4.441721e-004$
10 sec	μ	$-8.241392e-004$	$-8.902350e-005$	$-6.982898e-004$
	σ	$3.520071e-003$	$1.778551e-003$	$8.794129e-004$

Table B.77. Error residual for: 10 km relative orbit, 90° phase angle, $\bar{e} = 0.005$ reference orbit. Propagation model: J_2-Linearized. Measurement model: Non-Linear

dt	Statistic	δx	δy	δz
1 sec	μ	0.093145	−0.002805	0.055376
	σ	0.915732	0.529080	0.541765
10 sec	μ	0.047382	−0.515766	−0.287032
	σ	2.822173	1.193704	1.520284
dt	Statistic	δv_x	δv_y	δv_z
1 sec	μ	$6.421456e-004$	$-1.895623e-004$	$-8.071046e-004$
	σ	$1.115892e-002$	$5.633217e-003$	$2.799709e-003$
10 sec	μ	$-2.115656e-003$	$-1.592880e-003$	$-1.832018e-003$
	σ	$1.754534e-002$	$6.736363e-003$	$5.149732e-003$

Table B.78. Modeling error between CW and perturbed two-body; relative orbit of $\rho = 10$km and $\alpha = 90°$; elliptic reference orbit

State	Mean	Standard Deviation
δx	−125.529462	106.958637
δy	1507.258563	929.369460
δz	73.009059	45.809662
δv_x	$4.169489e-004$	$1.189043e-001$
δv_y	$2.469471e-001$	$2.375898e-001$
δv_z	$-2.094051e-004$	$6.041767e-002$

Table B.79. Error residual for: 10 km relative orbit, 90° phase angle, $\bar{e} = 0.005$ reference orbit. Propagation model: CW. Measurement model: Linear

dt	Statistic	δx	δy	δz
1 sec	μ	−0.020922	0.001200	0.013923
	σ	0.029639	0.028285	0.029753
10 sec	μ	−0.063364	0.002341	0.059728
	σ	0.086416	0.083313	0.085153
dt	Statistic	δv_x	δv_y	δv_z
1 sec	μ	$-2.089223e-003$	$5.593547e-005$	$1.397609e-003$
	σ	$1.413760e-003$	$1.363908e-003$	$1.603883e-003$
10 sec	μ	$-3.686985e-003$	$3.360581e-004$	$2.845794e-003$
	σ	$2.538999e-003$	$2.353331e-003$	$2.745635e-003$

Table B.80. Error residual for: 10 km relative orbit, 90° phase angle, $\bar{e} = 0.005$ reference orbit. Propagation model: CW. Measurement model: Non-Linear

dt	Statistic	δx	δy	δz
1 sec	μ	-0.867589	0.275414	0.386757
	σ	0.897256	0.614498	0.738871
10 sec	μ	-2.023365	0.649819	0.870164
	σ	3.059536	1.538473	1.834418
dt	Statistic	δv_x	δv_y	δv_z
1 sec	μ	$-1.472929e-002$	$2.384633e-003$	$5.470233e-003$
	σ	$8.316345e-003$	$5.903601e-003$	$6.241790e-003$
10 sec	μ	$-2.371985e-002$	$5.314108e-003$	$1.000949e-002$
	σ	$1.646849e-002$	$8.621850e-003$	$1.034587e-002$

B.3. Process Noise - Circular Reference Orbit

B.3.a. Relative Orbit: $\rho = 1km$, $\alpha = 0°$

B.3.a.i. GA-STM

The process noise covariance that was utilized for the estimators is as follows:

- Linear measurement with a sampling time of 1 second:

$$Q = diag([1.00e{-}015, 1.00e{-}016, 1.00e{-}015, 1.00e{-}016, 1.00e{-}015, 5.00e{-}017]) \tag{B.1}$$

- Linear measurement with a sampling time of 10 seconds:

$$Q = diag([1.00e{-}015, 1.00e{-}016, 1.00e{-}015, 1.00e{-}016, 1.00e{-}015, 5.00e{-}017]) \tag{B.2}$$

- Non-linear measurement with a sampling time of 1 second:

$$Q = diag([1.00e{-}015, 5.00e{-}017, 1.00e{-}015, 1.00e{-}017, 1.00e{-}015, 5.00e{-}017]) \tag{B.3}$$

- Non-linear measurement with a sampling time of 10 seconds:

$$Q = diag([1.00e{-}015, 1.00e{-}016, 1.00e{-}015, 1.00e{-}016, 1.00e{-}015, 5.00e{-}016]) \tag{B.4}$$

B.3.a.ii. J_2-Linearized EOM

The process noise covariance that was utilized for the estimators is as follows:

- Linear measurement with a sampling time of 1 second:

$$Q = diag([0.00e{+}000, 0.00e{+}000, 0.00e{+}000, 1.00e{-}018, 1.00e{-}018, 5.00e{-}018]) \tag{B.5}$$

- Linear measurement with a sampling time of 10 seconds:

$$Q = diag([0.00e{+}000, 0.00e{+}000, 0.00e{+}000, 1.00e{-}018, 1.00e{-}018, 1.00e{-}018]) \tag{B.6}$$

- Non-linear measurement with a sampling time of 1 second:

$$Q = diag([0.00e{+}000, 0.00e{+}000, 0.00e{+}000, 1.00e{-}017, 1.00e{-}017, 5.00e{-}017]) \tag{B.7}$$

- Non-linear measurement with a sampling time of 10 seconds:

$$Q = diag([0.00e{+}000, 0.00e{+}000, 0.00e{+}000, 1.00e{-}017, 1.00e{-}017, 5.00e{-}017]) \tag{B.8}$$

B.3.a.iii. CW EOM

The process noise covariance that was utilized for the estimators is as follows:

- Linear measurement with a sampling time of 1 second:

$$Q = diag([0.00e{+}000, 0.00e{+}000, 0.00e{+}000, 5.00e{-}016, 5.00e{-}016, 5.00e{-}016]) \tag{B.9}$$

- Linear measurement with a sampling time of 10 seconds:

$$Q = diag([0.00e{+}000, 0.00e{+}000, 0.00e{+}000, 5.00e{-}015, 5.00e{-}015, 5.00e{-}015]) \tag{B.10}$$

- Non-linear measurement with a sampling time of 1 second:

$$Q = diag([0.00e{+}000, 0.00e{+}000, 0.00e{+}000, 1.00e{-}015, 1.00e{-}015, 1.00e{-}015]) \tag{B.11}$$

- Non-linear measurement with a sampling time of 10 seconds:

$$Q = diag([0.00e{+}000, 0.00e{+}000, 0.00e{+}000, 5.00e{-}014, 5.00e{-}014, 5.00e{-}014]) \tag{B.12}$$

B.3.b. Relative Orbit: $\rho = 10km$, $\alpha = 0^\circ$

B.3.b.i. GA-STM

The process noise covariance that was utilized for the estimators is as follows:

- Linear measurement with a sampling time of 1 second:

$$Q = diag([1.00e{-}012, 1.00e{-}014, 1.00e{-}012, 1.00e{-}014, 1.00e{-}012, 1.00e{-}014]) \tag{B.13}$$

- Linear measurement with a sampling time of 10 seconds:

$$Q = diag([1.00e{-}012, 5.00e{-}013, 1.00e{-}012, 5.00e{-}013, 1.00e{-}012, 1.00e{-}013]) \tag{B.14}$$

- Non-linear measurement with a sampling time of 1 second:

$$Q = diag([1.00e{-}012, 5.00e{-}014, 1.00e{-}012, 5.00e{-}014, 1.00e{-}012, 7.50e{-}014]) \tag{B.15}$$

- Non-linear measurement with a sampling time of 10 seconds:

$$Q = diag([1.00e{-}012, 5.00e{-}013, 1.00e{-}012, 5.00e{-}013, 1.00e{-}012, 7.50e{-}013]) \tag{B.16}$$

B.3.b.ii. J_2-Linearized EOM

The process noise covariance that was utilized for the estimators is as follows:

- Linear measurement with a sampling time of 1 second:

$$Q = diag([0.00e{+}000, 0.00e{+}000, 0.00e{+}000, 5.00e{-}014, 1.00e{-}014, 5.00e{-}014]) \tag{B.17}$$

- Linear measurement with a sampling time of 10 seconds:

$$Q = diag([0.00e{+}000, 0.00e{+}000, 0.00e{+}000, 5.00e{-}014, 1.00e{-}014, 5.00e{-}014]) \tag{B.18}$$

- Non-linear measurement with a sampling time of 1 second:

$$Q = diag([0.00e{+}000, 0.00e{+}000, 0.00e{+}000, 5.00e{-}014, 1.00e{-}014, 1.00e{-}013]) \tag{B.19}$$

- Non-linear measurement with a sampling time of 10 seconds:

$$Q = diag([0.00e{+}000, 0.00e{+}000, 0.00e{+}000, 5.00e{-}014, 1.00e{-}014, 1.00e{-}013]) \tag{B.20}$$

B.3.b.iii. CW EOM

The process noise covariance that was utilized for the estimators is as follows:

- Linear measurement with a sampling time of 1 second:

$$Q = diag([0.00e{+}000, 0.00e{+}000, 0.00e{+}000, 1.00e{-}013, 5.00e{-}014, 5.00e{-}014]) \tag{B.21}$$

- Linear measurement with a sampling time of 10 seconds:

$$Q = diag([0.00e{+}000, 0.00e{+}000, 0.00e{+}000, 1.00e{-}012, 5.00e{-}013, 5.00e{-}013]) \tag{B.22}$$

- Non-linear measurement with a sampling time of 1 second:

$$Q = diag([0.00e{+}000, 0.00e{+}000, 0.00e{+}000, 5.00e{-}013, 1.00e{-}013, 1.00e{-}013]) \tag{B.23}$$

- Non-linear measurement with a sampling time of 10 seconds:

$$Q = diag([0.00e{+}000, 0.00e{+}000, 0.00e{+}000, 1.00e{-}011, 5.00e{-}012, 5.00e{-}012]) \tag{B.24}$$

B.3.c. Relative Orbit: $\rho = 1km$, $\alpha = 90^\circ$

B.3.c.i. GA-STM

The process noise covariance that was utilized for the estimators is as follows:

- Linear measurement with a sampling time of 1 second:

$$Q = diag([1.00e{-}014, 5.00e{-}018, 1.00e{-}014, 5.00e{-}017, 1.00e{-}014, 5.00e{-}018]) \tag{B.25}$$

- Linear measurement with a sampling time of 10 seconds:

$$Q = diag([1.00e{-}014, 1.00e{-}016, 1.00e{-}014, 1.00e{-}016, 1.00e{-}014, 5.00e{-}017]) \tag{B.26}$$

- Non-linear measurement with a sampling time of 1 second:

$$Q = diag([1.00e{-}014, 5.00e{-}018, 1.00e{-}014, 5.00e{-}017, 1.00e{-}014, 1.00e{-}017]) \tag{B.27}$$

- Non-linear measurement with a sampling time of 10 seconds:

$$Q = diag([1.00e{-}014, 5.00e{-}018, 1.00e{-}014, 5.00e{-}017, 1.00e{-}014, 5.00e{-}016]) \tag{B.28}$$

B.3.c.ii. J_2-Linearized EOM

The process noise covariance that was utilized for the estimators is as follows:

- Linear measurement with a sampling time of 1 second:

$$Q = diag([0.00e{+}000, 0.00e{+}000, 0.00e{+}000, 1.00e{-}017, 5.00e{-}018, 5.00e{-}018]) \tag{B.29}$$

- Linear measurement with a sampling time of 10 seconds:

$$Q = diag([0.00e{+}000, 0.00e{+}000, 0.00e{+}000, 1.00e{-}017, 5.00e{-}018, 5.00e{-}018]) \tag{B.30}$$

- Non-linear measurement with a sampling time of 1 second:

$$Q = diag([0.00e{+}000, 0.00e{+}000, 0.00e{+}000, 5.00e{-}017, 5.00e{-}017, 5.00e{-}017]) \tag{B.31}$$

- Non-linear measurement with a sampling time of 10 seconds:

$$Q = diag([0.00e{+}000, 0.00e{+}000, 0.00e{+}000, 1.00e{-}017, 1.00e{-}017, 1.00e{-}017]) \tag{B.32}$$

B.3.c.iii. CW EOM

The process noise covariance that was utilized for the estimators is as follows:

- Linear measurement with a sampling time of 1 second:

$$Q = diag([0.00e{+}000, 0.00e{+}000, 0.00e{+}000, 5.00e{-}016, 5.00e{-}016, 1.00e{-}016]) \tag{B.33}$$

- Linear measurement with a sampling time of 10 seconds:

$$Q = diag([0.00e{+}000, 0.00e{+}000, 0.00e{+}000, 5.00e{-}015, 5.00e{-}015, 1.00e{-}015]) \tag{B.34}$$

- Non-linear measurement with a sampling time of 1 second:

$$Q = diag([0.00e{+}000, 0.00e{+}000, 0.00e{+}000, 1.00e{-}014, 5.00e{-}015, 5.00e{-}015]) \tag{B.35}$$

- Non-linear measurement with a sampling time of 10 seconds:

$$Q = diag([0.00e{+}000, 0.00e{+}000, 0.00e{+}000, 5.00e{-}014, 1.00e{-}014, 1.00e{-}014]) \tag{B.36}$$

B.3.d. Relative Orbit: $\rho = 10km$, $\alpha = 90°$

B.3.d.i. GA-STM

The process noise covariance that was utilized for the estimators is as follows:

- Linear measurement with a sampling time of 1 second:

$$Q = diag([1.00e{-}012, 5.00e{-}014, 1.00e{-}012, 5.00e{-}014, 1.00e{-}012, 1.00e{-}014])) \tag{B.37}$$

- Linear measurement with a sampling time of 10 seconds:

$$Q = diag([1.00e{-}012, 1.00e{-}013, 1.00e{-}012, 5.00e{-}013, 1.00e{-}012, 1.00e{-}013]) \tag{B.38}$$

- Non-linear measurement with a sampling time of 1 second:

$$Q = diag([1.00e{-}012, 5.00e{-}013, 1.00e{-}012, 5.00e{-}013, 1.00e{-}012, 1.00e{-}013]) \tag{B.39}$$

- Non-linear measurement with a sampling time of 10 seconds:

$$Q = diag([1.00e{-}012, 5.00e{-}012, 1.00e{-}012, 5.00e{-}012, 1.00e{-}012, 1.00e{-}012]) \tag{B.40}$$

B.3.d.ii. J_2-Linearized EOM

The process noise covariance that was utilized for the estimators is as follows:

- Linear measurement with a sampling time of 1 second:

$$Q = diag([0.00e{+}000, 0.00e{+}000, 0.00e{+}000, 1.00e{-}014, 1.00e{-}014, 1.00e{-}014]) \tag{B.41}$$

- Linear measurement with a sampling time of 10 seconds:

$$Q = diag([0.00e{+}000, 0.00e{+}000, 0.00e{+}000, 5.00e{-}013, 1.00e{-}014, 1.00e{-}014]) \tag{B.42}$$

- Non-linear measurement with a sampling time of 1 second:

$$Q = diag([0.00e{+}000, 0.00e{+}000, 0.00e{+}000, 5.00e{-}014, 5.00e{-}014, 5.00e{-}014]) \tag{B.43}$$

- Non-linear measurement with a sampling time of 10 seconds:

$$Q = diag([0.00e{+}000, 0.00e{+}000, 0.00e{+}000, 5.00e{-}014, 5.00e{-}014, 5.00e{-}014]) \tag{B.44}$$

B.3.d.iii. CW EOM

The process noise covariance that was utilized for the estimators is as follows:

- Linear measurement with a sampling time of 1 second:

$$Q = diag([0.00e{+}000, 0.00e{+}000, 0.00e{+}000, 5.00e{-}014, 5.00e{-}014, 5.00e{-}014]) \tag{B.45}$$

- Linear measurement with a sampling time of 10 seconds:

$$Q = diag([0.00e{+}000, 0.00e{+}000, 0.00e{+}000, 5.00e{-}013, 5.00e{-}013, 5.00e{-}013]) \tag{B.46}$$

- Non-linear measurement with a sampling time of 1 second:

$$Q = diag([0.00e{+}000, 0.00e{+}000, 0.00e{+}000, 5.00e{-}012, 1.00e{-}012, 1.00e{-}012]) \tag{B.47}$$

- Non-linear measurement with a sampling time of 10 seconds:

$$Q = diag([0.00e{+}000, 0.00e{+}000, 0.00e{+}000, 5.00e{-}012, 1.00e{-}012, 1.00e{-}012]) \tag{B.48}$$

B.4. Process Noise - Elliptic Reference Orbit

B.4.a. Relative Orbit: $\rho = 1km$, $\alpha = 0^\circ$

B.4.a.i. GA-STM

The process noise covariance that was utilized for the estimators is as follows:

- Linear measurement with a sampling time of 1 second:

$$Q = diag([1.00e{-}014, 7.50e{-}018, 1.00e{-}014, 5.00e{-}017, 1.00e{-}014, 5.00e{-}018]) \tag{B.49}$$

- Linear measurement with a sampling time of 10 seconds:

$$Q = diag([1.00e{-}014, 5.00e{-}016, 1.00e{-}014, 5.00e{-}016, 1.00e{-}014, 1.00e{-}016]) \tag{B.50}$$

- Non-linear measurement with a sampling time of 1 second:

$$Q = diag([1.00e{-}014, 5.00e{-}017, 1.00e{-}014, 1.00e{-}017, 1.00e{-}014, 1.00e{-}016]) \tag{B.51}$$

- Non-linear measurement with a sampling time of 10 seconds:

$$Q = diag([1.00e{-}014, 5.00e{-}017, 1.00e{-}014, 5.00e{-}016, 1.00e{-}014, 5.00e{-}016]) \tag{B.52}$$

B.4.a.ii. J_2-Linearized EOM

The process noise covariance that was utilized for the estimators is as follows:

- Linear measurement with a sampling time of 1 second:

$$Q = diag([0.00e{+}000, 0.00e{+}000, 0.00e{+}000, 5.00e{-}018, 1.00e{-}018, 5.00e{-}018]) \tag{B.53}$$

- Linear measurement with a sampling time of 10 seconds:

$$Q = diag([0.00e{+}000, 0.00e{+}000, 0.00e{+}000, 1.00e{-}015, 7.50e{-}015, 1.00e{-}017]) \tag{B.54}$$

- Non-linear measurement with a sampling time of 1 second:

$$Q = diag([0.00e{+}000, 0.00e{+}000, 0.00e{+}000, 7.50e{-}014, 5.00e{-}015, 2.50e{-}017]) \tag{B.55}$$

- Non-linear measurement with a sampling time of 10 seconds:

$$Q = diag([0.00e{+}000, 0.00e{+}000, 0.00e{+}000, 7.50e{-}014, 5.00e{-}015, 2.50e{-}017]) \tag{B.56}$$

B.4.a.iii. CW EOM

The process noise covariance that was utilized for the estimators is as follows:

- Linear measurement with a sampling time of 1 second:

$$Q = diag([0.00e{+}000, 0.00e{+}000, 0.00e{+}000, 1.00e{-}015, 1.00e{-}015, 1.00e{-}015]) \tag{B.57}$$

- Linear measurement with a sampling time of 10 seconds:

$$Q = diag([0.00e{+}000, 0.00e{+}000, 0.00e{+}000, 1.00e{-}014, 1.00e{-}014, 1.00e{-}014]) \tag{B.58}$$

- Non-linear measurement with a sampling time of 1 second:

$$Q = diag([0.00e{+}000, 0.00e{+}000, 0.00e{+}000, 5.00e{-}015, 5.00e{-}015, 5.00e{-}015]) \tag{B.59}$$

- Non-linear measurement with a sampling time of 10 seconds:

$$Q = diag([0.00e{+}000, 0.00e{+}000, 0.00e{+}000, 5.00e{-}014, 5.00e{-}014, 5.00e{-}014]) \tag{B.60}$$

B.4.b. Relative Orbit: $\rho = 10km$, $\alpha = 0^\circ$

B.4.b.i. GA-STM

The process noise covariance that was utilized for the estimators is as follows:

- Linear measurement with a sampling time of 1 second:

$$Q = diag([1.00e{-}011, 1.00e{-}014, 1.00e{-}011, 5.00e{-}014, 1.00e{-}011, 5.00e{-}015]) \tag{B.61}$$

- Linear measurement with a sampling time of 10 seconds:

$$Q = diag([1.00e{-}011, 5.00e{-}013, 1.00e{-}011, 5.00e{-}013, 1.00e{-}011, 1.00e{-}013]) \tag{B.62}$$

- Non-linear measurement with a sampling time of 1 second:

$$Q = diag([1.00e{-}011, 1.00e{-}013, 1.00e{-}011, 1.00e{-}013, 1.00e{-}011, 1.00e{-}013]) \tag{B.63}$$

- Non-linear measurement with a sampling time of 10 seconds:

$$Q = diag([1.00e{-}011, 7.50e{-}013, 1.00e{-}011, 5.00e{-}013, 1.00e{-}011, 7.50e{-}013]) \tag{B.64}$$

B.4.b.ii. J_2-Linearized EOM

The process noise covariance that was utilized for the estimators is as follows:

- Linear measurement with a sampling time of 1 second:

$$Q = diag([0.00e{+}000, 0.00e{+}000, 0.00e{+}000, 1.00e{-}013, 5.00e{-}013, 5.00e{-}014]) \tag{B.65}$$

- Linear measurement with a sampling time of 10 seconds:

$$Q = diag([0.00e{+}000, 0.00e{+}000, 0.00e{+}000, 5.00e{-}013, 5.00e{-}013, 5.00e{-}014]) \tag{B.66}$$

- Non-linear measurement with a sampling time of 1 second:

$$Q = diag([0.00e{+}000, 0.00e{+}000, 0.00e{+}000, 5.00e{-}013, 5.00e{-}013, 5.00e{-}014]) \tag{B.67}$$

- Non-linear measurement with a sampling time of 10 seconds:

$$Q = diag([0.00e{+}000, 0.00e{+}000, 0.00e{+}000, 1.00e{-}012, 5.00e{-}013, 5.00e{-}014]) \tag{B.68}$$

B.4.b.iii. CW EOM

The process noise covariance that was utilized for the estimators is as follows:

- Linear measurement with a sampling time of 1 second:

$$Q = diag([0.00e{+}000, 0.00e{+}000, 0.00e{+}000, 1.00e{-}013, 1.00e{-}013, 1.00e{-}013]) \tag{B.69}$$

- Linear measurement with a sampling time of 10 seconds:

$$Q = diag([0.00e{+}000, 0.00e{+}000, 0.00e{+}000, 1.00e{-}012, 1.00e{-}012, 1.00e{-}012]) \tag{B.70}$$

- Non-linear measurement with a sampling time of 1 second:

$$Q = diag([0.00e{+}000, 0.00e{+}000, 0.00e{+}000, 1.00e{-}012, 1.00e{-}012, 1.00e{-}012]) \tag{B.71}$$

- Non-linear measurement with a sampling time of 10 seconds:

$$Q = diag([0.00e{+}000, 0.00e{+}000, 0.00e{+}000, 1.00e{-}011, 1.00e{-}011, 1.00e{-}011]) \tag{B.72}$$

B.4.c. Relative Orbit: $\rho = 1km$, $\alpha = 90^\circ$

B.4.c.i. GA-STM

The process noise covariance that was utilized for the estimators is as follows:

- Linear measurement with a sampling time of 1 second:

$$Q = diag([1.00e{-}015, 5.00e{-}018, 1.00e{-}015, 5.00e{-}017, 1.00e{-}015, 5.00e{-}018]) \tag{B.73}$$

- Linear measurement with a sampling time of 10 seconds:

$$Q = diag([1.00e{-}011, 5.00e{-}017, 1.00e{-}011, 5.00e{-}017, 1.00e{-}011, 5.00e{-}017]) \tag{B.74}$$

- Non-linear measurement with a sampling time of 1 second:

$$Q = diag([1.00e{-}015, 5.00e{-}018, 1.00e{-}015, 5.00e{-}017, 1.00e{-}015, 5.00e{-}018]) \tag{B.75}$$

- Non-linear measurement with a sampling time of 10 seconds:

$$Q = diag([1.00e{-}015, 5.00e{-}018, 1.00e{-}015, 5.00e{-}016, 1.00e{-}015, 1.00e{-}016]) \tag{B.76}$$

B.4.c.ii. J_2-Linearized EOM

The process noise covariance that was utilized for the estimators is as follows:

- Linear measurement with a sampling time of 1 second:

$$Q = diag([0.00e{+}000, 0.00e{+}000, 0.00e{+}000, 2.50e{-}015, 2.50e{-}016, 5.00e{-}018]) \tag{B.77}$$

- Linear measurement with a sampling time of 10 seconds:

$$Q = diag([0.00e{+}000, 0.00e{+}000, 0.00e{+}000, 5.00e{-}013, 5.00e{-}013, 5.00e{-}014]) \tag{B.78}$$

- Non-linear measurement with a sampling time of 1 second:

$$Q = diag([0.00e{+}000, 0.00e{+}000, 0.00e{+}000, 7.50e{-}015, 5.00e{-}016, 1.00e{-}017]) \tag{B.79}$$

- Non-linear measurement with a sampling time of 10 seconds:

$$Q = diag([0.00e{+}000, 0.00e{+}000, 0.00e{+}000, 7.50e{-}015, 5.00e{-}016, 1.00e{-}017]) \tag{B.80}$$

B.4.c.iii. CW EOM

The process noise covariance that was utilized for the estimators is as follows:

- Linear measurement with a sampling time of 1 second:

$$Q = diag([0.00e{+}000, 0.00e{+}000, 0.00e{+}000, 2.50e{-}015, 1.00e{-}015, 2.50e{-}015]) \tag{B.81}$$

- Linear measurement with a sampling time of 10 seconds:

$$Q = diag([0.00e{+}000, 0.00e{+}000, 0.00e{+}000, 2.50e{-}014, 1.00e{-}014, 2.50e{-}014]) \tag{B.82}$$

- Non-linear measurement with a sampling time of 1 second:

$$Q = diag([0.00e{+}000, 0.00e{+}000, 0.00e{+}000, 2.50e{-}014, 2.50e{-}015, 5.00e{-}015]) \tag{B.83}$$

- Non-linear measurement with a sampling time of 10 seconds:

$$Q = diag([0.00e{+}000, 0.00e{+}000, 0.00e{+}000, 2.50e{-}013, 5.00e{-}014, 7.50e{-}014]) \tag{B.84}$$

B.4.d. Relative Orbit: $\rho = 10km$, $\alpha = 90^\circ$

B.4.d.i. GA-STM

The process noise covariance that was utilized for the estimators is as follows:

- Linear measurement with a sampling time of 1 second:

$$Q = diag([1.00e{-}012, 5.00e{-}014, 1.00e{-}012, 5.00e{-}014, 1.00e{-}012, 1.00e{-}014]) \tag{B.85}$$

- Linear measurement with a sampling time of 10 seconds:

$$Q = diag([1.00e{-}012, 5.00e{-}013, 1.00e{-}012, 5.00e{-}013, 1.00e{-}012, 1.00e{-}013]) \tag{B.86}$$

- Non-linear measurement with a sampling time of 1 second:

$$Q = diag([1.00e{-}012, 5.00e{-}014, 1.00e{-}012, 7.50e{-}014, 1.00e{-}012, 2.50e{-}014]) \tag{B.87}$$

- Non-linear measurement with a sampling time of 10 seconds:

$$Q = diag([1.00e{-}012, 5.00e{-}013, 1.00e{-}012, 7.50e{-}013, 1.00e{-}012, 2.50e{-}012]) \tag{B.88}$$

B.4.d.ii. J_2-Linearized EOM

The process noise covariance that was utilized for the estimators is as follows:

- Linear measurement with a sampling time of 1 second:

$$Q = diag([0.00e{+}000, 0.00e{+}000, 0.00e{+}000, 5.00e{-}013, 5.00e{-}014, 1.00e{-}014]) \tag{B.89}$$

- Linear measurement with a sampling time of 10 seconds:

$$Q = diag([0.00e{+}000, 0.00e{+}000, 0.00e{+}000, 5.00e{-}013, 5.00e{-}014, 5.00e{-}014]) \tag{B.90}$$

- Non-linear measurement with a sampling time of 1 second:

$$Q = diag([0.00e{+}000, 0.00e{+}000, 0.00e{+}000, 1.00e{-}012, 1.00e{-}013, 1.00e{-}013]) \tag{B.91}$$

- Non-linear measurement with a sampling time of 10 seconds:

$$Q = diag([0.00e{+}000, 0.00e{+}000, 0.00e{+}000, 1.00e{-}012, 1.00e{-}013, 1.00e{-}013]) \tag{B.92}$$

B.4.d.iii. CW EOM

The process noise covariance that was utilized for the estimators is as follows:

- Linear measurement with a sampling time of 1 second:

$$Q = diag([0.00e{+}000, 0.00e{+}000, 0.00e{+}000, 1.00e{-}015, 1.00e{-}015, 1.00e{-}017]) \tag{B.93}$$

- Linear measurement with a sampling time of 10 seconds:

$$Q = diag([0.00e{+}000, 0.00e{+}000, 0.00e{+}000, 5.00e{-}012, 1.00e{-}012, 2.50e{-}012]) \tag{B.94}$$

- Non-linear measurement with a sampling time of 1 second:

$$Q = diag([0.00e{+}000, 0.00e{+}000, 0.00e{+}000, 2.50e{-}012, 5.00e{-}013, 7.50e{-}013]) \tag{B.95}$$

- Non-linear measurement with a sampling time of 10 seconds:

$$Q = diag([0.00e{+}000, 0.00e{+}000, 0.00e{+}000, 5.00e{-}011, 1.00e{-}011, 1.00e{-}011]) \tag{B.96}$$